

NONLINEAR DYNAMICS AND SYSTEMS THEORY

An International Journal of Research and Surveys

Volume 15 Number 1 2015

CONTENTS

Preface to the Special Issue: Experimental Approaches in Dynamical Analysis and Control of Mechanical Systems 1

Coupled Fractal Nanosystem: Trap Quasi-two-dimensional Structure 4
O.P. Abramova and S.V. Abramov

Differential Equations of Controlled Pneumatic Actuators for 6-DOF Stewart Platform 14
B. Andrievsky, D.V. Kazunin, D.M. Kostygova, et al

The Duffing Van der Pol Equation: Metamorphoses of Resonance Curves 25
J. Kyzioł and A. Okniński

Analytical and Experimental Investigation of Vertical Vibration of a Freight Wagon in the Presence of Mechanical Asymmetry 32
F.N. Nangolo, J. Soukup, A. Petrenko and J. Skocilas

Researches Defining the Characteristics of Hyperelastic and Composite Materials with Gas Phase in the Vehicle Pedestrian System 43
J. Osinski and P. Rumianek

Mathematical Modeling of the Hydro-Mechanical Fluid Flow System on the Basis of the Human Circulatory System 50
W. Parandyk, D. Lewandowski and J. Awrejcewicz

Six-Legged Robot Gait Analysis 63
B. Stańczyk and J. Awrejcewicz

Constrained Motion of Mechanical Systems and Tracking Control of Nonlinear Systems: Connections and Closed-form Results 73
Firdaus E. Udwadia and Harshavardhan Mylapilli

Transcritical-like Bifurcation in a Model of a Bioreactor 90
J. Villa, G. Olivar and F. Angulo

Cooperation of One and Multi-Joint Muscles 99
B. Zagrodny and J. Awrejcewicz

NONLINEAR DYNAMICS & SYSTEMS THEORY

Volume 15, No. 1, 2015

Nonlinear Dynamics and Systems Theory

An International Journal of Research and Surveys

EDITOR-IN-CHIEF A.A.MARTYNYUK

*S.P.Timoshenko Institute of Mechanics
National Academy of Sciences of Ukraine, Kiev, Ukraine*

REGIONAL EDITORS

P.BORNE, Lille, France
Europe

M.BOHNER, Rolla, USA
North America

T.A.BURTON, Port Angeles, USA
C.CRUZ-HERNANDEZ, Ensenada, Mexico
USA, Central and South America

AI-GUO WU, Harbin, China
China and South East Asia

K.L.TEO, Perth, Australia
Australia and New Zealand

Nonlinear Dynamics and Systems Theory

An International Journal of Research and Surveys

EDITOR-IN-CHIEF A.A.MARTYNYUK

The S.P.Timoshenko Institute of Mechanics, National Academy of Sciences of Ukraine,
Nesterov Str. 3, 03680 MSP, Kiev 57, UKRAINE / e mail: anmart@stability.kiev.ua
e mail: amartynyuk@volicable.com

MANAGING EDITOR I.P.STAVROULAKIS

Department of Mathematics, University of Ioannina
451 10 Ioannina, HELLAS (GREECE) / e mail: ipstav@cc.uoi.gr

REGIONAL EDITORS

AI-GUO WU (China), e-mail: agwu@163.com
P.BORNE (France), e-mail: Pierre.Borne@ec-lille.fr
M.BOHNER (USA), e-mail: bohner@mst.edu
T.A.BURTON (USA), e-mail: taburton@olypen.com
C. CRUZ-HERNANDEZ (Mexico), e-mail: ccruz@cicese.mx
K.L.TEO (Australia), e-mail: K.L.Teo@curtin.edu.au

EDITORIAL BOARD

Ahmed N.U. (Canada)	Khusainov, D.Ya. (Ukraine)
Aleksandrov, A.Yu. (Russia)	Kloeden, P. (Germany)
Artstein, Z. (Israel)	Kokologiannaki, C. (Greece)
Awrejcewicz J. (Poland)	Kuznetsov, N.V. (Finland)
Bajodah, A.H. (Saudi Arabia)	Lazar, M. (The Netherlands)
Benrejeb M. (Tunisia)	Leonov, G.A. (Russia)
Bevilaqua, R. (USA)	Limarchenko, O.S. (Ukraine)
Braiek, N.B. (Tunisia)	Lopez-Gutierrez, R.M. (Mexico)
Chen Ye-Hwa (USA)	Nguang Sing Kiong (New Zealand)
Corduneanu, C. (USA)	Okninski, A. (Poland)
D'Anna, A. (Italy)	Peng Shi (Australia)
De Angelis, M. (Italy)	Peterson, A. (USA)
Dshalalow, J.H. (USA)	Rushchitsky, J.J. (Ukraine)
Eke, F.O. (USA)	Shi Yan (Japan)
Enciso G. (USA)	Siljak, D.D. (USA)
Fabrizio, M. (Italy)	Sree Hari Rao, V. (India)
Georgiou, G. (Cyprus)	Stavrakakis, N.M. (Greece)
Guang-Ren Duan (China)	Vassilyev, S.N. (Russia)
Honglei Xu (Australia)	Vatsala, A. (USA)
Izobov, N.A. (Belarussia)	Wang Hao (Canada)
Karimi, H.R. (Norway)	

ADVISORY EDITOR

A.G.MAZKO, Kiev, Ukraine
e-mail: mazko@imath.kiev.ua

ADVISORY COMPUTER SCIENCE EDITORS

A.N.CHERNIENKO and L.N.CHERNETSKAYA, Kiev, Ukraine

ADVISORY LINGUISTIC EDITOR

S.N.RASSHYVALOVA, Kiev, Ukraine

© 2015, InforMath Publishing Group, ISSN 1562 8353 print, ISSN 1813 7385 online, Printed in Ukraine
No part of this Journal may be reproduced or transmitted in any form or by any means without
permission from InforMath Publishing Group.

INSTRUCTIONS FOR CONTRIBUTORS

(1) General. Nonlinear Dynamics and Systems Theory (ND&ST) is an international journal devoted to publishing peer-refereed, high quality, original papers, brief notes and review articles focusing on nonlinear dynamics and systems theory and their practical applications in engineering, physical and life sciences. Submission of a manuscript is a representation that the submission has been approved by all of the authors and by the institution where the work was carried out. It also represents that the manuscript has not been previously published, has not been copyrighted, is not being submitted for publication elsewhere, and that the authors have agreed that the copyright in the article shall be assigned exclusively to InforMath Publishing Group by signing a transfer of copyright form. Before submission, the authors should visit the website:

<http://www.e-ndst.kiev.ua>

for information on the preparation of accepted manuscripts. Please download the archive Sample NDST.zip containing example of article file (you can edit only the file Samplefilename.tex).

(2) Manuscript and Correspondence. Manuscripts should be in English and must meet common standards of usage and grammar. To submit a paper, send by e-mail a file in PDF format directly to

Professor A.A. Martynyuk, Institute of Mechanics,
Nesterov str.3, 03057, MSP 680, Kiev-57, Ukraine
e-mail: anmart@stability.kiev.ua; center@inmech.kiev.ua

or to one of the Regional Editors or to a member of the Editorial Board. Final version of the manuscript must typeset using LaTeX program which is prepared in accordance with the style file of the Journal. Manuscript texts should contain the title of the article, name(s) of the author(s) and complete affiliations. Each article requires an abstract not exceeding 150 words. Formulas and citations should not be included in the abstract. AMS subject classifications and key words must be included in all accepted papers. Each article requires a running head (abbreviated form of the title) of no more than 30 characters. The sizes for regular papers, survey articles, brief notes, letters to editors and book reviews are: (i) 10-14 pages for regular papers, (ii) up to 24 pages for survey articles, and (iii) 2-3 pages for brief notes, letters to the editor and book reviews.

(3) Tables, Graphs and Illustrations. Each figure must be of a quality suitable for direct reproduction and must include a caption. Drawings should include all relevant details and should be drawn professionally in black ink on plain white drawing paper. In addition to a hard copy of the artwork, it is necessary to attach the electronic file of the artwork (preferably in PCX format).

(4) References. References should be listed alphabetically and numbered, typed and punctuated according to the following examples. Each entry must be cited in the text in form of author(s) together with the number of the referred article or in the form of the number of the referred article alone.

Journal: [1] Poincare, H. Title of the article. *Title of the Journal* Vol. 1 (No.1), Year, Pages. [Language]

Book: [2] Liapunov, A.M. *Title of the book*. Name of the Publishers, Town, Year.

Proceeding: [3] Bellman, R. Title of the article. In: *Title of the book*. (Eds.). Name of the Publishers, Town, Year, Pages. [Language]

(5) Proofs and Sample Copy. Proofs sent to authors should be returned to the Editorial Office with corrections within three days after receipt. The corresponding author will receive a sample copy of the issue of the Journal for which his/her paper is published.

(6) Editorial Policy. Every submission will undergo a stringent peer review process. An editor will be assigned to handle the review process of the paper. He/she will secure at least two reviewers' reports. The decision on acceptance, rejection or acceptance subject to revision will be made based on these reviewers' reports and the editor's own reading of the paper.

NONLINEAR DYNAMICS AND SYSTEMS THEORY

An International Journal of Research and Surveys
Published by InforMath Publishing Group since 2001

Volume 15

Number 1

2015

CONTENTS

Preface to the Special Issue: Experimental Approaches in Dynamical Analysis and Control of Mechanical Systems	1
Coupled Fractal Nanosystem: Trap – Quasi-two-dimensional Structure . 4 <i>O.P. Abramova and S.V. Abramov</i>	
Differential Equations of Controlled Pneumatic Actuators for 6-DOF Stewart Platform	14
<i>B. Andrievsky, D.V. Kazunin, D.M. Kostygova, et al</i>	
The Duffing–Van der Pol Equation: Metamorphoses of Resonance Curves	25
<i>J. Kyzioł and A. Okniński</i>	
Analytical and Experimental Investigation of Vertical Vibration of a Freight Wagon in the Presence of Mechanical Asymmetry	32
<i>F.N. Nangolo, J. Soukup, A. Petrenko and J. Skocilas</i>	
Researches Defining the Characteristics of Hyperelastic and Composite Materials with Gas Phase in the Vehicle–Pedestrian System	43
<i>J. Osinski and P. Rumianek</i>	
Mathematical Modeling of the Hydro-Mechanical Fluid Flow System on the Basis of the Human Circulatory System	50
<i>W. Parandyk, D. Lewandowski and J. Awrejcewicz</i>	
Six-Legged Robot Gait Analysis	63
<i>B. Stańczyk and J. Awrejcewicz</i>	
Constrained Motion of Mechanical Systems and Tracking Control of Nonlinear Systems: Connections and Closed-form Results	73
<i>Firdaus E. Udvardia and Harshavardhan Mylapilli</i>	
Transcritical-like Bifurcation in a Model of a Bioreactor	90
<i>J. Villa, G. Olivar and F. Angulo</i>	
Cooperation of One and Multi-Joint Muscles	99
<i>B. Zagrodny and J. Awrejcewicz</i>	

Founded by A.A. Martynyuk in 2001.

Registered in Ukraine Number: KB 5267 / 04.07.2001.

NONLINEAR DYNAMICS AND SYSTEMS THEORY

An International Journal of Research and Surveys

Impact Factor from SCOPUS for 2013: SNIP – 1.108, IPP – 0.809, SJR – 0.496

Nonlinear Dynamics and Systems Theory (ISSN 1562–8353 (Print), ISSN 1813–7385 (Online)) is an international journal published under the auspices of the S.P. Timoshenko Institute of Mechanics of National Academy of Sciences of Ukraine and Curtin University of Technology (Perth, Australia). It aims to publish high quality original scientific papers and surveys in areas of nonlinear dynamics and systems theory and their real world applications.

AIMS AND SCOPE

Nonlinear Dynamics and Systems Theory is a multidisciplinary journal. It publishes papers focusing on proofs of important theorems as well as papers presenting new ideas and new theory, conjectures, numerical algorithms and physical experiments in areas related to nonlinear dynamics and systems theory. Papers that deal with theoretical aspects of nonlinear dynamics and/or systems theory should contain significant mathematical results with an indication of their possible applications. Papers that emphasize applications should contain new mathematical models of real world phenomena and/or description of engineering problems. They should include rigorous analysis of data used and results obtained. Papers that integrate and interrelate ideas and methods of nonlinear dynamics and systems theory will be particularly welcomed. This journal and the individual contributions published therein are protected under the copyright by International InforMath Publishing Group.

PUBLICATION AND SUBSCRIPTION INFORMATION

Nonlinear Dynamics and Systems Theory will have 4 issues in 2015, printed in hard copy (ISSN 1562–8353) and available online (ISSN 1813–7385), by InforMath Publishing Group, Nesterov str., 3, Institute of Mechanics, Kiev, MSP 680, Ukraine, 03057. Subscription prices are available upon request from the Publisher (<mailto:anmart@stability.kiev.ua>), EBSCO Information Services (<mailto:journals@ebSCO.com>), or website of the Journal: <http://e-ndst.kiev.ua>. Subscriptions are accepted on a calendar year basis. Issues are sent by airmail to all countries of the world. Claims for missing issues should be made within six months of the date of dispatch.

ABSTRACTING AND INDEXING SERVICES

Papers published in this journal are indexed or abstracted in: Mathematical Reviews / MathSciNet, Zentralblatt MATH / Mathematics Abstracts, PASCAL database (INIST–CNRS) and SCOPUS.



Special Issue
Experimental Approaches in Dynamical Analysis and
Control of Mechanical Systems

Preface

Identification of system parameters is usually a very troublesome problem. It encloses a multidisciplinary approaches ranging from systems theory, methods of nonlinear dynamics, the measurement signal treatment, the experimental engineering procedures, and many other. The more the system of analysis is complicated, which is often related to its multi-dimensional modeling, the more laborious its parameters are possible to estimate. Usually, a dynamical process subject to one of the above itemized approaches behaves unpredictably, and may be identified only partially. Therefore, the Special Issue extends selected papers presented during the international conference on *Dynamical Systems – Theory and Applications* held on December 2-5, 2013 in Lodz, Poland. Main areas of modern experimental and numerical analysis taken into consideration by authors of these papers could be mentioned: bifurcations and chaos in dynamical systems, stability of dynamical systems, original numerical methods of vibration analysis, non-smooth systems, engineering systems and differential equations, control in dynamical systems, asymptotic methods in nonlinear dynamics, vibrations of lumped and continuous systems, dynamics in life sciences and bioengineering. In particular, the following areas of nonlinear dynamics and systems theory with respect to the Mathematics Subjects Classification are covered: stability, nonlinear resonances, bifurcations and instability, general systems, mathematical modeling (models of systems, model-matching), system identification, control systems and adaptive control. A brief description of contents of this Special Issue follows.

The theory of fractional calculus and the concept of fractals is studied by Abramova and Abramov. Various types of fractal nanotraps based on quasi-two-dimensional fractal structures are obtained by the method of sections. It is shown that the behavior of the deformation field for the coupled state of the fractal nano-system is essentially different from the deformation field for the uncoupled state. It is proposed to use fractal nanotraps for trapping individual particles or groups of particles in order to study their physical properties. Stanczyk and Awrejcewicz present results of investigations of real six-legged robot called hexapod. Due to specific construction of legs having three degrees-of-freedom, a prototype allows to model gait of reptiles and insects. Applied mathematical model yields identification of the angular velocity, acceleration and moments generated by each of the robot cells, separately. As a result it is possible to determine quality coefficients of different gait patterns of the robot, i.e. maximal speed or maximal load depending on the number of moving legs. Obtained results are confronted with a theoretical model of differential equations regulating gait of the hexapod.

A study by Osinski and Rumianek is carried out to develop the methods of describing some properties of investigated materials. The knowledge of basic materials and gas pressure formed during foaming using the theory of hyperplastic materials, and in particular, Ogden's model and its modifications is extended. The aim also goes on to analyze the possibility of energy dissipation between a pedestrian and a vehicle on impact. The energy created during the impact is dissipated by the element of protection made of a hyperdeformable material. The presented methods and applications of the characteristics of hyper elastic materials and composites with the gas phase are used to determine the proper selection of material properties, increasing the opportunities for a proper assessment of the effectiveness of safety devices.

Kyziol and Okninski study dynamics of the Duffing - Van der Pol driven oscillator. Periodic steady-state solutions of the corresponding equation are determined within the Krylov-Bogoliubov-Mitropolsky approach to yield dependence of amplitude on forcing frequency as an implicit function, referred to as resonance curve or amplitude profile. Equations for singular points of resonance curves are solved exactly. Authors investigate metamorphoses of the computed amplitude profiles induced by changes of control parameters near singular points of these curves since qualitative changes of dynamics occur in neighborhoods of singular points. More exactly, conditions for birth of resonances as well as for attractor crises are found. Bifurcation diagrams are estimated to show good agreement with the predictions of theoretical analysis.

An analysis of equations describing single and multi-joint muscles cooperation during movement of limb segments is presented by Zagrodny and Awrejcewicz. The Pareto-optimum problem is considered for the human upper limb in a case of movement in the sagittal plane. Uncertainty of this problem and some additional physiological restrictions are described. Moreover, effects of practical verification based on the video analysis of the volunteer's arm movement and its lack of reproducibility is addressed. Examination of the artificial arm prototype shows similar behavior to the human biological musculo-skeletal system.

Production and construction asymmetry of railway vehicles in the presence of multiple track irregularities on the rail influences the time flow of the wheel. It has an influence on wheel and rail wear defects, especially on driving safety. Production and construction asymmetry is found during the experimental investigation of the basic parameters of mechanical properties of a double-axel freight wagon of Smmps type. The contribution by Nangulo et al. introduces a methodology of analytical solution of the influence of production and construction asymmetry on the vertical dynamic response of a double-axel freight wagon in the presence of multiple track irregularities. Measured field data are used to validate the model.

A non-standard bifurcation, similar to a transcritical one, in a model of a bioreactor is detected by Villa et al. This happens in a periodically-forced system with restrictions on the state space. The bioreactor is periodically fed with substrate. In the mathematical model, a periodic orbit approaches (without hitting) the restriction surface as a bifurcation parameter is varied. The way the orbit approaches the switching surface in the three-dimensional state space is such that it becomes parallel to the restriction surface. This phenomenon is somehow analogous to a transcritical bifurcation, which is described, since another periodic orbit exists inside the restriction surface, but they do not collide.

The objective of the study carried out by Parandyk et al. is to examine a human/mammal circulatory system. Considering structures and operating rules of a nat-

ural, biological circulatory system it can be easily stated that it is possible to create an analogous hydromechanical dynamic system. Noting the similarities and taking into account blood and vessels features there is mathematical model given that include differential equations of the fluid mechanics. Additionally a stand/analog consisted of hydraulic and electronics elements is presented. A prototype of the circulatory system is proposed with a construction of the heart as a bicapsular pumping unit powered by external pneumatic system. Solving the equations describing biological system, it gives opportunities to examine some external and internal risk factors, model input signals and activity under different conditions.

Udwadia and Mylapilli expose the connections between the determination of the equations of motion of constrained systems and the problem of tracking control of nonlinear mechanical systems. The new duality between the imposition of constraints on a mechanical system and the trajectory requirements for tracking control is exposed through the use of a simple example. It is shown that given a set of constraints, d'Alembert's principle corresponds to the problem of finding the optimal tracking control of a mechanical system for a specific control cost function that Nature seems to choose. The way Nature seems to handle the tracking control problem of highly nonlinear systems suggests ways in which authors are able to develop new control methods that do not make any approximations and/or linearizations related to the nonlinear system dynamics. More general control costs are used and Nature's approach is thereby extended to general control problems.

Finally, it should be emphasized that the selected papers are mainly oriented toward modeling and identification of mechanical systems. They have been reviewed to satisfy the journal's standards.

In addition, J. Awrejcewicz, a Guest Editor of this Special Issue, greatly appreciates a kind invitation of Professor A.A. Martynyuk to publish the recommended papers. Furthermore, a professional help of the NDST's staff in the final production process is acknowledged.

Guest Editor:

Jan Awrejcewicz,

Lodz University of Technology, Department of Automation, Biomechanics and Mechatronics, 1/15 Stefanowski Str., 90-924 Lodz, Poland

and

Institute of Vehicles, Warsaw University of Technology, 84 Narbutta st., 02-524, Warsaw, Poland;

`mailto:jan.awrejcewicz@p.lodz.pl`



Coupled Fractal Nanosystem: Trap – Quasi-two-dimensional Structure

O.P. Abramova* and S.V. Abramov

Donetsk National University, 24 University st., Donetsk, 83001, Ukraine

Received: March 31, 2014; Revised: December 17, 2014

Abstract: For a model nanosystem various types of quasi-two-dimensional fractal structures are obtained. To this end the theory of fractional calculus and the concept of fractal are used. Various types of fractal nanotraps based on quasi-two-dimensional fractal structures are obtained by the method of sections. It is shown that the behavior of the deformation field for the coupled state of the fractal nanosystem is essentially different from the behavior of the deformation field for the uncoupled state. It is proposed to use fractal nanotraps for trapping individual particles or groups of particles in order to study their physical properties.

Keywords: *quasi-two-dimensional fractal structures; fractional calculus; nanosystem; nanotraps; numerical modeling.*

Mathematics Subject Classification (2010): 93A10, 93A30.

1 Introduction

Investigating the fundamental properties of nanosystems and nanomaterials of a new generation [9–11, 14] is actual for the modern areas of nanotechnology, structural and nonlinear mechanics [8]. The active nanostructural elements in real nanomaterials are clusters, pores, quantum dots, wells, two-dimensional quantum billiards (quantum corals) [17]. These elements can find their application in quantum information science, nanomechanics, quantum optics, and for the quantum computers, molecular spin memory devices [14]. The theoretical description of the chaotic states in the structural mechanics, analysis of nonlinear dynamical models of attractors and the chaotic simulation are discussed in the books [8, 16–18].

Quasi-two-dimensional fractal structures such as fractal linear, elliptic and hyperbolic dislocations, fractal quantum dots (particles or groups of particles) [3–6] may occur in

* Corresponding author: <mailto:oabramova@ua.fm>

model nanosystems. The location of the singular points (attractors) of the deformation field in the core of fractal structures is typical for linear dislocation, real ellipse, hyperbola or an imaginary ellipse. In the general case the behavior of the deformation field near these singular points is stochastic and has unusual quantum statistical properties [3–6], there is the presence of quantum chaos [17].

For theoretical description of fractal objects it is proposed to use the theory of fractional calculus [15], the Hamilton operators [1, 2] and the concept of fractal [12]. For experimental investigations of physical properties of individual atoms (electrons, photons) and quantum measurement it is needed to create special traps: nanosystems are represented by a trapped particle (or a group of particles) in the trap. W. Paul [13] considered the electromagnetic traps for charged and neutral particles (having a dipole moment). In [17] the traps (quantum corrals) constructed experimentally from individual atoms (molecules) are considered. Physical properties of the particles placed in such traps qualitatively differ from those of free particles. If we have single atom in the trap, it is possible to observe the interaction of the atom with the radiation field and the statistical behavior of a single atom in a pure form. Using the variety of external actions (acoustic, electromagnetic, mechanical excitation, laser cooling, etc.), we can change the state of the atoms in the trap [11, 14, 17]. In papers [9, 10] the experimental methods that made it possible to measure and govern individual quantum systems are proposed.

The purpose of this paper is to investigate the possibility of constructing fractal nanotraps based on quasi-two-dimensional fractal structures and governing the behavior of coupled systems: fractal trap – fractal structure.

2 Fractal Structures and Fractal Traps

We consider a model nanosystem [3–6]: volumetric discrete lattice $N_1 \times N_2 \times N_3$, whose nodes are given by integers n, m, j , ($n = \overline{1, N_1}$; $m = \overline{1, N_2}$; $j = \overline{1, N_3}$). The dimensionless variable displacement u of lattice nodes in a fractal trap is described by analogy with [3–6], but with a changed value Q

$$u = (1 - \alpha)(1 - 2sn^2(u - u_0, k))/Q. \quad (1)$$

Here α is the fractal dimension of the deformation field u along the Oz -axis ($\alpha \in [0, 1]$); u_0 is the constant (critical) displacement; k is the modulus of the elliptic sine.

The changed value Q considers both the interaction of the nodes in the main plane of rectangular discrete lattice and the interplanar interactions by an angular parameter $\varphi(j)$. This allows to fulfill a stochastic (due to changes in the internal parameters, the process of self-organization) governing of the alteration of these structures. The initial expression for Q in the coordinate system nOm has the form

$$Q = p'_0 + q_1 + q_2; \quad q_1 = p'_1 n + p'_2 m; \quad q_2 = -(p_{11} n^2 - 2p_{12} nm + p_{22} m^2). \quad (2)$$

Here the functions q_1, q_2 are linear quadratic forms with respect to the independent variables n, m . The expression (2) has six parameters. The parameter p'_0 is independent of the variables n, m ; parameters p'_1, p'_2 are included in the linear form; parameters p_{11}, p_{12}, p_{22} determine the behavior of the quadratic form.

The rotation operation of the coordinate axes by angle $\varphi > 0$ is used to go from the coordinate system nOm to the coordinate system $n'Om'$ according to the formulas

$$n' = n \cos \varphi - m \sin \varphi; \quad m' = n \sin \varphi + m \cos \varphi. \quad (3)$$

Doing the operation of parallel translation of the coordinate system we obtain an expression for Q

$$Q = p_0 - b_1(n' - n_0)^2/n_c^2 - b_2(m' - m_0)^2/m_c^2. \quad (4)$$

Here, the previous parameters are related with the new parameters by expressions

$$\begin{aligned} p'_0 &= p_0 - b_1 n_0^2/n_c^2 - b_2 m_0^2/m_c^2; & p'_1 &= 2n_0 b_1 \cos \varphi/n_c^2 + 2m_0 b_2 \sin \varphi/m_c^2; \\ p'_2 &= 2m_0 b_2 \cos \varphi/m_c^2 - 2n_0 b_1 \sin \varphi/n_c^2; & p_{11} &= b_1 \cos^2 \varphi/n_c^2 + b_2 \sin^2 \varphi/m_c^2; \\ p_{22} &= b_1 \sin^2 \varphi/n_c^2 + b_2 \cos^2 \varphi/m_c^2; & p_{12} &= (b_1/n_c^2 - b_2/m_c^2) \sin \varphi \cos \varphi. \end{aligned} \quad (5)$$

Parameters $(n'_c)^2 = p_0 n_c^2/b_1$, $(m'_c)^2 = p_0 m_c^2/b_2$ play the role of semi-axes of quasi-two-dimensional structures of the type of elliptical or hyperbolic dislocation in a coordinate system $n'Om'$. To classify the type of fractal structures, we introduce a row-vector $b = (b_1, b_2, p_0)$.

When $b = b_{11} = (1, 1, p_{01})$, $p_{01} > 0$ a fractal elliptical dislocation at state 1 (ED1) is obtained. When $b = b_{12} = (-1, -1, -p_{01})$ a fractal elliptical dislocation in state 2 (ED2) is obtained.

For fractal hyperbolic dislocation we have four states HD1, HD2, HD3, HD4 with $b = b_{21} = (1, -1, p_{02})$, $b = b_{22} = (1, -1, -p_{02})$, $b = b_{23} = (-1, 1, p_{02})$, $b = b_{24} = (-1, 1, -p_{02})$, respectively, where $p_{02} > 0$.

The fractal quantum dot in the two states QD1, QD2 is obtained at $b = b_{31} = (1, 1, -p_{03})$, $b = b_{32} = (-1, -1, p_{03})$, respectively, where $p_{03} > 0$.

The set of fractal quantum dots (the imaginary line dislocations) can be in four states SQD1, SQD2, SQD3, SQD4 with $b = b_{41} = (1, 0, -p_{04})$, $b = b_{42} = (0, 1, -p_{04})$, $b = b_{43} = (-1, 0, p_{04})$, $b = b_{44} = (0, -1, p_{04})$, respectively, where $p_{04} > 0$.

Fractal linear split dislocation can be in four states LSD1, LSD2, LSD3, LSD4 with $b = b_{51} = (1, 0, p_{05})$, $b = b_{52} = (0, 1, p_{05})$, $b = b_{53} = (-1, 0, -p_{05})$, $b = b_{54} = (0, -1, -p_{05})$, respectively, where $p_{05} > 0$.

The stochastic state of the whole lattice can be realized in two states SSL1, SSL2 with $b = b_{61} = (0, 0, p_{06})$, $b = b_{62} = (0, 0, -p_{06})$, respectively, where $p_{06} > 0$.

The initial fractal quasi-two-dimensional structures are obtained by using the iterative method to solve the equation (1) with Q in the form (2) for the angular parameter $\varphi = 0$, for the values of other constant parameters $\alpha = 0.5$, $k = 0.5$, $u_0 = 29.537$, $n_0 = 14.3267$, $n_c = 9.4793$, $m_0 = 19.1471$, $m_c = 14.7295$, $N_1 = 30$, $N_2 = 40$.

Using the method of sections of original fractal structures (Fig. 1) other sectioned fractal structures (Fig. 2) can be obtained. The original structures are shown in Fig. 1: structure SSL1 for parameter $p_{06} = 0.1523$ (Fig. 1 (a)); structure ED1 for parameter $p_{01} = 1.0123$ (Fig. 1 (b)); structure QD2 for parameter $p_{03} = -3.457 \cdot 10^{-11}$ (Fig. 1 (c)).

Sectioned fractal structures can be used as fractal traps for trapping or capturing other fractal quasi-two-dimensional structures (particles or groups of particles) in order to investigate their physical properties. The deformation field of fractal traps is essentially stochastic both in the area core and inside the fractal structure (Figs. 1, 2). The state of fractal trap at the transition from one node plane to another ($j = \overline{1, N_3}$) can be changed by using the parameter $\varphi(j)$. Sectioned fractal traps (Fig. 2) allow to obtain porous traps: the pores can be on the boundary nodal planes and inside the bulk nanosystem.

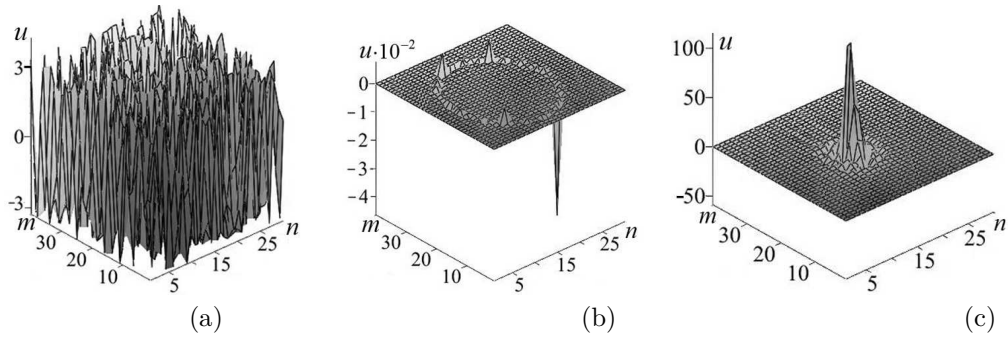


Figure 1: The behavior of the functions u of the original fractal structures on n, m for $\varphi = 0$: SSL1, $p_{06} = 0.1523$ (a); ED1, $p_{01} = 1.0123$ (b); QD1, $p_{03} = -3.457 \cdot 10^{-11}$ (c).

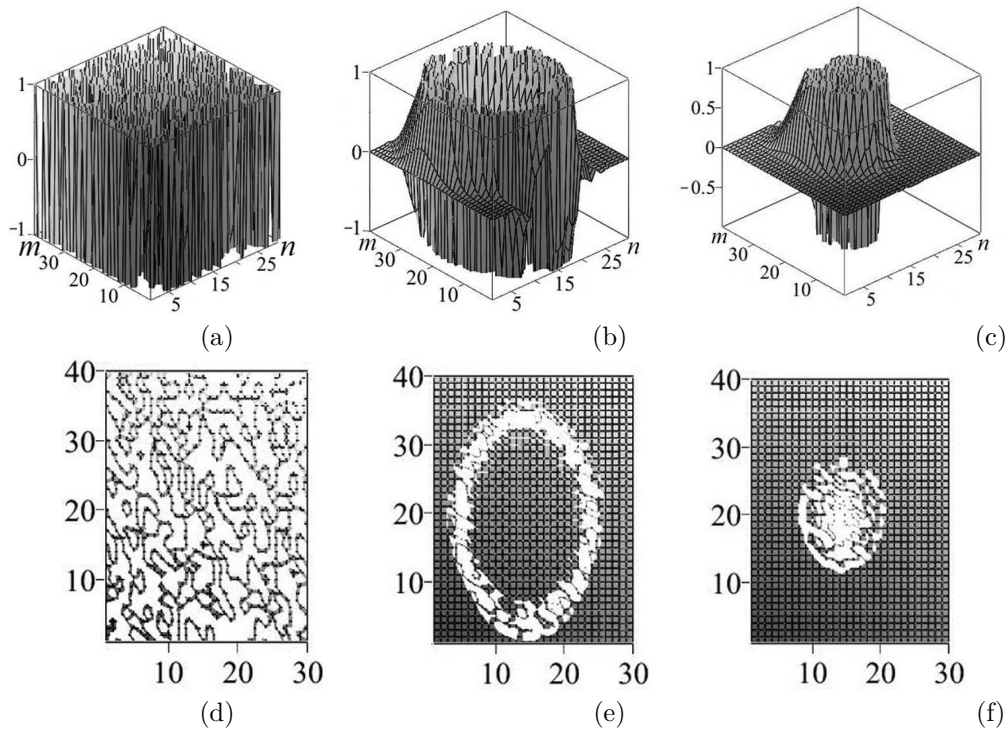


Figure 2: The behavior of the functions u of sectioned structures (a, b, c) and their cuts (d, e, f) $u \in [-1, 1]$ (top view) on n, m for $\varphi = 0$: SSL1 (a, d); ED1 (b, e); QD1 (c, f).

3 Coupled Systems: Fractal Trap - Fractal Structure

We investigate the state of the system: the fractal trap – fractal structure (Figs. 3, 4). The state of such a system is significantly different depending on the choice of the type of the iteration process when solving the basic non-linear equations.

As fractal traps the fractal structures SSL1 (Fig. 1 (a)), ED1 (Fig. 1 (b)) are used. As fractal structures the structures QD1 (Fig. 1 (c)); SQD1 with $p_{04} = 3.457 \cdot 10^{-11}$ are chosen.

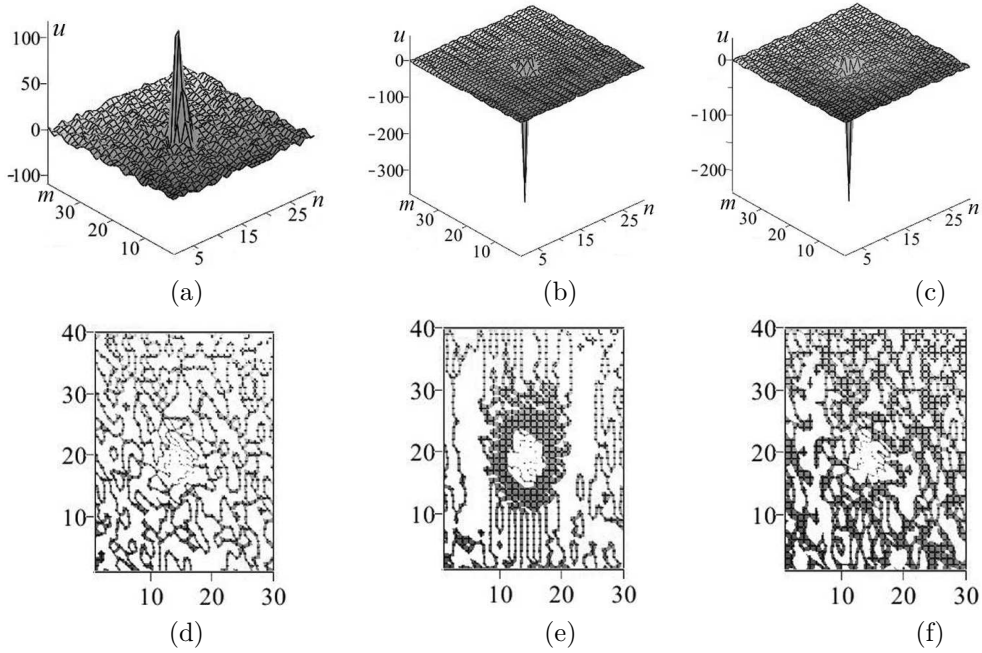


Figure 3: The behavior of u of structure SSL1-QD1 (a, b, c) and cuts (d, e, f) $u \in [-1, 1]$ on n, m for $\varphi = 0$: uncoupled state A (a, d); coupled state B (b, e); deviation δ (c, f).

We investigate the states of the following systems: SSL1-QD1; ED1-QD1; SSL1-SQD1; ED1-SQD1. Independent displacement functions for trap u_1 and structure u_2 are determined by using the iteration method with its values Q_1 and Q_2 structures for selected higher structures by the solution of independent nonlinear equations, respectively

$$u_1 = (1 - \alpha)(1 - 2sn^2(u_1 - u_0, k))/Q_1; \quad (6)$$

$$u_2 = (1 - \alpha)(1 - 2sn^2(u_2 - u_0, k))/Q_2. \quad (7)$$

In this case, the displacement function of the system is given by $u_A = u_1 + u_2$ (uncoupled state A). For the coupled system the nonlinear equation for the displacement function u (coupled state B) is given in the form

$$u = (1 - \alpha)(1 - 2sn^2(u - u_0, k))/Q_1 + (1 - \alpha)(1 - 2sn^2(u - u_0, k))/Q_2; \quad u_B = u. \quad (8)$$

The deviation of the displacement system (state B from state A) is described by the function

$$\delta = (u_B - u_A)/2. \quad (9)$$

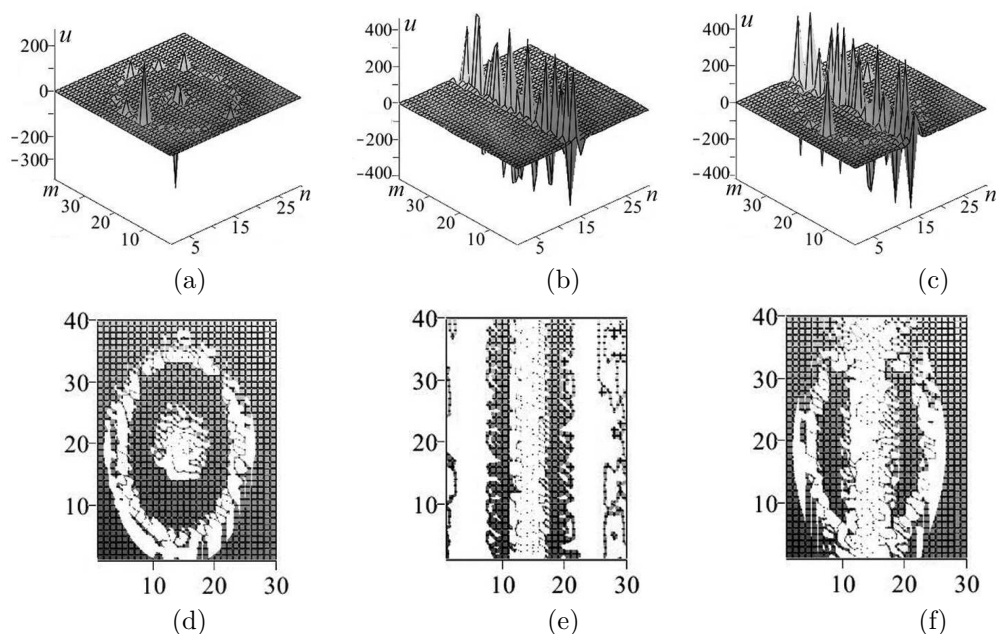


Figure 4: The behavior of the functions u of structures ED1-QD1 (a); SSL1-SQD1 (b); ED1-SQD1 (c) and cuts (d, e, f) $u \in [-1, 1]$ (top view) on n, m for $\varphi = 0$ in state B.

The fractal trap SSL1 (Fig. 1 (a)) and the fractal structure QD1 (Fig. 1 (c)) are selected to investigate the displacement function u of system SSL1-QD1 (Fig. 3). For the uncoupled state A (Figs. 3 (a, d)) the behavior of the displacement function is significantly different from that of the displacement function for the coupled state B (Figs. 3 (b, e)). This changes the direction and the amplitude of the main peak and the behavior of the deformation field in the whole area $N_1 \times N_2$ of the nodal plane of the lattice. The dependency of the deviation δ for these states from n, m is given in Figs. 3 (c, f). Some other types of coupled structures (in state B) are shown in Fig. 4.

For these structures the behavior of the displacement functions for coupled state B is also essentially different from that of the displacement function for the uncoupled state A. In this case, the fractal structure QD1 can play the role of a single particle, and the fractal structure SQD1 - the role set of particles.

4 The Influence of Translation and Rotation on the State of the Coupled System

We investigate the influence of the angular parameters $\varphi = \varphi_{61}$ (for the traps SSL1), and $\varphi = \varphi_{31}$ (for the fractal structure QD1) on the state of the coupled system SSL1-QD1.

The initial state of this coupled system for $\varphi_{61} = 0$ and $\varphi_{31} = 0$ is given in Figs. 3 (b, e). Fractal trap SSL1 remains in the initial state with $\varphi = \varphi_{61} = 0$, then from (2), (5) for Q_1 we obtain

$$Q_1 = p_{06}; \quad p'_0 = p_{06}; \quad p'_1 = p'_2 = p_{11} = p_{22} = p_{12} = 0. \quad (10)$$

For the structure QD1 being captured at $\varphi = \varphi_{31} \neq 0$ from (2), (5) we find the expression for Q_2

$$Q_2 = p'_0 + p'_1 n + p'_2 m - p_{11} n^2 + 2p_{12} nm - p_{22} m^2; \quad (11)$$

$$\begin{aligned} p'_0 &= -p_{03} - n_0^2/n_c^2 - m_0^2/m_c^2; & p'_1 &= 2n_0 \cos \varphi_{31}/n_c^2 + 2m_0 \sin \varphi_{31}/m_c^2; \\ p'_2 &= 2m_0 \cos \varphi_{31}/m_c^2 - 2n_0 \sin \varphi_{31}/n_c^2; & p_{11} &= \cos^2 \varphi_{31}/n_c^2 + \sin^2 \varphi_{31}/m_c^2; \\ p_{22} &= \sin^2 \varphi_{31}/n_c^2 + \cos^2 \varphi_{31}/m_c^2; & p_{12} &= (1/n_c^2 - 1/m_c^2) \sin \varphi_{31} \cos \varphi_{31}. \end{aligned} \quad (12)$$

The displacement function $u_B = u$ of the coupled system SSL1-QD1 (Fig. 5) is determined when solving the nonlinear equation (8) with the values for Q_1 from (10) and Q_2 from (11)-(12) for the angular parameter $\varphi_{31} = \pi/8$ (right polarization) and $\varphi_{31} = -\pi/8$ (left polarization).

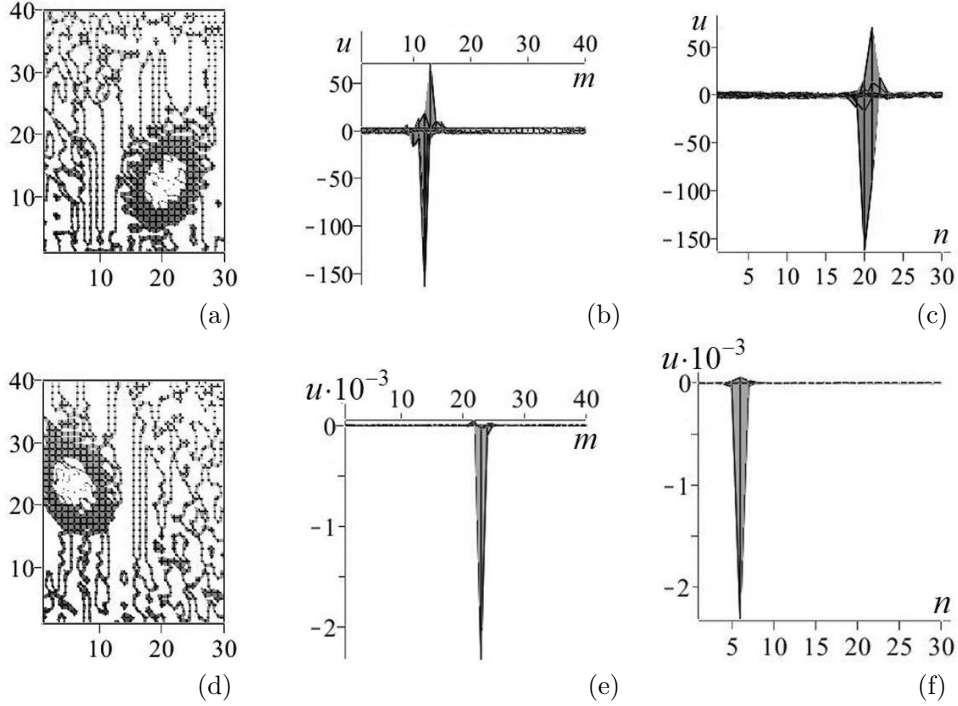


Figure 5: Dependencies of cuts $u \in [-1, 1]$ (a, d) and projections (b, c, e, f) of u on φ_{31} for structure SSL1-QD1 (state B): $\varphi_{31} = \pi/8$ (a, b, c); $\varphi_{31} = -\pi/8$ (d, e, f).

The projections of the displacement function on the planes mOu (Fig. 5 (b, e)), nOu (Fig. 5 (c, f)) allow us to determine the coordinates of the main peak. We introduce the state vector $M = (m, n, u)$. Then for the peak down with right polarization $M = M_1 = (12, 20, -160)$ are found. Then for the peak down with left polarization $M = M_2 = (23, 6, -2300)$ are found. The state vector $M = M_0 = (19, 14, -360)$ of the peak down with $\varphi_{31} = 0$ is found from Fig. 3 (b). We investigate the influence of the angular parameters $\varphi = \varphi_{11}$ (for the trap ED1) and $\varphi = \varphi_{31}$ (for the fractal structure QD1) on the state of the coupled system ED1-QD1.

The initial state of this coupled system for $\varphi_{11} = 0$ and $\varphi_{31} = 0$ is given in Fig. 4 (a, d). Fractal trap ED1 remains in the initial state with $\varphi = \varphi_{11} = 0$, then from (2), (5) for Q_1 we obtain

$$Q_1 = p'_0 + p'_1 n + p'_2 m - p_{11} n^2 + 2p_{12} nm - p_{22} m^2; \quad p'_0 = p_{01} - n_0^2/n_c^2 - m_0^2/m_c^2; \quad (13)$$

$$p'_1 = 2n_0/n_c^2; \quad p'_2 = 2m_0/m_c^2; \quad p_{11} = 1/n_c^2; \quad p_{22} = 1/m_c^2; \quad p_{12} = 0. \quad (14)$$

For the captured structure QD1 at $\varphi = \varphi_{31} \neq 0$ the expressions for Q_2 (11) - (12) are used. The displacement function $u_B = u$ of the coupled system ED1-QD1 (Fig. 6) is determined when solving the nonlinear equation (8) with the values for Q_1 from (13)-(14) and Q_2 from (11)-(12) for the angular parameter $\varphi_{31} = \pi/8$ (right polarization) and $\varphi_{31} = -\pi/8$ (left polarization).

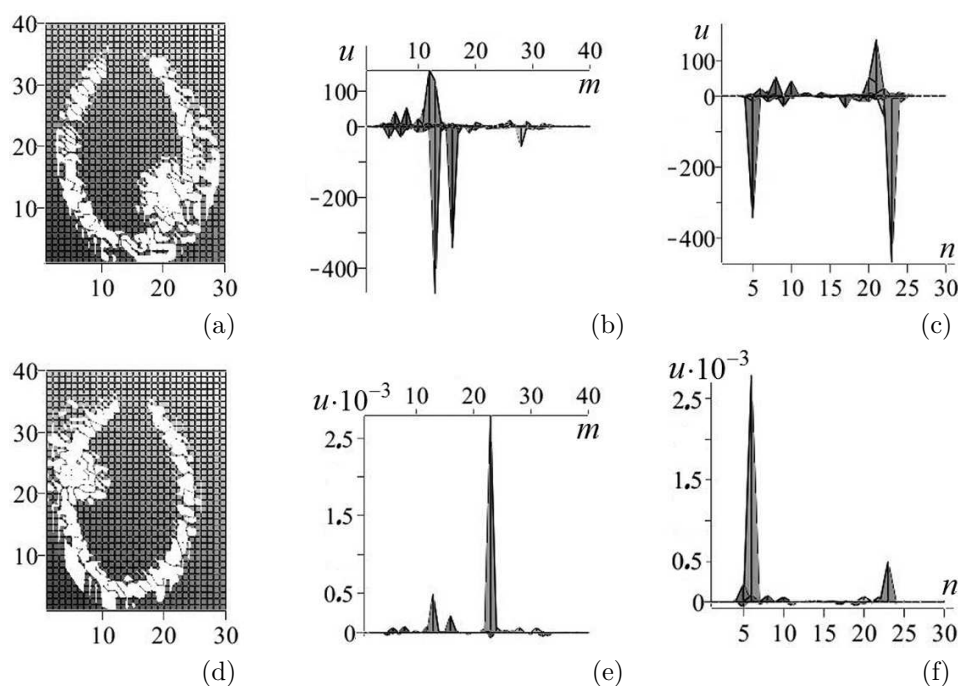


Figure 6: Dependencies of cuts $u \in [-1, 1]$ (a, d) and projections (b, c, e, f) of u on φ_{31} for structure ED1-QD1 (state B): $\varphi_{31} = \pi/8$ (a, b, c); $\varphi_{31} = -\pi/8$ (d, e, f).

The projections of the displacement function on the planes mOu (Fig. 6 (b, e)), nOu (Fig. 6 (c, f)) allow us to determine the coordinates of the main peak. For the main peak down with right polarization $M = M_1 = (13, 23, -440)$ are found. For the peak up with left polarization $M = M_2 = (23, 6, 2800)$ are found. The state vector $M = M_0 = (19, 14, -400)$ of the main peak down with $\varphi_{31} = 0$ is found from Fig. 4 (a).

Changing the angle parameter $\varphi = \varphi_{31}$ for the fractal structure QD1, captured by fractal traps SSL1 with $\varphi_{61} = 0$ or ED1 with $\varphi_{11} = 0$ leads to essential changes of the deformation field, location, amplitudes of the main peaks and the effect of the reorientation of the main peaks of the coupled systems SSL1-QD1 or ED1-QD1.

It is also possible to carry out operations of translation and rotation of the fractal traps only (by changing the angular parameter φ of the trap), leaving a fixed capturing fractal structure or to carry out operations of translation and rotation jointly (both for traps and structures). This offers additional possibilities to govern the coupled systems: fractal trap – fractal structure.

5 Conclusions

The possibility of creating fractal nanotraps based on quasi-two-dimensional fractal structures is shown. By using the method of sections sectioned fractal traps are obtained. The deformation field of fractal traps is essentially stochastic. Sectioned fractal traps allow to obtain porous traps: the pores can be both on the boundary nodal planes and inside the bulk nanosystems. It is proposed to use fractal traps to capture the fractal structures in order to investigate their physical properties in a trap, and also the behavior of the coupled system: fractal trap - fractal structure. It is shown that the behavior of the deformation field for the coupled state of the system (fractal trap – fractal structure) is essentially different from the behaviour of the deformation field for the uncoupled state. By varying the angular parameters it is possible to govern both the states of a separate trap and a captured structure and the state of the whole coupled system.

Acknowledgement

The materials of this work were presented at the 12th Conference on Dynamical Systems Theory and Applications (DSTA 2013) in Poland, Lodz, December 2-5, 2013 [7].

References

- [1] Abramov, V.S. Fractal dislocation as one of non-classical structural objects in the nano-dimensional systems. *Metallofiz. i Noveishie Tekhnologii* **33**(2) (2011) 247–251.
- [2] Abramov, V.S. Behavior of a soft mode type for inverse structural states of fractal dislocation in the model nanosystem. In: *Topical problems of deformable solid mechanics*. The Proc. of VII Int. Scientific. Conf. Melekino, Vol. 1, June 11–14, Ukraine. Donetsk: DonNU, P. 13–17, 2013.
- [3] Abramova, O.P. and Abramov, S.V. Alteration of the deformation field of fractal quasi-two-dimensional structures in nanosystems. In: *Physical and mathematical modeling of systems*. Materials IX Intern. Seminar, November 30 - December 1, Voronezh, Russia, Part 1, P. 3–10, 2012.
- [4] Abramova, O.P. and Abramov, S.V. Features of behaviour of the deformation field of fractal quasi-two-dimensional structures. *Bul. of Donetsk Nat. Univers. Ser. A* (1) (2013) 9–17.
- [5] Abramova, O.P. and Abramov, S.V. Governance of alteration of the deformation field of fractal quasi-two-dimensional structures in nanosystems. In: *Abstracts of the 6th Chaotic Modeling and Simulation International Conference*. Istanbul, Yeditepe Univers. Turkey, 11-14 June, (Christos H. Skiadas, ed.) P. 11–12, 2013.
- [6] Abramova, O.P. and Abramov, S.V. Structural transitions of fractal quasi-two-dimensional deformation fields in nanosystems. In: *Topical problems of deformable solid mechanics*. The Proc. of VII Int. Scientific. Conf. Melekino, June 11-14, Vol. 1, Ukraine, Donetsk: DonNU, P. 18–22, 2013.

- [7] Abramova, O.P. and Abramov, S.V. Fractal nanotraps based on quasi-two-dimensional fractal structures. In: *Dynamical Systems Theory* (J. Awrejcewicz, et. al., eds.) Lodz, December 2-5, P. 71–80, Poland, 2013.
- [8] Awrejcewicz, J. and Krysko, V.A. *Chaos in Structural Mechanics*. Springer-Verlag, Berlin, Heidelberg, 2008.
- [9] Chou, C.W., Hume, D.B. Rosenband, T. and Wineland, D.J. *Optical clocks and relativity*. *Science* **329** (2010) 1630–1633.
- [10] Gleyzes, S., Kuhr, S., Guerlin, C. et al. Quantum jumps of light recording the birth and death of a photon in a cavity. *Nature* **446** (2007) 297–300.
- [11] Kahra, S., Leschhorn, G., Kowalewski, M. et al. A molecular conveyor belt by controlled delivery of single molecules into ultrashort laser pulses. *Nature Physics* **8**(3) (2012) 238–242.
- [12] Mandelbrot, B.B. *The Fractal Geometry of Nature*. Freeman, New York, 1982.
- [13] Paul, W. Electromagnetic traps for charged and neutral particles. *Rev. of Modern Physics* **62**(3) (1990) 531–543.
- [14] Raman, K.V., Kamerbeek, A.M., Mukherjee, A. et al. Interface-engineered templates for molecular spin memory devices. *Nature* **493** (7433) (2013) 509–513.
- [15] Samko, S.G., Kilbas, A. and Marichev, O. *Fractional Integrals and Derivatives. Theory and Applications*. Gordon and Breach Sci. Publ., New York, 1990.
- [16] Skiadas, C. H. and Skiadas, C. *Chaotic Modeling and Simulation: Analysis of Chaotic Models, Attractors and Forms*. Taylor and Francis/CRC, London, 2009.
- [17] Stockmann, H.-J. *Quantum Chaos. An Introduction*. Cambridge Univers. Press, 1999.
- [18] Zakrzhevsky, M.V., Smirnova, R.S., Schukin, I.T., Yevstignejev, V.Yu. et. al. *Nonlinear Dynamics and Chaos. Bifurcation Groups and Rare Attractors*. Riga, RTU, Publishing House, 2012.



Differential Equations of Controlled Pneumatic Actuators for 6-DOF Stewart Platform

B. Andrievsky^{1,2}, D.V. Kazunin^{1,3}, D.M. Kostygova³, N.V. Kuznetsov^{1,4*},
G.A. Leonov^{1,2}, P. Lobanov³, A.A. Volkov¹

¹ *St. Petersburg State University, Russia*

² *Institute for Problems of Mechanical Engineering of RAS, Russia*

³ *Transas Group, Saint Petersburg, Russia*

⁴ *University of Jyväskylä, Finland*

Received: April 6, 2014; Revised: January 27, 2015

Abstract: In the paper, the differential equations of the controlled pneumatic actuators as a part of simulator for training drivers of freight vehicles based on 6-DOF Stewart Platform are presented. The sliding-mode control strategy is proposed and studied by simulations. The experimental results for the existing on-off logical control algorithm are given, showing potential advantage of the sliding-mode controller for tracking fast reference signals.

Keywords: *Stewart platform; control; pneumatic actuator; nonlinear dynamics.*

Mathematics Subject Classification (2010): 00A06, 00A69, 00A72, 03C98, 34L30.

1 Introduction

The present paper is devoted to designing a simulator for training of freight KamAZ vehicle drivers. The simulator is currently under construction by the Transas Co. The car cab is mounted on the Gough–Stewart platform for reproducing the desired motions of the cab. The distinguish feature of the simulator is employing pneumatic servo as actuators.

Pneumatic systems are widely used in many applications, but the control of such systems poses difficult problems due to the nonlinear behavior of friction-like phenomena and great variation of the system properties associated with the system state.

During the last decades, the control/tracking problem for pneumatic actuators has been extensively studied in the literature. The authors of [1] presented results on the

* Corresponding author: <mailto:nkuznetsov239@gmail.com>

modeling and the control of a heavy pneumatic machine designed for handling logs. The paper shows that a significant improvement in performance results from modified self tuning generalized predictive control of pneumatic systems. In [2] it is demonstrated that low friction pneumatic cylinders offer real potential for the precision control systems and the self-tuning strategy is proposed to obtain correct operating parameters at the start of a session. In [2] the low-friction cylinder is compared to conventional, sealed cylinders showing the enhanced performance. An experimental comparison between six different techniques to control the position of a pneumatic actuator, such as PID control, fuzzy control, PID control with pressure feedback, fuzzy control with pressure feedback, sliding mode control and neuro-fuzzy control is given in [3]. It is stressed that the nonlinear nature of pneumatic systems together with the large uncertainty in the model parameters does not allow a realistic comparison using only mathematical models and simulations. The authors conclude that in terms of both error and complexity of design and cost, the Fuzzy logic controller with neural estimator instead of the pressure sensor has some advantages as compared with other control methods. Results of the experimental comparison of PID control and the nonlinear robust tracking control strategy for servo-controlled pneumatic systems are presented in [4], demonstrating some advantages of the proposed nonlinear controller design. A combination of a fuzzy-PID controller used to ensure tracking performance with an adaptable wavelet neuro compensator, used to compensate for the time delay resulting from the control valve is proposed in [5]. By simulation of the linear time delayed model of the pneumatic system, the authors show that the system without delay-time compensation may become unstable when the delay time exceeds 0.02 s, and that the adaptable neural network ensures performance robustness in the face of environment and physical variations. Possibility of chaotic motion in nonlinear systems is discussed in [6].

The paper is organized as follows. The car simulator based on the Stewart platform is briefly described in Section 2, where Gough–Stewart platform construction is recalled, and specifications for control system of the platform are given. The model of the pneumatic actuator is presented in Section 3. The fluid servodrive of the Transas car simulator and the control algorithms are described in Section 4. Results of the simulation and experimental study are given in Section 5. Concluding remarks and the future work intentions are presented in Section 6.

2 Freight Vehicle Simulator Based on Stewart Platform

2.1 Gough–Stewart platform

The *Stewart* (or *Gough–Stewart*) *platform* is a six-degree-of-freedom parallel manipulator. This platform being representative of the class of parallel manipulators, the concepts applicable for it have direct relevance to the entire class [7]. The Stewart platform has 6 degrees of freedom, such as:

- three spatial coordinates: x, y, z ;
- three angular coordinates: yaw ψ , pitch ϑ and roll γ .

Schematic view of the Stewart platform is shown in Fig. 1.

Dynamics of the Stewart platform, arbitrarily placed on six rods of variable length, with allowance for the inertia and weight rods is described as a special case of rigid body motion in [8,9]. The equation of motion of the center of gravity C of the loaded platform

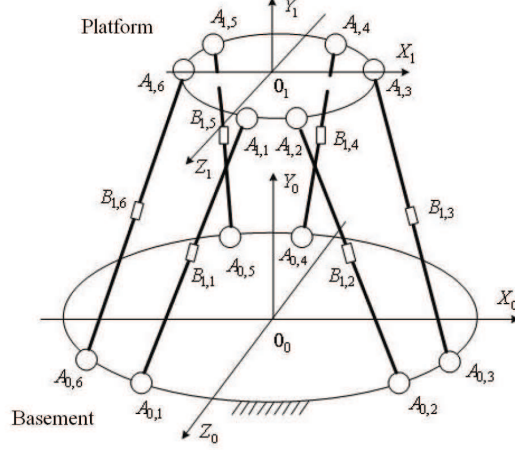


Figure 1: Schematic view of the Stewart platform.

in the fixed reference frame may be written as follows:

$$\begin{aligned} m(\ddot{\mathbf{r}}^0 + \dot{\boldsymbol{\omega}}^0 \times \mathbf{r}_c^0 + \boldsymbol{\omega}^0 \times (\boldsymbol{\omega}^0 \times \mathbf{r}_c^0)) + mg\mathbf{k}_0, \\ \mathbf{r}_c^0 = \mathbf{P} \cdot \mathbf{r}_c, \end{aligned} \quad (1)$$

where $\mathbf{F}^0 = \sum_{k=1}^6 F_k \mathbf{e}_{kt}^0$, F_k ($k = 1, \dots, 6$) are the forces, acting to the platform from the side of the pneumatic actuators, m denotes the mass of the platform with a load, g is the gravity acceleration, $\overrightarrow{OC} = \mathbf{r}_c$ is the radius vector of the center of gravity platform in the moving reference frame, $\ddot{\mathbf{r}}^0$ stands for the acceleration of point O .

The equation of moments with respect to the center of gravity C in the moving reference frame has the following form

$$\begin{aligned} J_c \cdot \dot{\boldsymbol{\omega}} + \boldsymbol{\omega} \times (J_c \cdot \boldsymbol{\omega}) = \mathbf{M}, \\ \mathbf{e}_{kt} = \mathbf{P}^T \cdot \mathbf{e}_{kt}^0, \quad \boldsymbol{\omega} = \mathbf{P}^T \cdot \boldsymbol{\omega}^0, \end{aligned} \quad (2)$$

where $\mathbf{M} = \sum_{k=1}^6 F_k (\mathbf{a}_k - \mathbf{r}_c) \times \mathbf{e}_{kt}$, J_c is the inertia tensor with respect to point C , \mathbf{F}^0 and \mathbf{M} denote the principal forces vector and the principal torque, respectively, acting to the platform from the side of the pneumatic cylinders.

Kinematics of the platform is described by the following matrix equation

$$\mathbf{A} \cdot \mathbf{V}^0 = \dot{\mathbf{i}}, \quad \dot{\mathbf{i}} = (\dot{i}_1, \dots, \dot{i}_6)^T, \quad (3)$$

where matrix \mathbf{A} is composed from the row-vectors

$$\mathbf{L}_k \cdot \mathbf{V}^0 = \dot{i}_k, \quad k = 1, \dots, 6, \quad (4)$$

$(\cdot)^T$ denotes the transpose operation (see [8] for more details).

In the projections on the coordinate axes X, Y, Z , system (1), (2), (3) has the following form:

$$\begin{aligned}
J_x \dot{\omega}_x + (J_z - J_y) \omega_y \omega_z &= \sum_{k=1}^6 F_k (a_{ky} e_{kz} - a_{kz}^* e_{ky}), \\
J_y \dot{\omega}_y + (J_x - J_z) \omega_z \omega_x &= \sum_{k=1}^6 F_k (a_{kz}^* e_{kx} - a_{kx} e_{kz}), \\
J_z \dot{\omega}_z + (J_y - J_x) \omega_x \omega_y &= \sum_{k=1}^6 F_k (a_{kx} e_{kx} - a_{ky} e_{kx}), \\
a_{kz}^* &= a_{kz} - z_c.
\end{aligned} \tag{5}$$

$$\begin{aligned}
m(\ddot{x} + z_c \dot{\omega}_y + z_c \omega_x \omega_z) &= \sum_{k=1}^6 F_k e_{kx} + mg \sin \vartheta, \\
m(\ddot{y} - z_c \dot{\omega}_y + z_c \omega_y \omega_z) &= \sum_{k=1}^6 F_k e_{ky} - mg \cos \vartheta \sin \gamma, \\
m(\ddot{z} - z_c(\omega_x^2 + \omega_y^2)) &= \sum_{k=1}^6 F_k e_{kz} - mg \cos \vartheta \cos \gamma,
\end{aligned} \tag{6}$$

$$\begin{aligned}
\dot{\vartheta} &= \omega_y \cos \gamma - \omega_z \sin \gamma, \\
\dot{\gamma} &= \omega_z + \dot{\psi} \sin \vartheta, \\
\dot{\psi} &= (\omega_y \sin \gamma + \omega_z \cos \gamma) \cdot (\cos \vartheta)^{-1}.
\end{aligned} \tag{7}$$

The system of equations (5)–(7) is of order 12. This system should be supplemented by equations of the external forces F_k ($k = 1, \dots, 6$), acting to the platform from the side of pneumatic actuators.

2.2 Freight vehicle simulator of Transas Co.

The present paper deals with a pneumatically actuated Stewart platform, which serves as a computer-controlled mobile base of the simulator for training of freight KamAZ vehicle drivers. An axonometric plan of the Stewart platform used as a part of the Transas car simulator is presented in Fig. 2.

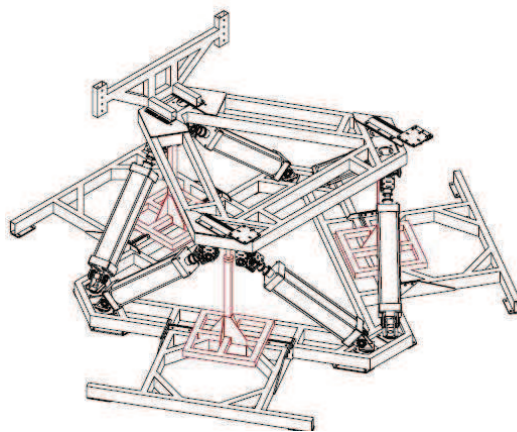


Figure 2: Axonometric plan of the Stewart platform of Transas car simulator.

The considered system peculiarity is the usage of pneumatic servosystems instead of the hydraulic ones. The advantage of pneumatic actuators is the design simplicity and relative ease of operation and maintenance. Besides, they are relatively cheap and functional flexible. As well as the hydraulic systems, they may reproduce forward movement without gears.

Pneumatic actuators have the following advantages over the hydraulic ones:

- Their actuators have higher operating speed and lower cost;

— Return lines are much shorter, since the air can be vented to the atmosphere from any point of the system;

— There is an unlimited supply of air as the working fluid.

However, pneumatic actuators of the same dimension as the hydraulic ones, are producing the smaller force due to the higher fluid pressure in the hydraulic actuators. In addition, it is difficult to ensure sufficient control accuracy by the pneumatic actuators due to the air compressibility. This imposes special requirements to the control system design.

2.3 Specifications for control system of the platform

The control system is aimed at providing prescribed motion of the platform center-of-gravity, and the angular position of the platform, ensuring tracking of the reference signal produced by the higher level of the simulator control. Adaptability of the control system is required for ensuring stable platform behavior in the total region of admissible variables and parameters.

The control algorithm should involve the procedure for converting the input data, removing the platform from the admissible region, to the acceptable one.

The requirements on the tracking precision should be fulfilled by means of minimal frequency of pneumatic valve actuations.

From the experience of the operation of such kind of platforms it is known that, due to leaks in pneumatic equipment, the parasitic oscillations occur in the quiescent state. These oscillations should be suppressed.

Additionally, the control system must ensure fulfillment of the above stated requirements for the case of increasing the mass of the service load up to 400 kg above its nominal value.

3 Pneumatic Actuator Model

3.1 Basic relations

Equations (5)–(7) should be considered jointly with the following equations for pressures p_1 and p_2 in the working and exhaust cavities of the pneumatic cylinder [10, 11]:

$$\dot{p}_1 = \frac{k f_1^{\text{ef}} K p_h \sqrt{RT_h}}{F_1(x_{01} + x)} \varphi(\sigma_1) - \frac{k p_1}{x_{01} + x} \cdot \dot{x}, \quad (8)$$

$$\sigma_1 = p_1/p_h; \quad K = \sqrt{2gk/(k-1)}; \quad x_{01} = V_{01}/F_1;$$

where p_h and T_h denote the air pressure and temperature (respectively) in the header pipe; $f_1^{\text{ef}} = \mu_1 f_1$ is the effective area of the inlet hole; μ_1 denotes the flow coefficient of the inlet pipe; f_1 is the inlet area; x_{01} stands for the initial piston position; V_{01} is the initial working chamber space; k denotes the adiabatic index (for standard air, $k = 1.4$); g is the acceleration of gravity¹. Nonlinear *discharge function* $\varphi(\cdot)$ in (8) has the following form [10, 11]:

$$\varphi(\sigma) = \begin{cases} \sqrt{\sigma^{\frac{2}{k}} - \sigma^{\frac{k+1}{k}}}, & \text{if } 0.528 < \sigma < 1; \\ 0.2588, & \text{if } 0 < \sigma < 0.528. \end{cases} \quad (9)$$

¹ In the present work all the values are given in the engineer's system of units.

Initial values of x_{01} and V_{01} include not only the initial volume of the chamber (the so-called *clearance space*), but also the volume of the pipeline from the distributor to the working cylinder.

Equation for pressure p_2 in the exhaust chamber 2 differs from (8) not only by signs of its members and the piston coordinate, but by the fact that it includes a varying temperature T_2 in the exhaust chamber instead of the constant air temperature T_h in the header pipe:

$$\dot{p}_2 = -\frac{k f_2^{\text{ef}} K \sqrt{RT_2}}{F_2(s + x_{02} - x)} \varphi\left(\frac{\sigma_a}{\sigma_2}\right) + \frac{kp_2}{s + x_{02} - x} \cdot \dot{x}, \quad (10)$$

where $\sigma_2 = \frac{p_2}{p_h}$; $x_{02} = \frac{V_{02}}{F_1}$; $f_2^{\text{ef}} = \mu_2 f_2$, $\varphi(\cdot)$ is given by (9).

Since the adiabatic process occurs in the absence of the heat exchange in the exhaust chamber, the temperature T_2 in (10) may be expressed in terms of p_2 as

$$\frac{p_2}{p_1} = \left(\frac{v_1}{v_2}\right)^k, \quad \frac{p_2}{p_1} = \left(\frac{T_2}{T_1}\right)^{\frac{k}{k-1}}, \quad \frac{T_2}{T_1} = \left(\frac{v_1}{v_2}\right)^{k-1}.$$

Then (10) reads as follows:

$$\dot{p}_2 = -\frac{k f_2^{\text{ef}} K p_2^{\frac{3k-1}{2k}} \sqrt{RT_h}}{F_2(s + x_{02} - x) p_h^{\frac{k-1}{2k}}} \varphi\left(\frac{\sigma}{\sigma_2}\right) + \frac{kp_2}{s + x_{02} - x} \cdot \dot{x}. \quad (11)$$

4 Fluid Servodrive of Transas Car Simulator

4.1 Dynamics model of tracking pneumo actuator

Foregoing equations (5)–(7), (8), (9), (11) make it possible to study motion of the pneumo valve under the variations of the load and the inlet and outlet areas, but these equations do not take into account that input and output cavities are not fixed during the motion control, they may be referred to upper and to lower parts of the pneumatic cylinder, depending on the current control action. Besides, it should be also considered that in the particular servo system, the pressure force is controlled by means of air *exhaust* (not air injection) from the corresponding chamber of the pneumatic cylinder. This is made by means of three controlled outlet valves with different selectional areas, which makes possible to compose the 3-bit control signal (for each direction). Air pressure in the cavities is restored from the surge vessel, which is connected with the compressor, via two uncontrolled valves (one for each chamber). Additionally, in what follows it is taken into account that the weight of the piston is negligibly small in comparison with the load forces applied from the moving platform with the cab, mounted on it.

Following [9, 12], to describe motion of the pneumatic actuator let us introduce the dimensionless controlling parameter $-1 \leq \alpha \leq 1$ such as $f_1 = f_2 = |\alpha| f_{\max}$, where f_{\max} denotes the maximal area of the outlet hole, assuming that if $\alpha > 0$ then the outlet hole of the upper chamber is connected to the atmosphere, and visa versa, if $\alpha < 0$ then this is made for the lower chamber. If $\alpha = 0$ then both chambers are closed off for the air discharge. As is stated above, parameter α is represented by 4 binary digits (one bit is for the sign).

Finally, the following model for air pressures in the chambers is obtained:

$$\begin{aligned} \dot{p}_1 = & \frac{k f_0 K p_h \sqrt{RT_h}}{F_1(x_{01} + x)} \varphi(\sigma_1) - \frac{k p_1}{x_{01} + x} \cdot \dot{x} \\ & - \begin{cases} 0, & \text{if } \alpha > 0, \\ \frac{k f_1^{\text{ef}} K p_1^{\frac{3k-1}{2k}} \sqrt{RT_h}}{F_1(x_{01} + x) p_h^{\frac{k-1}{2k}}} \varphi\left(\frac{p_a}{p_1}\right), & \text{otherwise,} \end{cases} \end{aligned} \quad (12)$$

$$\begin{aligned} \dot{p}_2 = & \frac{k f_0 K p_h \sqrt{RT_h}}{F_2(s + x_{02} - x)} \varphi(\sigma_2) + \frac{k p_2}{s + x_{02} - x} \cdot \dot{x} \\ & - \begin{cases} \frac{k f_2^{\text{ef}} K p_2^{\frac{3k-1}{2k}} \sqrt{RT_h}}{F_2(s + x_{02} - x) p_h^{\frac{k-1}{2k}}} \varphi\left(\frac{p_a}{p_2}\right), & \text{if } \alpha > 0, \\ 0, & \text{otherwise,} \end{cases} \end{aligned} \quad (13)$$

where $K = \sqrt{2gk/(k-1)}$, $x_{01} = V_{01}/F_1$, $x_{02} = V_{02}/F_1$, $f_1 = f_2 = f_{\max}|\alpha|$, $f_1 = f_2 = f_{\max}|\alpha|$, $f_0 = \mu_0 f_{\max}$, $f_1^{\text{ef}} = \mu_1 f_1$, $f_2^{\text{ef}} = \mu_2 f_2$, $\sigma_1 = p_1/p_h$, $\sigma_2 = p_2/p_h$. The first term in (12), (13) describes air feeding the chambers from the compressor over the valve with a sectional area f_0 .

4.2 Sliding-mode control of pneumatic actuator

Let $x^*(t)$ be the reference signal, representing the desired piston position (and, consequently, the running-out of the rod).

To ensure the high tracking accuracy along with robustness to parametric uncertainties, unmodelled nonlinearities and the external disturbances (such as varying forces applied from the load), the following sliding-mode controller may be used [3, 13, 14, 16]:

$$u(t) = e(t) + k_D \dot{e}(t), \quad (14)$$

$$\alpha(t) = \text{sat}\left(\kappa \text{sign}(u) \cdot \sqrt{|u|}\right), \quad (15)$$

where $e(t) = x^*(t) - x(t)$ denotes the tracking error, k_D stands for the damping gain, ensuring ‘‘smooth’’ sliding motion [13–15]. In what follows, after some trial and error iterations, the ‘‘guessed’’ values $k_D = 0.4$ s/m, $\kappa = 15$ have been taken.

5 Simulation and Experimental Results

The simulations of the closed-loop system (12), (13) with sliding-mode controller (14) for all six ‘‘legs’’ of the platform was studied by the simulations. In our study the various reference signals on platform coordinates x_c^* , y_c^* , z_c^* , ψ^* , ϑ^* , γ^* have been converted by means of the kinematic equations (see, e.g. [17]) to the reference signals on the each leg $x_i^*(t)$, $i = 1, \dots, 6$ of the pneumatic servo systems. Then the actual running-out of each rod $x_i(t)$ has been re-converted by means of the inverse kinematic relations [17] to the actual platform coordinates $x_c(t)$, $y_c(t)$, $z_c(t)$, $\psi(t)$, $\vartheta(t)$, $\gamma(t)$ for accuracy evaluation.

One example of the simulation results is demonstrated in Figs. 3–5. The harmonic reference signal on the vertical platform coordinate z_c has been taken, the other reference variables have been taken zeros.

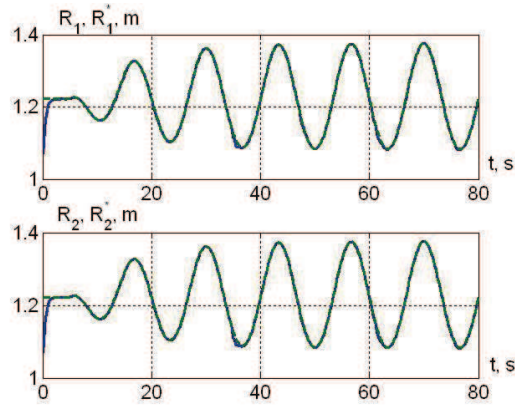


Figure 3: Model (12), (13), controller (14). Legs 1–4 lengths vs t . Solid line – actual value, dashed line – desired value.

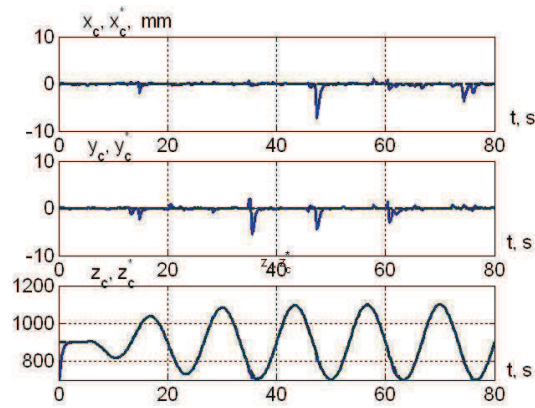


Figure 4: Model (12), (13), controller (14). Platform translational coordinates vs t . Solid line – actual value, dashed line – desired value.

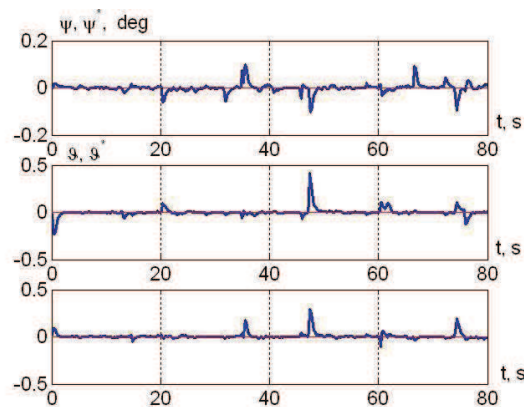


Figure 5: Model (12), (13), controller (14). Platform angular coordinates vs t .

As is seen from the plots, control law (14) ensures high precision and operating speed of tracking process.

The same reference signals have been applied to the real-world set-up (see Fig. 6), which is supplied with the on-off logic controller, which has been borned by the typical solutions for pneumatic automation systems. It is seen from the plots (Figs. 7–9), that the tracking error for the siding mode controller is up to 5 time less than that for the on-off logic controller.



Figure 6: Performing the experiments.

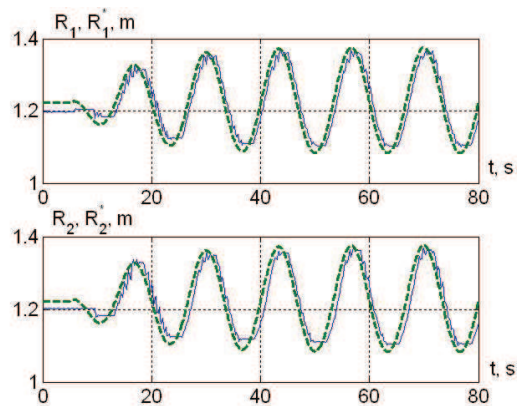


Figure 7: Experimental results. On-off logic control. Legs 1–4 lengths vs t . Solid line – actual value, dashed line – desired value.

6 Conclusions

In the paper the problem of pneumatic actuators control by switching the valves is considered. The actuators are the part of the simulator for training drivers of freight vehicles, based on the 6-DOF Stewart Platform.

The sliding-mode control strategy is proposed and studied by simulations. The experimental results for the existing on-off logical control algorithm are given. Comparison of the results demonstrates possibility for improvement of the stimulator performance based on the sliding-mode controller.

The future work intentions are the implementation of the proposed control law on the real-world pneumatic actuators for experimental valuation of the robustness properties of the sliding-mode controller with respect to the unmodelled plant dynamics, uncertainties and varying external disturbances from the load.

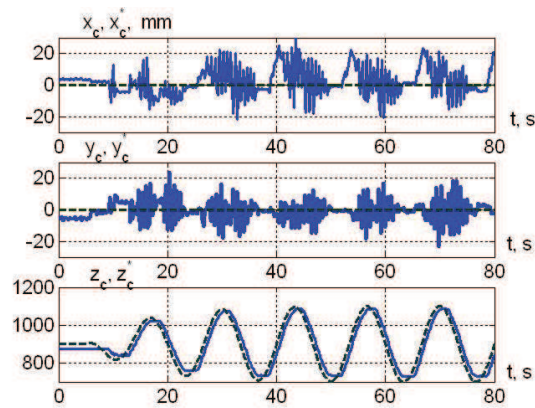


Figure 8: Experimental results. On-off logic control. Platform translational coordinates vs t . Solid line – actual value, dashed line – desired value.

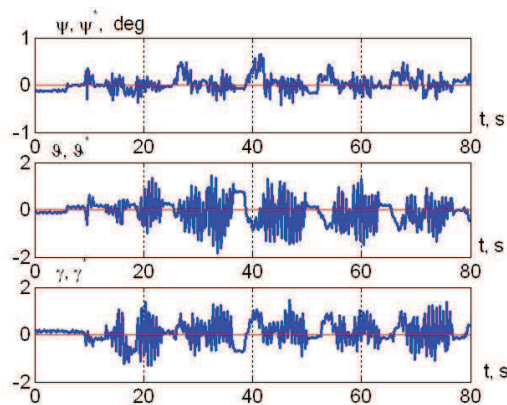


Figure 9: Experimental results. On-off logic control. Platform angular coordinates vs t .

Acknowledgment

This work was supported by Russian Scientific Foundation (project 14-21-00041) and Saint-Petersburg State University.

References

- [1] Wang, X. and Kim, C.K.-H. Improved control of pneumatic lumber-handling systems. *IEEE Trans. Control Syst. Technol.* **9** (3) (2001) 458–472.
- [2] Richardson, R., Plummer, A. and Brown M. Self-tuning control of a low-friction pneumatic actuator under the influence of gravity. *IEEE Trans. Control Syst. Technol.* **9** (2) (2001) 330–334.
- [3] Chillari, S., Guccione, S. and Muscato G. An experimental comparison between several pneumatic position control methods. In: *Proc. 40th IEEE Conf. Decision and Control (CDC 2001)*, Orlando, Florida, USA, 2001, 1168–1173.
- [4] Yin, Y. and Wang, J. A nonlinear feedback tracking control for pneumatic cylinders and experiment study. In: *Proc. American Control Conf. (ACC 2009)*, St. Louis, MO, USA, 2009, 3476–3481.
- [5] Lin, C.-L. and Chen C.-H. Design of a dead time controller for pneumatic systems. In: *Proc. American Control Conf. (ACC 2003)*, Denver, Colorado, USA, 2003, 1715–1720.
- [6] Leonov, G. A. Strange Attractors and Classical Stability Theory. *Nonlinear Dynamics and System Theory* **8** (1) (2008) 49–96.
- [7] Dasgupta, B. and Mruthyunjaya, T. The Stewart platform manipulator: a review. *Mechanism and Machine Theory* **35** (1) (2011) 15–40.
- [8] Leonov, G., Zegzhda, S., Kuznetsov, N., Tovstik, P., Tovstik, T. and Yushkov, M. Motion of a solid driven by six rods of variable length. *Doklady Physics* **59** (3) (2014) 153–157.
- [9] Andrievsky, B., Kazunin, D., Kuznetsov, N., Kuznetsova, O., Leonov, G. and Seledzhi, S. Modeling, simulation and control of pneumatically actuated Stewart platform with input quantization. In: *European Modelling Symposium EMS2014*, Pisa, Italy, 2014.
- [10] Gerc, E. and Krejcin, G. *Raschoet Pnevmoprivodov. Spravochnoe Posobie (Pneumatic Actuators Design. A Handbook)*. Mashinostroenie, Moscow, 1975 (in Russian).
- [11] Harris, P.G., O'Donnell, G.E. and Whelan T. Modelling and identification of industrial pneumatic drive system. *Int. J. Adv. Manuf. Technol.* **58** (2012) 1075–1086.
- [12] Andrievsky, B., Kazunin, D.V., Kostygova, D.M., Kuznetsov, N.V., Leonov, G.A., Lobanov, P.N. and Volkov A.A. Control of pneumatically actuated 6-DOF Stewart platform for driving simulator. In: *Proc. 19th Int. Conf. Methods and Models in Automation and Robotics (MMAR 2014)*. Miedzydroje, Poland, 2014, 663–668.
- [13] Yakubovich, V., Leonov, G. and Gelig A. *Stability of Stationary Sets in Control Systems with Discontinuous Nonlinearities*. Singapore, World Scientific, 2004.
- [14] Utkin, V. *Sliding Modes in Control and Optimization*. Springer-Verlag, 1992.
- [15] Leonov, G. A. and Shumafov, M.M. Stabilization of Controllable Linear Systems. *Nonlinear Dynamics and System Theory* **10** (3) (2010) 235–268.
- [16] Moreau, R., Pham, M.T., Tavakoli, M., Le, M.Q. and Redarce, T. Sliding-mode bilateral teleoperation control design for master–slave pneumatic servosystems. *Control Engineering Practice* **20** (2012) 584–597.
- [17] Harib, K. Srinivasan, K. Kinematic and dynamic analysis of Stewart platform-based machine tool structures. *Robotica* **21** (2003) 541–554.



The Duffing–Van der Pol Equation: Metamorphoses of Resonance Curves

J. Kyzioł and A. Okniński*

Politechnika Świętokrzyska, Kielce, Poland

Received: March 31, 2014; Revised: December 17, 2014

Abstract: We study dynamics of the Duffing–Van der Pol driven oscillator. Periodic steady-state solutions of the corresponding equation are determined within the Krylov-Bogoliubov-Mitropolsky approach to yield dependence of amplitude on forcing frequency as an implicit function, referred to as resonance curve or amplitude profile. Equations for singular points of resonance curves are solved exactly. We investigate metamorphoses of the computed amplitude profiles induced by changes of control parameters near singular points of these curves since qualitative changes of dynamics occur in neighbourhoods of singular points. More exactly, conditions for birth of resonances as well as for attractor crises are found. Bifurcation diagrams are computed to show good agreement with theoretical analysis.

Keywords: *oscillators; resonance curves; singular points.*

Mathematics Subject Classification (2010): 34C15, 70K30, 37G10.

1 Introduction

Nonlinear oscillators have many important applications in various areas of science and engineering [1, 2]. In this paper we investigate Duffing–Van der Pol oscillator which has been extensively studied due to potential applications in physics, chemistry, biology, engineering, electronics, and many other fields, see [3, 4] and references therein.

The periodically forced Duffing – Van der Pol oscillator (DvdP) is written as:

$$\frac{d^2x}{dt^2} - (b - cx^2) \frac{dx}{dt} + ax + dx^3 = f \cos \omega t. \quad (1)$$

There are three main cases of the Duffing potential $V(x) = \frac{1}{2}ax^2 + \frac{1}{4}dx^4$: (i) single well ($a > 0$, $d > 0$), (ii) double well ($a < 0$, $d > 0$), and (iii) double hump ($a > 0$, $d < 0$).

* Corresponding author: <mailto:fizao@tu.kielce.pl>

In the present paper we consider cases (i), (iii) and it is thus assumed that $a, b, c, f, \omega > 0$ while d is arbitrary.

There are many numerical and analytical methods to solve nonlinear oscillator equations. Analytical methods lead to complicated (approximate) formulae and analysis of such solutions is difficult. In the present work we analyse such approximate analytic solutions using the theory of algebraic curves. More exactly, we determine periodic steady-state solutions of the DvdP equation within the Krylov-Bogoliubov-Mitropolsky approach to get dependence of amplitude on forcing frequency as an implicit function, referred to as resonance curve or amplitude profile. We investigate metamorphoses of the computed amplitude profiles induced by changes of control parameters near singular points of these curves since qualitative changes of dynamics occur in neighbourhoods of singular points, see [5] and references therein. We have learned recently that idea to use Implicit Function Theorem in this context was put forward in [6].

The paper is organized as follows. In Section 2 the Van der Pol – Duffing equation is written in nondimensional form and implicit equation for resonance curves $L(\Omega, A) = 0$ is derived via the Krylov-Bogoliubov-Mitropolski (KBM) approach. In Section 3 theory of algebraic curves is applied to compute singular points on the amplitude profiles. Equations for singular points are solved and in Section 4 the solutions are used to study birth of resonances as well as attractor crises. We summarize our results in the last Section 5.

2 Nonlinear Resonances via KBM Method

We apply the Krylov-Bogoliubov-Mitropolsky (KBM) perturbation approach [7, 8] to equation (1). Substituting into (1):

$$x = \sqrt{\frac{b}{c}}z, \quad t = \frac{1}{\sqrt{a}}\tau, \quad b = \sqrt{a}\mu, \quad \omega = \sqrt{a}\Omega, \quad (2)$$

we get the DvdP in nondimensional form:

$$\frac{d^2z}{d\tau^2} - \mu(1 - z^2)\frac{dz}{d\tau} + z + \lambda z^3 = G \cos(\Omega\tau), \quad (3)$$

$\mu, G, \Omega > 0, \lambda - \text{arbitrary},$

where $\lambda = \frac{bd}{ac}$, $G = \frac{f}{a}\sqrt{\frac{c}{b}}$.

The equation (3) is written in the following form:

$$\frac{d^2z}{d\tau^2} + \Omega^2 z + \varepsilon(\sigma z + g) = 0, \quad (4)$$

where

$$\left. \begin{aligned} g &= -\Theta_0^2 z - \mu_0 \frac{dz}{d\tau} + \mu_0 z^2 \frac{dz}{d\tau} + \alpha_0 z + \lambda_0 z^3 - G_0 \cos(\Omega\tau), \\ \Theta_0^2 &= \frac{\Theta^2}{\varepsilon}, \quad \mu_0 = \frac{\mu}{\varepsilon}, \quad \alpha_0 = \frac{1}{\varepsilon}, \quad \lambda_0 = \frac{\lambda}{\varepsilon}, \quad G_0 = \frac{G}{\varepsilon}, \quad \varepsilon\sigma = \Theta^2 - \Omega^2. \end{aligned} \right\} \quad (5)$$

According to the KBM method we assume for small nonzero ε that the solution for 1 : 1 resonance can be written as:

$$z = A(\tau) \cos(\Omega\tau + \varphi(\tau)) + \varepsilon z_1(A, \varphi, \tau) + \dots \quad (6)$$

with slowly varying amplitude and phase:

$$\frac{dA}{d\tau} = \varepsilon M_1(A, \varphi) + \dots, \tag{7}$$

$$\frac{d\varphi}{d\tau} = \varepsilon N_1(A, \varphi) + \dots. \tag{8}$$

Computing now derivatives of z from equations (6), (7), (8) and substituting to equations (4), (5), eliminating secular terms and demanding $M_1 = 0, N_1 = 0$ we obtain the following equations for the amplitude and phase of steady states:

$$A^2 \left(\mu^2 \Omega^2 \left(1 - \frac{1}{4} A^2 \right)^2 + \left(1 + \frac{3}{4} \lambda A^2 - \Omega^2 \right)^2 \right) = G^2. \tag{9}$$

3 General Properties of the Amplitude Profile $A(\Omega)$

After introducing new variables, $\Omega^2 = X, A^2 = Y$, the equation (9) defining the amplitude profile reads $L(X, Y) = 0$, where:

$$L(X, Y; \lambda, \mu, G) \stackrel{df}{=} \mu^2 XY \left(1 - \frac{1}{4} Y \right)^2 + Y \left(1 + \frac{3}{4} \lambda Y - X \right)^2 - G^2. \tag{10}$$

Singular points of $L(X, Y)$ are computed from equations [9]:

$$L = 0, \tag{11a}$$

$$\frac{\partial L}{\partial X} = 0, \tag{11b}$$

$$\frac{\partial L}{\partial Y} = 0. \tag{11c}$$

There are several classes of physically acceptable solutions of equations (11), i.e. solutions fulfilling conditions: $X > 0, Y > 0, \mu > 0$.

1. Firstly, if we fix values of X, μ , then the solution reads:

$$\left. \begin{aligned} 3mY^3 - 36mY^2 + (144m - 64 + 256X)Y - 192m + 256 - 512X &= 0, \\ \lambda = \frac{16m - 8mY + mY^2 - 32 + 32X}{24Y}, \quad g = -\frac{mY}{48} (XY^2 - 16X + 8Y - 16 - Y^2), \end{aligned} \right\} \tag{12}$$

where $m \equiv \mu^2, g \equiv G^2$ and a special solution for the unforced case ($G = 0$) is:

$$Y = 4, \quad \lambda = -\frac{1}{3} + \frac{1}{3}X, \quad G = 0 \quad (\mu - \text{arbitrary}). \tag{13}$$

2. In the second case, when λ, μ are fixed, we obtain the special solution (13) again as well as equation for Y :

$$\begin{aligned} A_3 Y^3 + A_2 Y^2 + A_1 Y + A_0 &= 0, \\ A_3 = 5\mu^2, \quad A_2 = -192\lambda - 44\mu^2, \\ A_1 = 112\mu^2 + 384\lambda - 192, \quad A_0 = 256 - 64\mu^2, \end{aligned} \tag{14}$$

equation for Z :

$$\begin{aligned} Z^2 &= B_6 \mu^6 + B_4 \mu^4 + B_2 \mu^2 + B_0, \\ B_6 &= -4(Y - 4)^2, \\ B_4 &= (39\lambda + 20)Y^2 - (144\lambda + 152)Y + 336\lambda + 416, \\ B_2 &= (2232\lambda^2 + 660\lambda)Y^2 - (6048\lambda^2 + 192\lambda - 480)Y \\ &\quad + 2304\lambda^2 - 1344\lambda - 640, \\ B_0 &= 2304\lambda^2 (3\lambda Y^2 + (-6\lambda + 3)Y - 4), \end{aligned} \tag{15}$$

and, finally, after solving equations (14), (15), we can compute X, G :

$$X = -\frac{1}{32}\mu^2 Y^2 + \frac{1}{4}(\mu^2 + 3\lambda)Y + 1 - \frac{1}{2}\mu^2, \quad G = \frac{1}{10\mu}Z. \quad (16)$$

3. On the other hand, if we fix values of X, Y , then we get:

$$\begin{aligned} G^2 &= \frac{4}{9}(YX + 4X - Y + 4)(4YX - 8X - Y + 4) \frac{Y}{(Y-4)^2}, \\ \mu^2 &= -\frac{64}{3} \frac{4YX - 8X - Y + 4}{(Y-4)^3}, \\ \lambda &= -\frac{4}{9} \frac{5YX + Y - 4X - 4}{Y(Y-4)}. \end{aligned} \quad (17)$$

Necessary conditions: $\mu^2 > 0$, $G^2 > 0$ lead to:

Y	X	λ
$0 < Y < 2$	$0 < X < \frac{Y-4}{4(Y-2)}$	$\text{sign}(\lambda) = \text{sign}(s)$
$2 < Y < 4$	$0 < X$	$\text{sign}(\lambda) = \text{sign}(s)$
$4 < Y$	$0 < X < \frac{Y-4}{4(Y-2)}$	$\lambda < 0$

(18)

where $s = X + \frac{Y-4}{5Y-4}$.

4 Computational Results

In this Section singular points of amplitude profiles – solutions of equations (10), (11) – are studied. In the first Subsection we shall consider the special solution (13), corresponding to the amplitude profile with isolated point. On the other hand, this solution describes birth of a limit cycle in the unforced case ($G = 0$). In Subsection 4.2 we consider the second class of solutions defined by equations (14), (15), (16). In this case metamorphosis of the resonance corresponds to change of attractor size (crisis).

4.1 Birth of resonances from isolated points

The solution (13) yields for $X = \Omega^2 = 4$ the following values: $Y = A^2 = 4$, $\lambda = 1$ and we choose $\mu = 0.5$. Since $G = 0$, this solution corresponds to a resonance in the unforced case living exactly at this critical value $X = \Omega^2 = 4$. On the plot $L(\Omega^2, A^2) = 0$ this resonance is represented by an isolated point. For increasing values of G this point gives rise to growing ovals and thus the corresponding resonances (limit cycles) exist in a broader and broader range of Ω . In Fig. 1 implicit plots $L(\Omega^2, A^2; \lambda, \mu, G) = 0$ are shown for $\mu = 0.5$, $\lambda = 1$ and $G = 0.01, 0.10, 0.20, 0.50$.

We have computed bifurcation diagrams for $\mu = 0.5$, $\lambda = 1$ and $G = 0.01, 0.05, 0.10, 0.20$ to show birth and growth of the resonance. This scenario is shown in Fig. 2. It can be seen that for decreasing values of G the resonance shrinks around $\Omega \cong \sqrt{4} = 2$ with amplitude $A \cong \sqrt{4} = 2$, in good agreement with (13). More exactly, the resonance appears at $\Omega = 1.92$ rather than $\Omega = 2$ thus providing estimate of the KBM method's error.

4.2 Metamorphoses of resonances in the neighbourhood of self-intersection

Let us consider the second class of solutions described in Section 3. For example, for $\lambda = 1$, we compute from equation (13) $X = 4$, $Y = 4$, $G_{cr}^{(1)} = 0$ and we choose $\mu = 0.5$. Now for $\lambda = 1$ and $\mu = 0.5$ we get from equations (14), (15), (16) one physical solution

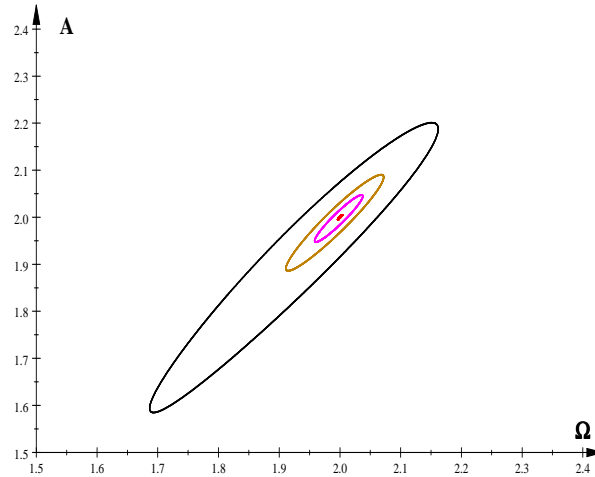


Figure 1: Implicit plots $L(\Omega^2, A^2; \lambda, \mu, G) = 0$ where $\mu = 0.5$, $\lambda = 1$ and $G = 0.01$ (red line), 0.10 (magenta), 0.20 (sienna), 0.50 (black).

$X = 2.28921783344$, $Y = 1.77072449936$, $G_{cr}^{(2)} = 0.563412500579$. The first solution represents isolated point and describes birth of a resonance in the unforced case ($G = 0$), while the second solution corresponds to a self-intersection of the resonance curve. Both solutions are shown in Fig. 3.

Now, for $G = 0$ and increasing we have to do with scenario described in Subsection 4.1. Black curve in Fig. 3 corresponds to $G = 0.5 < G_{cr}^{(2)}$. The attractor is shown in Fig. 4 (left figure). There is only one stable solution corresponding to black oval in Fig. 3, the lower black branch being unstable. Then for $G = 1.5 > G_{cr}^{(2)}$ (the corresponding amplitude profile is represented by green line in Fig. 3) the attractor increases its size, cf. Fig. 4 where bifurcation diagrams are shown. Let us add here that for smaller values of G but greater than $G_{cr}^{(2)}$, say for $G = 0.75$, the resonance is stable on a smaller interval of Ω .

5 Summary and Discussion

In this work we have studied dynamics of the periodically forced Duffing-van der Pol equation. Steady-state nonlinear resonances have been determined within the Krylov-Bogoliubov-Mitropolsky approach. We have applied theory of algebraic curves [9] to determine singular points of the computed resonance profiles since qualitative changes of dynamics occur in neighbourhood of singular points [5]. Resonance curves (9) have two classes of singular points: isolated points as well as self-intersections. We have found that a family of resonances (limit cycles) of the unforced DvdP equation ($G = 0$) is born when the amplitude profile of the forced equation, computed according to the KBM method has singular point for $G = 0$, see Subsection 4.1. It is possible to control value of Ω at which the resonance appears for $G > 0$, see equation (13). For growing values of forcing amplitude G stability range in the Ω space is growing as well. On the other hand, in the neighbourhood of self-intersections of resonance curves there are crises – the corresponding attractor changes its size. We have computed several bifurcation diagrams

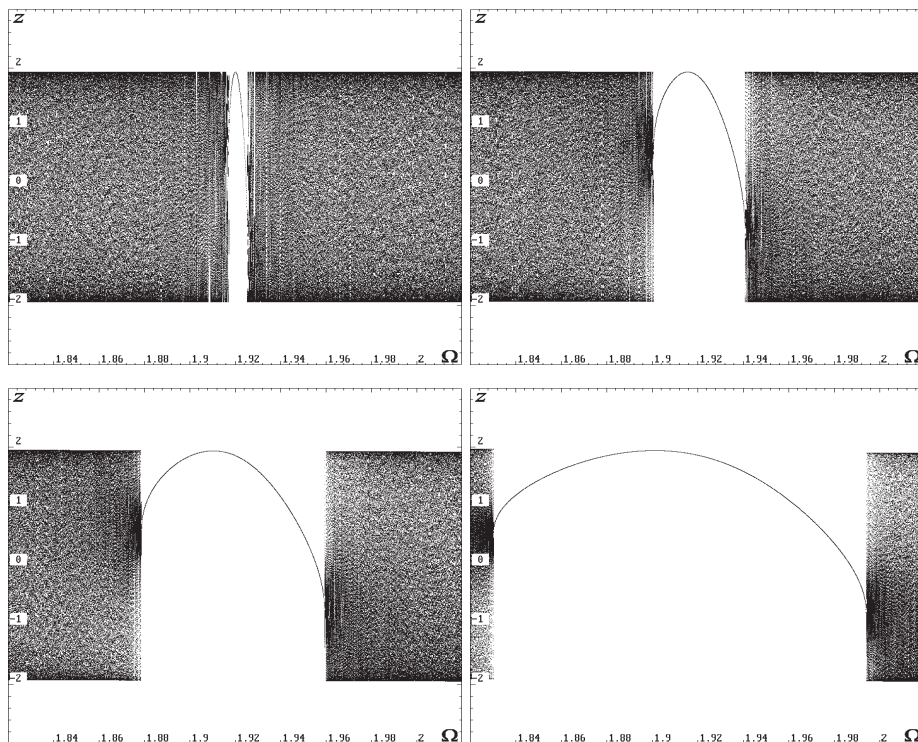


Figure 2: Bifurcation diagrams, $\mu = 0.5$, $\lambda = 1$ and $G = 0.01$, $G = 0.05$, $G = 0.10$, $G = 0.20$ (left to right, top to bottom).

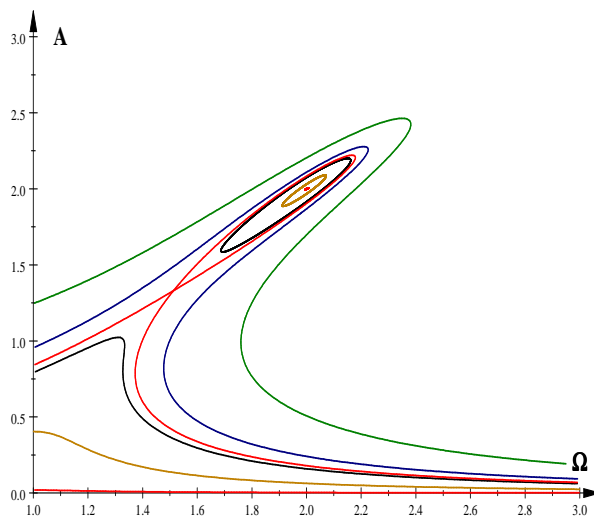


Figure 3: Implicit plots $L(\Omega^2, A^2; \lambda, \mu, G) = 0$ where $\mu = 0.5$, $\lambda = 1$ and $G = 0.01$ (red), $G = 0.20$ (sienna), $G = 0.50$ (black), $G = G_{cr}^{(2)}$ (red), $G = 0.75$ (blue), $G = 1.50$ (green).

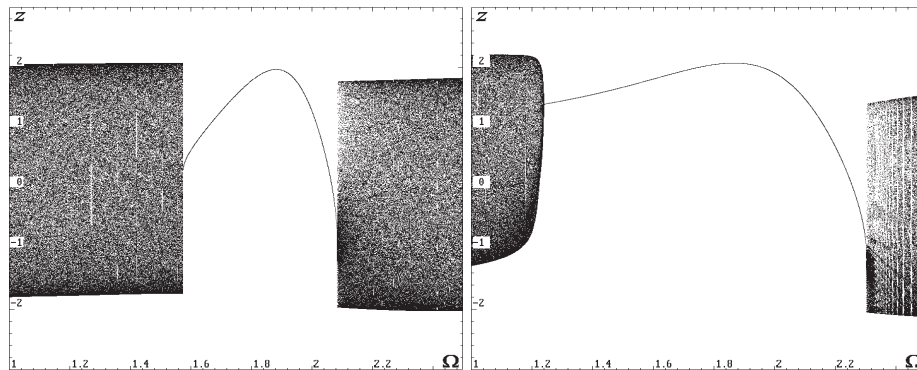


Figure 4: Bifurcation diagrams, $\mu = 0.5$, $\lambda = 1$, and $G = 0.5$ (left figure), $G = 1.5$ (right figure).

documenting qualitative changes of dynamics in the neighbourhood of metamorphoses of resonance curves.

Acknowledgement

The paper has been presented during the 12th Conference on Dynamical Systems – Theory and Applications, December 2-5, 2013, Lodz, Poland.

References

- [1] Pikovsky, A., Rosenblum, M. and Kurths, J. *Synchronization. A Universal Concept in Non-linear Sciences*. New York, Cambridge University Press, 2001.
- [2] Awrejcewicz, J. *Bifurcation and Chaos in Coupled Oscillators*. New Jersey, World Scientific, 1991.
- [3] Szemplińska-Stupnicka, W. and Rudowski, J. The coexistence of periodic, almost-periodic and chaotic attractors in the Van der Pol – Duffing oscillator. *J. Sound Vibr.* **199**(2) (1997) 165–175.
- [4] Chudzik, A., Perlikowski, P., Stefański, A. and Kapitaniak, T. Multistability and rare attractors in van der Pol-Duffing oscillator. *Int. J. Bif. Chaos* **21**(7) (2011) 1907–1912.
- [5] Kyzioł, J. and Okniński, A. Exact nonlinear fourth-order equation for two coupled oscillators: metamorphoses of resonance curves. *Acta Phys. Polon.* **B44**(1) (2013) 35–47.
- [6] Awrejcewicz, J. Modified Poincaré method and implicit function theory. In: *Nonlinear Dynamics: New Theoretical and Applied Results* (J. Awrejcewicz, ed.) Akademie Verlag, Berlin, 1995, P. 215–229.
- [7] Nayfeh, A. H. *Introduction to Perturbation Techniques*. New York, John Wiley & Sons, 1981.
- [8] Awrejcewicz, J. and Krysko, V. A. *Introduction to Asymptotic Methods*. New York, Chapman and Hall (CRC Press), 2006.
- [9] Wall, C. T. C. *Singular Points of Plane Curves*. New York, Cambridge University Press, 2004.



Analytical and Experimental Investigation of Vertical Vibration of a Freight Wagon in the Presence of Mechanical Asymmetry

F.N. Nangolo^{1*}, J. Soukup¹, A. Petrenko¹ and J. Skocilas²

¹ *UJEP in Usti nad Labem, Faculty of Production Technology and Management, 1001 Na Okraji, 40001 Usti nad Labem, Czech Republic.*

² *CTU in Prague, Faculty of Mechanical Engineering, 4 Technicka, 16607 Prague, Czech Republic.*

Received: March 31, 2014; Revised: January 29, 2015

Abstract: Production and construction asymmetry of railway vehicles in the presence of multiple track irregularities on the rail influences the time flow of the wheel. It has an influence on wheel and rail wear defects, especially on driving safety. Production and construction asymmetry was found during the experimental investigation of the basic parameters of mechanical properties of a double-axel freight wagon of Smmps type. This was an impulse for a systematic investigation of the influence of production and construction asymmetry on the vertical dynamic of complex mechanical systems, such as a railway vehicle. The current contribution introduces a methodology of analytical solution of the influence of production and construction asymmetry on the vertical dynamic response of a double-axel freight wagon in the presence of multiple track irregularities. Measured field data were used to validate the model.

Keywords: *asymmetry; analytical model; experiment; vertical vibration.*

Mathematics Subject Classification (2010): 93A10.

* Corresponding author: <mailto:nangolo@fvtm.ujep.cz>

1 Introduction

This paper was successfully presented at the conference of Dynamic Systems Theory in Lodz, Poland, 2013. In the present paper, an analytical method to study the effects of production and construction asymmetry on the vertical vibration response of a railway wagon in the presence of multiple track irregularities and their consequences is presented. A review of published material on the subject revealed that many analyses [18] have been made from which general conclusions regarding the dynamic behavior of complex mechanical systems were drawn. The fundamentals of this subject are covered in detail in [3], and will not be treated here. The reader is referred to [4,5,12] for further background.

Investigation of the influence of asymmetry on ground vehicles as a simple model was introduced in 1925 and today it is mostly used as a textbook example in vibration of mechanical system with two degrees of freedom [2, 5]. The full vehicle model dealing with the influence of production and construction asymmetry on the vertical vibration response of a railway wagon in the presence of multiple track irregularities is rarely described in literatures. Therefore, it is the intention of this work to extend preceding analysis by introducing the effect of production and construction asymmetry on the vertical vibration response of complex mechanical systems under multiple track excitations. In this paper a double-axel freight wagon modeled as a 9 DOF three-dimensional system intended for the investigation of the effect of production and construction asymmetry on vertical vibration response in the presence of multiple track irregularities and their consequences is presented.

2 Literature Review

In analyzing the interaction between the train and the track, the vehicle system can be modeled as one-dimensional, two-dimensional, or three-dimensional model. The simplest vehicle model is a single degree of freedom (DOF) one-dimensional model, which considers a single wheel with static force representing the static load due to the car-body and bogie where the contact between the wheel and rail is maintained by either linear or non-linear spring. This model has been applied in a number of published studies concerned with dynamic wheel-rail interaction; see for example [9]. The single DOF is considered sufficient for high frequency vibration analysis considering the interaction between the wheel and rail with surface irregularities. However, this model is insufficient to analyze the contributions due to pitch and roll motions of the vehicle on wheel-rail impact load or to investigate the effect of multiple defects in different wheel-sets and/or multiple surface irregularities on the rail.

Alternatively, two-dimensional models that include half of the car-body and two bogies and four wheel-sets have been most widely formulated and applied for studies on wheel-rail interactions. *Nielsen and Igeland* [17], developed a four-DOF two-dimensional pitch plane model in order to study the influence of wheel and rail imperfections on vehicle-track interaction. This model has been further employed by *Dong* [15] and *Cai* [16] in order to simulate the vehicle-track interaction under wheel defects. Several two-dimensional vehicle models have also been formulated with 10-14 DOF that consist of half bogie and a quarter of the car-body weight and include the pitch motion of both the car-body and bogie [13, 14]. Such a model would be sufficient to analyze the dynamic interaction between the leading and trailing bogie and wheels and effect of the cross wheel defects. However, contributions due to either pitch or roll motion of the

car-body and bogies have to be neglected in such models.

Three-dimensional vehicle models have been developed incorporating a full or half of the car-body, two bogies and two wheel-sets. Such models permit dynamic coupling between the leading and trailing bogies. *Sun et al.* [10] developed a comprehensive three-dimensional vehicle model in order to study lateral and vertical dynamics of the wagon-track system [11]. Such a model provides all the advantages of roll, pitch plane models and is quite adequate for the investigation of the influences of coupled vertical, the pitch and lateral dynamics of the vehicle [7]. The pitch and roll motions of the car-body and bogie that could enhance the wheel-rail impact force caused by the wheel and rail irregularities can be adequately investigated. However, the effects of production and construction asymmetry on the vertical vibration response in the presence of multiple track irregularities and their consequences have never been investigated with this full three-dimensional vehicle model. Therefore it is the intension of this paper to introduce an analytical method to solve vertical vibration response of complex mechanical system with multi-DOF. This method is limited to vertical vibration responses only.

3 Railway Vehicle Model

In the present paper an analytical model of a railway vehicle was developed as illustrated in Figure 1. The model consists of a car body, two bogie frames and four wheel-sets. The car body is modeled as a rigid body having a mass m , and having moment of inertia J_x and J_y about the transverse and longitudinal centroidal horizontal axes, respectively. While the bogie frames are considered as rigid bodies with m_1 and m_2 , with moment of inertia J_{x1} and J_{y1} for the front bogie and similarly rear bogie having moment of inertia J_{x2} and J_{y2} about the transverse and longitudinal centroidal horizontal axes, respectively. The springs in the primary and secondary suspension system are characterized by spring stiffness constant k_{jki} and damping coefficient b_{jki} , where $j = 1, 2$, quadrant $k = 1, 2, 3, 4$ and spring position orders $i = 1, \dots, n$. Assuming small vertical motion and the vehicle car body to be rigid, its motion may be described by the relative vertical displacement w_t and rotations about the main longitudinal horizontal axis φ_x and about main the transverse horizontal axis φ_y . Likewise, the motions of the two bogie frames are described by $w_1, \varphi_{x1}, \varphi_{y2}$ for the front bogie frame and $w_2, \varphi_{x2}, \varphi_{y2}$ for the rear bogie frame each about their centroidal. The railway wagon is thus represented by a 9 DOF mechanical system.

4 Analytical Method and Solution

A number of analytical solutions to vehicle dynamic response have been developed in the past. Some authors have considered the mechanical analog of the DNA base pair oscillations to analysis rotational oscillations of a DNA fragment in detail, see [8]. To facilitate analyse, it is essential to reduce the complex vehicle vibrating system to its simplest elements. At the same time, careful judgment is called for to avoid assumptions that are not in accord with the basic realities of the situation. Hence with this point in mind, in the present paper the analytical solution of the railway vehicle is considered to be a system of three rigid bodies with 9 degrees of freedom coupled by spring-damper elements with the consideration of linear viscous damping, as shown in Figure 2.

The equations of motion for the railway model considered in this paper are derived from the Lagrange equation of motion and therefore it is necessary to determine the

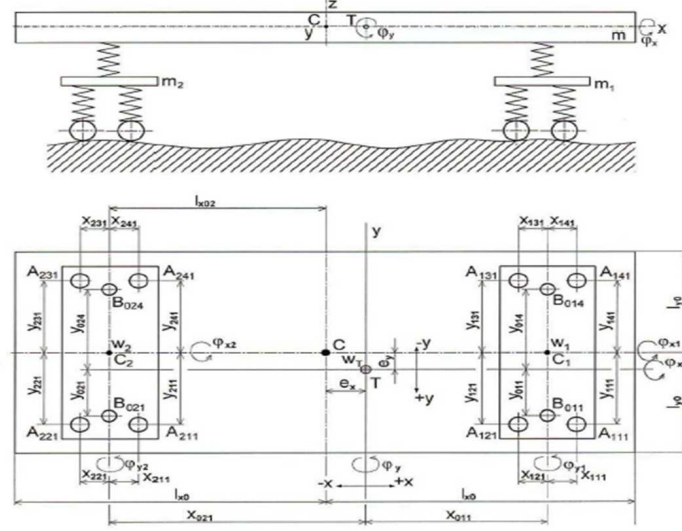


Figure 1: The analytical model.

kinetic energy E_k , potential energy E_p and Rayleigh dissipation function R_d of the mechanical system. The vectors of generalized coordinates system are given as

$$q_j(t) = [w, w_1, w_2, \varphi_x, \varphi_y, \varphi_{x1}, \varphi_{y1}, \varphi_{x2}, \varphi_{y2}]^T, \dot{q}_j(t), \ddot{q}_j(t). \quad (1)$$

The kinetic energy:

$$E_k = \frac{1}{2}m\dot{w}^2 + \frac{1}{2}(J_x\dot{\varphi}_x^2 + J_y\dot{\varphi}_y^2 - 2D_{xy}\dot{\varphi}_x\dot{\varphi}_y) + E_{k1} + E_{k2}, \quad (2)$$

where

$$E_{k1} = \frac{1}{2}m_1\dot{w}_1^2 + \frac{1}{2}J_{x1}\dot{\varphi}_{x1}^2 + \frac{1}{2}J_{y1}\dot{\varphi}_{y1}^2, \quad E_{k2} = \frac{1}{2}m_2\dot{w}_2^2 + \frac{1}{2}J_{x2}\dot{\varphi}_{x2}^2 + \frac{1}{2}J_{y2}\dot{\varphi}_{y2}^2.$$

To determine the potential energy of the mechanical system, it is necessary to determine the displacements, marked by A_{jki} , of the individual springs in the primary and secondary suspension system w_{jki} characterized by spring stiffness constant k_{jki} , where $j = 1, 2$, quadrant $k = 1, 2, 3, 4$ and spring position orders $i = 1, \dots, n$.

Points	Vertical displacements	Constant stiffness
A111	$w_{111} = w_1(t) - y_{111}\varphi_{x1}(t) + x_{111}\varphi_{y1}(t) - h_{111}$	k_{111}
A121	$w_{121} = w_1(t) - y_{121}\varphi_{x1}(t) + x_{121}\varphi_{y1}(t) - h_{121}$	k_{121}
A131	$w_{131} = w_1(t) - y_{131}\varphi_{x1}(t) + x_{131}\varphi_{y1}(t) - h_{131}$	k_{131}
A141	$w_{141} = w_1(t) - y_{141}\varphi_{x1}(t) + x_{141}\varphi_{y1}(t) - h_{141}$	k_{141}

Table 1: Front bogie (m_1) for $j = 1$.

Points	Vertical displacements	Constant stiffness
A211	$w_{211} = w_2(t) - y_{211}\varphi_{x2}(t) + x_{211}\varphi_{y2}(t) - h_{211}$	k_{211}
A221	$w_{221} = w_2(t) - y_{221}\varphi_{x2}(t) + x_{221}\varphi_{y2}(t) - h_{221}$	k_{221}
A231	$w_{231} = w_2(t) - y_{231}\varphi_{x2}(t) + x_{231}\varphi_{y2}(t) - h_{231}$	k_{231}
A241	$w_{241} = w_2(t) - y_{241}\varphi_{x2}(t) + x_{241}\varphi_{y2}(t) - h_{241}$	k_{241}

Table 2: Rear bogie (m_2) for $j = 2$.

In case of the car body (m), with the point marked by B_{jki} , their coordinates x_{jki} , y_{jki} , $j = 0$, $k = 1, 2$ respectively, $i = 1, 4$ and the k_{jki} individual springs as shown in Figure 2, are:

Points	Vertical displacements	Const. stiff.
B011	$w_{011} = w(t) - y_{011}\varphi_x(t) + x_{011}\varphi_y(t) - w_1 + (y_{011} + e_y)\varphi_{x1}$	k_{011}
B014	$w_{014} = w(t) - y_{014}\varphi_x(t) + x_{014}\varphi_y(t) - w_1 + (y_{014} + e_y)\varphi_{x1}$	k_{014}
B021	$w_{021} = w(t) - y_{021}\varphi_x(t) + x_{021}\varphi_y(t) - w_2 + (y_{021} + e_y)\varphi_{x2}$	k_{021}
B024	$w_{024} = w(t) - y_{024}\varphi_x(t) + x_{024}\varphi_y(t) - w_2 + (y_{024} + e_y)\varphi_{x2}$	k_{024}

Table 3: Car body (m).

The potential energy is:

$$E_p = \frac{1}{2} \sum_{j=1}^2 \sum_{k=1}^4 \sum_{i=1}^{k_j} k_{jki} w_{jki}^2 + \frac{1}{2} \sum_{j=0} \sum_{k=1,2} \sum_{i=1,4} k_{jki} w_{jki}^2. \quad (3)$$

The Rayleigh dissipation function is:

$$R_d = \frac{1}{2} \sum_{j=1}^2 \sum_{k=1}^4 \sum_{i=1}^{k_j} b_{jki} \dot{w}_{jki} + \frac{1}{2} \sum_{j=0} \sum_{k=1,2} \sum_{i=1,4} b_{jki} \dot{w}_{jki}. \quad (4)$$

The equations of motion for the railway model considered in this paper are derived from the Lagrange equation of motion (5). By substituting equations (2), (3) and (4) into equation (5) and after the derivation of equation (5) we have

$$\frac{d}{dt} \left(\frac{\partial E_k}{\partial \dot{q}_j} \right) - \frac{\partial E_k}{\partial q_j} + \frac{\partial E_p}{\partial q_j} + \frac{\partial R_d}{\partial \dot{q}_j} = Q_j \quad (5)$$

for $j=1, \dots, p=9$. According to [1] and [4], in the time domain the equations of motion for this system may be obtained in the general form as

$$\mathbf{M}\ddot{\mathbf{q}}(t) + \mathbf{B}\dot{\mathbf{q}}(t) + \mathbf{K}\mathbf{q}(t) = \mathbf{Q}_j(t), \quad (6)$$

where \mathbf{M} is the mass matrix, \mathbf{B} is the damping matrix, \mathbf{K} is the stiffness matrix and for generalization, all elements of matrix \mathbf{B} and \mathbf{K} are considered not to equal zero.

$$\mathbf{q}_j(t) = [w, w_1, w_2, \varphi_x, \varphi_y, \varphi_{x1}, \varphi_{y1}, \varphi_{x2}, \varphi_{y2}]^T, \dot{\mathbf{q}}_j(t), \ddot{\mathbf{q}}_j(t)$$

are the vectors of the generalized coordinates and $\mathbf{Q}_j(t)$ is the vector of the generalized kinematic excitation functions. After dividing equation (6) by the respective diagonal

element of the mass matrix \mathbf{M} and after the Laplace transformation for the zero initial conditions $q(0)$ and $\dot{q}(0)$, the system of differential equations is transformed to the system of algebraic equations

$$\mathbf{G}\bar{q}(s) = \bar{f}(s), \tag{7}$$

where s is the parameter of transformation, $\bar{q}(s)$ and $\bar{f}(s)$ are the vectors of the generalized coordinates $q(t)$ and forces $f(t)$. It holds for the elements of the matrix \mathbf{G} :

$$\begin{aligned} g_{ij} &= s^2 + \beta_{ij}s + \kappa_{ij}, && \text{for } i = j, \\ g_{ij} &= -\delta_{ij}s^2 + \beta_{ij}s + \kappa_{ij}, && \text{for } i \neq j \text{ and for } i = 4, 6, 8 \text{ and } j = i + 1, \\ g_{ij} &= \beta_{ij}s + \kappa_{ij}, && \text{for } i \neq j \text{ and for } i = 5, 7, 9, \\ &&& \text{and } j = i - 1 \text{ for } i = 3, \dots, 9 \text{ and } j = 1, \dots, 9, \end{aligned}$$

where $\delta_{12} = -\frac{D_{xy}}{J_x}$ and $\delta_{21} = -\frac{D_{xy}}{J_y}$ are the elements representing the influence of asymmetric distribution of the sprung mass.

For solving the system of algebraic equations (7), it is possible due to small number of equations, to apply the Cramer rule [1] as follows

$$\bar{q}_j(s) = \sum_{i=1}^{n/2} (-1)^{j+i} \bar{f}_i(s) \frac{D_{ji}(s)}{D(s)}, \quad j = 1, 2, \dots, n/2, \quad n = 18. \tag{8}$$

This method is suitable regarding the process of obtaining the vector of the generalized coordinates $q(t)$ by the inverse transformation. In order to determine the original $q_j(t)$ of the corresponding image $\bar{q}_j(s)$ it is necessary to transform equation (8) to the form of convolution integral. Therefore, it is necessary to find the poles of the characteristic polynomial $D(s)$ of equation (8) [1]. The poles are supposed to be in the form of complex conjugates $s_i = -Res_k \pm Im s_k$, for $k = 1, 2, \dots, n/2$. To evaluate the poles of the characteristic equation $D(s)$, it is necessary to equate the polynomial in the form of the product of the quadratic polynomials using the product of the roots factors $s^2 + p_k s + r_k$, for $k = 1, 2, \dots, n/2$. The polynomial responding to the sub-determinant $D_{ji}(s)$ is determined using the same algorithm.

In order to determine the original $q_j(t)$ of the corresponding image $\bar{q}_j(s)$ it is suitable to transform equation (8) to the form of convolution. Therefore it is possible to transfer the ratio of the determinants in equation (8) to the sum of partial fractions in the form

$$\frac{D_{ij}(s)}{D(s)} = \frac{\sum_{r=1}^{n/2} \left[(K_{ji,r}s + L_{ji,r}) \prod_{k=1, k \neq i}^{n/2} (s^2 + p_k s + r_k) \right]}{\prod_{k=1}^{n/2} (s^2 + p_k s + r_k)} = \sum_{r=1}^{n/2} \frac{K_{ji,r}s + L_{ji,r}}{s^2 + p_k s + r_k}, \tag{9}$$

where the constants $K_{ji,r}$ and $L_{ji,r}$ for $j = 1, 2, \dots, n/2$, $i = 1, 2, \dots, n/2$, $r = 1, 2, \dots, n/2$, can be determine from the condition of the coefficients equality of the identical powers of the parameter s in the numerator of the fractional equation (9). By substituting equation (9) into equation (8) for the determination of the image of the generalized coordinates $\bar{q}(s)$, for $j = 1, 2, \dots, n/2$, the latter can be modified as follows

$$\bar{q}_j(s) = \sum_{i=1}^{n/2} (-1)^{j+i} \bar{f}_i(s) \sum_{k=1}^{n/2} \frac{K_{ji,k}s + L_{ji,k}}{s^2 + p_k s + r_k}. \tag{10}$$

After inverse transformation of equation (10) for the function of the generalized coordinate $q_j(t)$, for $j = 1, 2, 3, \dots, 9$, the form of the sum of convolution integrals is obtained as follows

$$q_j(t) = \sum_{i=1}^9 (-1)^{j+i} \sum_{k=1}^9 [G_1 + G_2], \quad (11)$$

where

$$G_1 = K_{ji,k} \int_0^t F_i(\tau) e^{-\beta_k(t-\tau)} \cos[\Omega_k(t-\tau)] d\tau,$$

$$G_2 = \frac{L_{ji,k} - \beta_k K_{ji,k}}{\Omega_k} \int_0^t F_i(\tau) e^{-\beta_k(t-\tau)} \sin[\Omega_k(t-\tau)] d\tau.$$

Equation (11) shows the solution for a linear viscous damped mechanical system, where j -th component of vector of generalized coordinates $q_j(t)$ is the sum of convolution integrals, multiplied by i -th generalized kinematic excitation elements $F_i(t)$ designated by the product of spring constant and height of the road or rail surface unevenness and by product of damping coefficient b_{jik} , and time derivative of height contact place of the m -index wheel at specific crossing velocity, to the k -th harmonic component with its own natural frequency Ω_k . K_{jik} and L_{jik} are unknown coefficients of amplitude, depending on the mechanical properties of the system under consideration. Vector components of the kinematic excitation function $F_i(t)$ are given in the range of $0 \leq t$.

5 Production and Construction Asymmetry of the Mechanical System

In this paper asymmetry of the distributed sprung mass of the railway vehicle is simulated as shown in Figure 2, where Figure 2a shows the symmetrical case, where $T = C$, $e_x = e_y = 0$ and Figure 2b shows the asymmetrical case, where $T \neq C$, $e_x \neq 0$ and $e_y \neq 0$. The position of the external weight placed on the surface of the wagon introduces weight eccentricities due to the uneven distribution of the sprung mass of the mechanical system. This effect causes the center of mass to be arbitrarily positioned so that no symmetry exists in the system, as a result of this the system center of mass T is shifted along the x -axis and y -axis directions with respect to the system's geometrical center. Meanwhile, Figure 2 shows the arrangement of rail defects as kinematic excitations; Figure 2c shows the symmetrical arrangement of the multiple track irregularities on the track, while Figure 2d shows the asymmetrical arrangement of rail defects. Meanwhile Figure 3 shows different cases of asymmetry and the arrangement of the multiple track irregularities (kinematic excitation) on both rails. In this paper the multiple track irregularities are modeled as a unit step function.

6 Experimental Tests

Experimental tests were done on a four-axel freight wagon of *Smmps* type. The railway freight wagon was modified in a way to be in accordance with the requirements of the analytical model derivate in Section 2. The original bogies were removed from the wagon and replaced by another bogie of Y25 type from a passenger freight car. The outer springs of the primary spring system of these bogie frames were removed and secondary spring system, consisting of three springs was fitted to the bogie frames. The bogie frames were

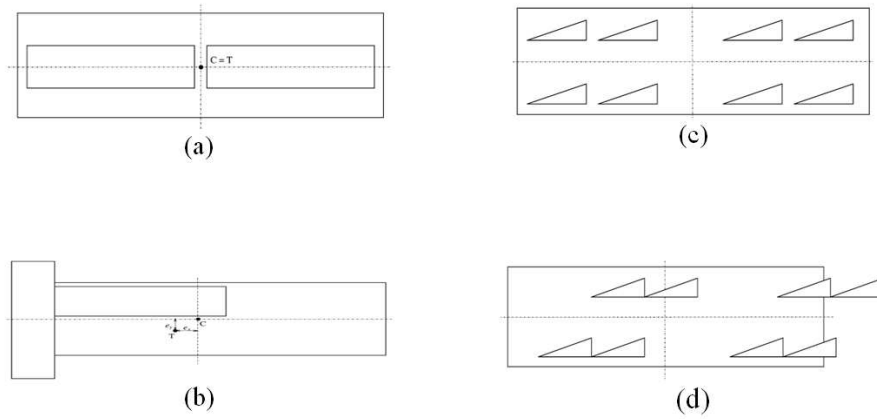


Figure 2: The analytical - symmetry and asymmetrical model, (a) Symmetrical and (b) asymmetrical distribution of the sprung mass (c) Symmetrical and (d) asymmetrical of multiple track irregularities.

Chocks p. of loads	Chocks					
	I	II	III	IV	V	VI
A	A - I	A - II	A - II	A - IV	A - V	A - VI
B	B - I	B - II	B - III	B - IV	B - V	B - VI
C	C - I	C - II	C - II	C - IV	C - V	C - VI
D	D - I	D - II	D - II	D - IV	D - V	D - VI
E	E - I	E - II	E - III	E - IV	E - V	E - VI

Figure 3: Symmetric and asymmetric model.

fixed to the wagon by means of wire ropes net to keep the car body in equilibrium, see Figure 4 and Figure 5 respectively.



Figure 4: Secondary spring system.



Figure 5: Connection of bogie frame to car body.

6.1 Test procedures

The vertical vibration responses of the freight wagon were done as follows:

- The freight wagon loaded as illustrated in Table 1 was towed by a shunting locomotive to move over track irregularities. The locomotive was connected to the car body with a wire rope. The wedge blocks stimulated the Heaviside unit function.
- The measurements were sensed by means of HBM amplifiers, signals went through the low-pass filter 32 kHz into the digital-to-analogue system DAS 48.
- Each test was repeated 2 – 3 times. A total of 89 tests were measured. Twenty quantities were measured during the tests – the bogie frames relative vertical vibration response with respect to the axle-box (9 sensors), car body relative vertical vibration response with respect to the front and the rear bogie frames (4 sensors), vertical acceleration of the car body (5 sensors) and finally, acceleration of the bogie frames (2 sensors). The purpose of these tests was to determine and record time histories of relative vertical vibration response of the freight wagon in the presence of production and construction asymmetry and multiple general kinematic excitations to verify the theoretical model in Section 2.

7 Analytical Solutions

Two types of analysis were performed in this paper in order to investigate the effects of production and construction asymmetry on the vertical vibration response of the railway vehicle in the presence of multiple track irregularities. The first analysis was done for simulated analytical data set and the second was for experimental data to validate the analytical model. The analytical data was processed using a MatLab code, which was written specifically for this investigation. In regard of large amount of collected data, it was not possible to process and include all the results into this one investigation report, because of its very limited extent. Therefore, the present work comprises only general conclusions. Figure 6, shows the analytical results processed using a MatLab code for the symmetrical (a) and asymmetrical (b) distribution of the sprung mass running over uneven track irregularities (d), as shown in Figure 2. The results showed the expected

trends of vertical vibration response of the model with no definite cut off between stable and unstable behavior.

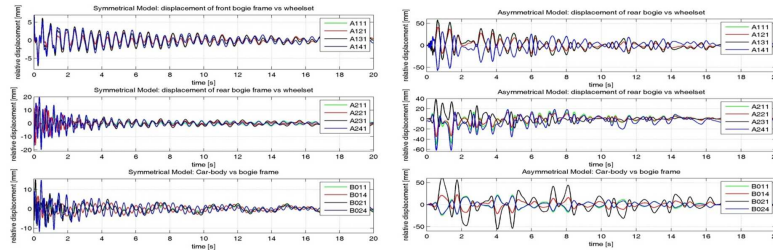


Figure 6: Vertical dynamic response due to a single unit step on all wheels on the right side of the wagon.

8 Validation of the Developed Model

The developed model has been validated using the experimental data reported by *J.Soukup* and *J.Volek*, see [1] for more detail. The parameters employed in the simulation are obtained from reported studies [6]. The comparisons between the responses obtained by the developed model in Section 4 with that of the reported study are shown in Figure 7. The results showed expected trends of vertical vibration response in the presence of production and construction asymmetry of the mechanical system. It is quite evident, that good agreement with a 9DOF vehicle model has been achieved, but several limitations of the model have been identified. The significance of these limitations is currently being investigated with more additional degrees of freedom. It can be concluded that, the influence of production and construction asymmetry on the vertical vibration response in the presence of multiple track irregularities is obvious. Hence detail analysis of this phenomenon is a necessity in railway vehicle design process.

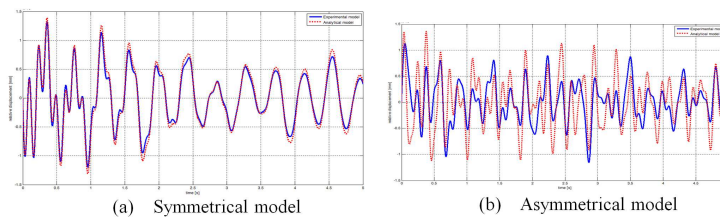


Figure 7: The comparisons between the responses obtained by the developed model with that of the reported study.

9 Conclusion

The present paper confirmed the influence of production and construction asymmetry of railway vehicle in the presence of multiple track irregularities inputs. In regard to

the large amount of collected data, it was not possible to process and include all the results into this one investigation report, because of its very limited extent. Therefore, the present work comprises only general conclusions.

Acknowledgment

The research work is supported by the Student Grant Agency (SGA) UJEP, Czech Republic. The current paper has been successfully presented during the 12th Conference on Dynamical Systems Theory and Applications (DSTA), in Lodz, Poland (2013).

References

- [1] Soukup, J., Volek, J. et. al. *Vibration of Mechanic Systems-Vehicles*. UJEP, Usti nad Labem, 2008.
- [2] Ellis, J.R. *Road Vehicle Dynamics*. J. R. Ellis, Ahron, USA, 1989.
- [3] Wang, T. L. Impact in a Railway Truss Bridge. *Computers and structures journal* **49** (6) (1993) 1045–1054.
- [4] Gillespie, T.D. *Fundamental of Vehicle Dynamics*. SAE international, 1992.
- [5] Karl, P. and Werner, S. *Ground Vehicle Dynamics*. Stuttgart, Germany, 1993.
- [6] Nangolo, N. and Soukup J. *Modeling of Vertical Dynamic Response of Railway Vehicle System with Experimental Validation*. Machine Modeling and Simulation. Poland, 2012.
- [7] Gerlici, J. and Lack, T. Modified HHT Method for Vehicle Vibration Analysis in Time Domain Utilisation. *Applied Mechanics and Materials* **486** (2013) 396–405.
- [8] Yakushevich, L. V., Gapa, S. and Awrejcewicz, J. Mechanical Analog of the DNA Base pair. In: *Dynamical Systems Theory and Applications*. Lodz, 2010, 879–886.
- [9] Wu, T. X. and Thompson, D. J. On the impact noise generation of due to a wheel passing over rail joints. *Journal of Sound and Vibrations* **267** (3) (2003) 485–496.
- [10] Sun, Y. Q., Dhanasekar, M. and Roach, D. A three-dimensional model for the lateral and Vertical Dynamics of wagon-track system. *Journal of Rail and Rapid Transit* **217** (1) (2003) 31–45.
- [11] Wen, Z., Xiao, G., Xiao, X., Jin, X., Zhu, M. Dynamic vehicle-track interaction and plastic deformation of rail at rail welds. *Engineering Failure Analysis* **16** (4) (2009) 1221–1237.
- [12] Andersson, C. and Abrahamsson, T. Simulation of interaction between a train in general motion and a track. *Vehicle System Dynamics: International Journal of Vehicle Mechanics and Mobility* **38** (6) (2002) 433–455.
- [13] Zhai, W. and Cai, Z. Dynamic interaction between a lumped mass vehicle and a discretely supported continuous rail track. *Computers & Structures* **63** (5) (1997) 987–997.
- [14] Zhai, W. M., Cai, C. B., Wang, Q. C., Lu, Z.W. and Wu., X. S. Dynamic effects of Vehicles on Tracks in the case of raising train speed. *Journal of Rail and Rapid Transit* **215** (2001) 125–135.
- [15] Dong, R.G. *Vertical Dynamics of Railway Vehicle-Track System*. PhD Thesis, Dept. of Mechanical and Industrial Engineering, Concordia University, Montreal, Canada, 1994.
- [16] Cai, Z. *Modeling of Rail Track Dynamics and Wheel Rail Interaction*. PhD thesis, Dept. of Civil Engineering, Queens University, Kingston, Ontario, Canada, 1992.
- [17] Nielsen J.C.O. and Igeland A. Vertical dynamic interaction between train and track influence of wheel and track imperfections. *Journal of Sound and Vibration* **187** (5) (1995) 825–839.
- [18] Pilipchuk, V. Acceleration Control in Nonlinear Vibrating Systems Based on Damped Least Squares. *Journal of Sound and Vibration* **13** (2) (2013) 181–192.



Researches Defining the Characteristics of Hyperelastic and Composite Materials with Gas Phase in the Vehicle–Pedestrian System

J. Osinski* and P. Rumianek

Warsaw University of Technology, The Institute of Machine Design Fundamentals, 84 Narbutta Str., 02-524 Warsaw, Poland

Received: March 31, 2014; Revised: December 22, 2014

Abstract: The aim of this work is to develop methods of describing the properties of materials based on knowledge of: basic materials, technologies (gas pressure formed during foaming) using the theory of hyperplastic materials, in particular using Ogden’s model and its modifications. The aim also goes on to analyze the possibility of energy dissipation between a pedestrian and a vehicle on impact. The energy created during the impact will be dissipated by the element of protection made of a hyperdeformable material. The resulting description can be used for the applicability of hyperelstic models, and therefore in the whole range of deformation of the polymer-based composites and elastic composites of metals (excluding plasticity). This thesis further presents analytical methods of hyperelastic materials using Finite Elements Method. Using FEM it is possible to verify used materials, define the materials models and show the effectiveness of the designed component without performing any expensive impact tests. The presented methods and applications of the characteristics of hyper elastic materials and composites with the gas phase are used to determine the proper selection of parameters (material properties), increasing the opportunities for a proper assessment of the effectiveness of safety devices.

Keywords: *energy dissipation; intensive construction; hyperelstic materials; gas phase; gasar; crushable foam.*

Mathematics Subject Classification (2010): 93A30.

* Corresponding author: <mailto:jerzy.osinski@ipbm.simr.pw.edu.pl>

1 Introduction

Hyperelastic materials and composites with the gas phase have wide applications due to their thermal properties and ability to absorb energy tremendously. The structure of these materials resembles closed cells, in which we find two phases: the solid phase, from which the material is formed and the gas phase, which is formed as a result of ongoing physical or chemical phenomena during the stages of production. The relevant properties of the structure are obtained not only by the choice of the way of producing, but also through appropriate selection of materials and proper design of the structure geometry.

The study's aim is to develop a methodology and an overall assessment of the analysis of elements made of hyperelastic foams and composites with gas phase. The main aspect that has been considered is to determine the properties of the materials, as well as to assess the potential energy dissipation by elements made of the above-mentioned materials. The methods of modeling hyper elastic materials and composites with the gas phase are applicable to the structure to increase the safety of the passengers in the vehicle and outside the vehicle as well as of the materials used in motorcycle and bicycle helmets. The used materials have a high capacity to transfer the kinetic energy during impact, which is compensated by the destruction process (crushing, breaking). The developed methodology of analysis using the Finite Element Method allows to not only determine the properties of the tested materials, evaluate the ability to dissipate energy, but above all, without the need for costly impact tests, to show the effectiveness of the protective elements.

To determine the properties of any selected materials two experimental stages are involved, which take into account the intended use [5]. The first step is to conduct experimental research carried out in accordance with standard specifications: PN-EN ISO 604:2004, PN-EN ISO 604:2006, PN-H-04320:1957 [2].

In the second stage, using the theory of hyperelastic materials and MES - Abaqus, simulating the specified data set experimentally during the first stage, we select the appropriate model, the description of which is the most consistent. Owing to the simulation we can properly determine the coefficients of the model. For the analysis it is necessary to use polynomial models, such as Ogdens model or hyperfoam model. Conducted experimental studies were performed using strength machines located at the Faculty of Automotive and Construction Machinery Engineering and Department of Materials Science and Engineering of the Warsaw University of Technology.

2 The Material

Tests of samples, made of foamed polypropylene used for the implementation of the protective elements, which is a plastic material having the form of interconnected gas filled granules, were carried out. After several studies it can be noticed that there are bubbles in the interior of the granules called the cell structure. Due to the type used for research of the testing machine, the samples were made in two sizes: 80mm x 80mm and height of 40mm, and 20mm x 20mm and 30mm height. The variety of foams having a density from 25 to 220 g/dm³. Tests were also carried out for samples of different shape, which made it possible to assess the impact on the mechanical ability of the shape of the material [6, 7].

Also, the tests were carried out of pedestrian protection element used in the VW car Skoda Fabia II (Figure 1). For energy absorber (pedestrian protection element) a fastening element was made, which makes it possible to mount the machine for strength

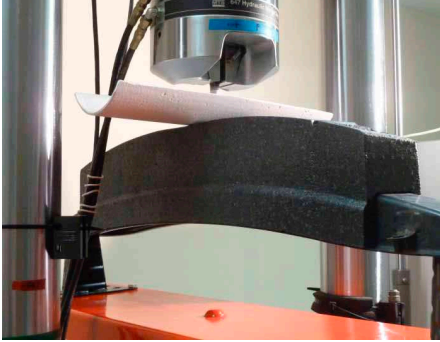


Figure 1: Energy absorber used in the VW car Skoda Fabia II.

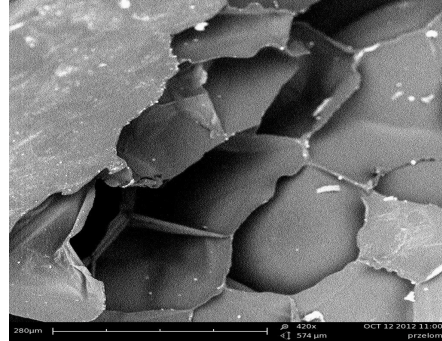


Figure 2: SEM image of pedestrian safety element fracture made of polypropylene foam.

research.

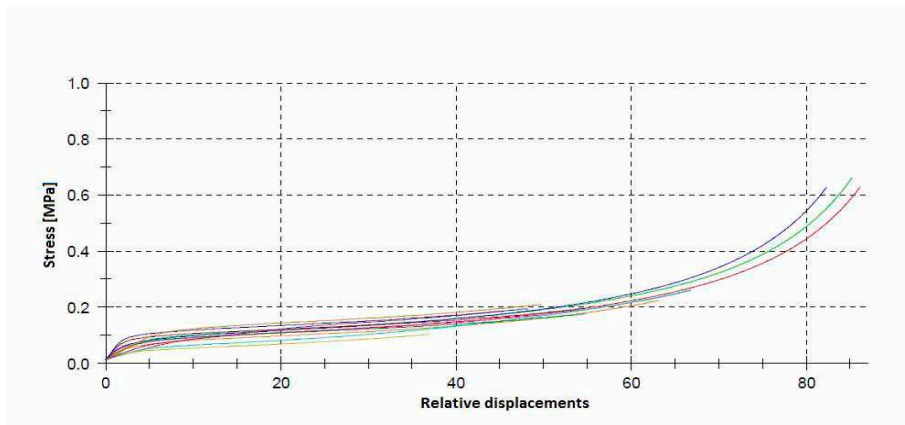


Figure 3: Series of compression curves set experimentally.

3 Methodology of Research

3.1 Determination of structure of the material

The material from which the sample was made, was not linked to the other form of gas-filled granules. Material with such structure is suitably formed in forming machines, during the formation of the granules taking the form of closed-cell structures creating a material having a relatively high rigidity (Figure 2). The use of granules of different sizes effects on the alteration properties of the foam. To determine the properties of the structure it was necessary to conduct a study which was carried out in the Department of Integrated Process Engineering at the Faculty of Chemical and Process Engineering of Warsaw University of Technology.

During the study, there were no adhesive substances between the granules. The material has a high temperature resistance, up to about 150°C, excellent thermoformability

and shape memory (large capacity to return to its original shape after static and dynamic loads). Due to the fact that the process of formation of the foam is expanding - foaming granules of material such as polypropylene with water vapor and using pressure, the granules are combined with each other while increasing the volume. More than 90% of the volume of foam produced in the process is air.

3.2 Experimental studies

Static test for plastic compression is different, due to the nature of the deformation. Stress-strain characteristics obtained in the compression test for the tested materials are shown in the drawing (Figure 3).

In all tests the temperature changes have been recorded by the pyrometer. The compressive strength was determined using a sample testing machine Q-test 10 of MTS and Zwick / Roell Z005. The samples were prepared in the form of cuboids. The research component of pedestrian protection, due to the large size, compression test took place only on the first machine. The compression rate at 23°C for the first machine was 5 mm/min, the second machine – 1 mm/s. Tests were also made for the cold samples, which were cooled with dry ice. During the course of the test, recordings were made according to the compression force between the piston and the piston displacement, which constituted the first part of the experimental testing. On this basis, the following samples were made for graphs showing the dependence of the deformation stress. Taking into account the effect of the initial temperature, the samples were studied with the initial temperature 23°C and -15°C. On this basis, the hysteresis loop was determined as in the case of quasi-static compression.

3.3 The simulation studies

Analysis of simulation models was made using a system Abaqus FEA (Finite Element Method), which allows us to fit models that exist in the database, according to the theory of hyperelastic materials. Simulations were made by using the EXPLICIT module. Numerical analyses were performed for the samples appropriately modeled and for the security of the element. The models were constructed using the Catia V5R19. During the simulation, the effect of friction during deformation of the foam structure led to the crimping of a gas-filled cell. For safety element model, the structure model takes into account the issue of the structure of the material contact problem. The evaluation of dynamic loads: stresses, accelerations and deformations occurring during the impact against a pedestrian, allows for the ability of a material to absorb the energy. Except for the actual values of the coefficients, α_i leads to a nonlinear model, which allows for the description of materials and compressibility [4].

Ogden's model can include different cases (Figure 4). If we accept the description of the coefficients $\alpha_i = 2, 4, 6, \dots$, then we have a polynomial model, including various special cases: models of Mooney-Rivlin (Figure 5), Yeoch and Neo-Hookean (Figure 6). By introducing the equation of α_i coefficients with fractional values, we obtained nonlinear model already in the first approximation [4]. The values of the coefficients are determined based on experimentally defined approximations of the stress - strain. The data of Ogden's material model were determined on the basis of research conducted at the Institute of Mechanical Engineering at the Faculty of Automotive and Construction Machinery Engineering and Department of Materials Science and Engineering, Warsaw University of Technology. The material has been described by the third row of the

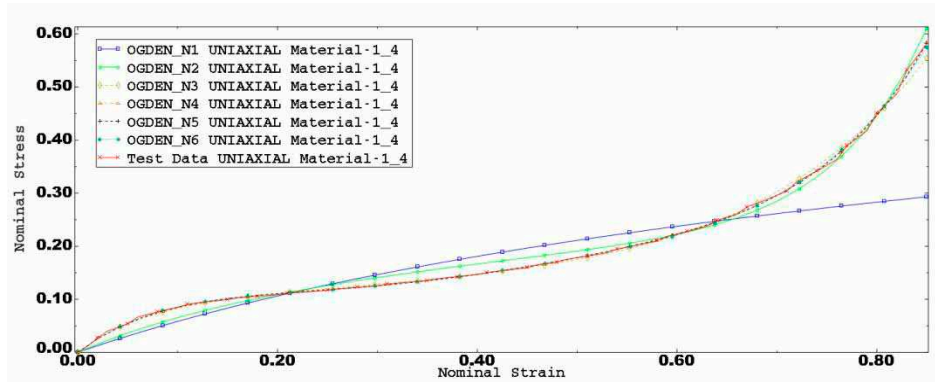


Figure 4: Series of compression curves set experimentally. Ogden's models.

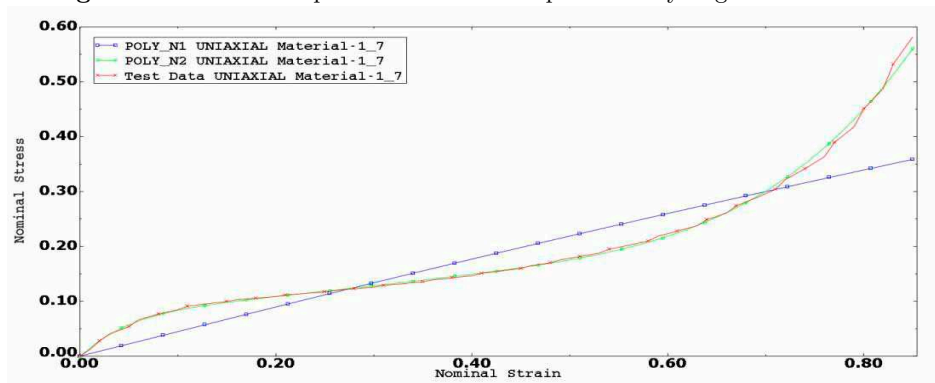


Figure 5: Series of compression curves set experimentally. Polynomial- Mooney-Rivlin model.

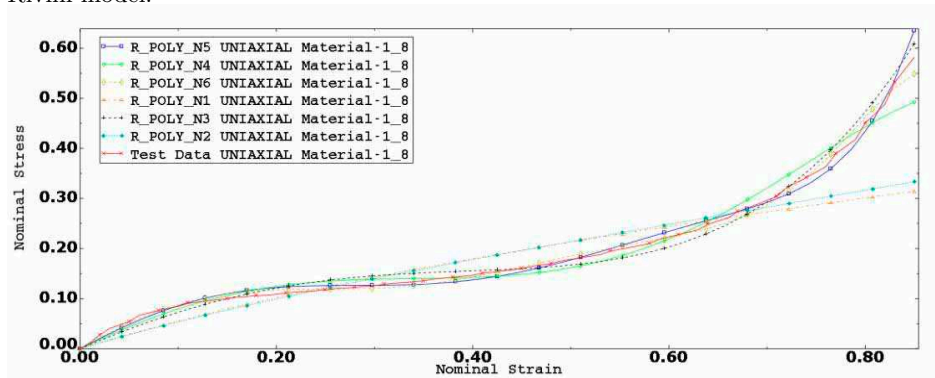


Figure 6: Series of compression curves set experimentally. Reduced Polynomial-Neo-Hookean model.

Ogden's model [1]. The coefficients of Ogden's material impact attenuator model, used in the simulation, are presented in Table 1.

For modeling foam, we can modify the Ogden's model with the introduction of real

i	μ_i	α_i	D_i
1	-1062310,50	7,701	8,6448
2	781324,564	8,0848	0
3	776736,53	-11,4395	0

Table 1: Description of the foam properties of the third row Ogden's model – coefficients.

exponent in the second part of the equation which describes the volume deformations (in this case, they are also non-linear dependances) (Table 2). In the calculations using the FEM application we can choose the hyperelastic model, for which the set of properties have been described.

i	μ_i	α_i	D_i
1	-832131,49	16,20948	8,935334
2	831230,727	16,21166	0
3	-2528968,43	-1,172925	0

Table 2: Description of the foam properties of the hyperfoam model – coefficients.

To select the model which reflects the actual behavior of the material for which we carry out experimental studies, the results from both studies should be compared (compare the results with the results of experimental tests of the numerical model). For the materials considered, series of comparisons have been made for different types of models. The final results of the process revealed that the most consistent stresses waveforms in the real and numerical studies have occurred for the Ogden's model.

4 Conclusions

The results of the analyses allow us to conclude that the testing methodology and impact simulation of element (pedestrian protection element) and test samples can assess the effectiveness of the protection of pedestrians and assessment of hyperelastic materials and composites with the gas phase. Research has shown that during the tests the energy dissipation is followed by the foam elements. The study of these documents and the existing elements of pedestrian protection is very important because it not only makes it possible to determine the extent to which we can protect the victims of accidents, but also reduce the consequences of such accidents. Detailed research and analysis allow us to see what events occur during a crash in the applied material. Model foam structures take into account the phenomenon of energy dissipation. The nature of the energy dissipation phenomena varies with the speed of deformation. Such dependencies are determined by numerical simulation of deformation. To build the model, the information on the manner of their production emanate from the achievements of material engineering.

It is important to analyze the problems occurring at the interface between the contact surface and within the material at the contact surfaces of the hyperdeformable element (foamed structure) with other structural elements made of steel or other materials. This thesis affords us the ability to integrate aspects of material engineering in the making of foam structures to the mechanics of materials and structural strength (evaluation of

elastic and plastic properties in terms of high-speed deformation) and the operation of vehicles in the range of passive safety. Compression tests of executed samples of the material were carried out to develop models that correspond to the material used. This thesis further contributes to the development of the use of Finite Element Method to simulate rapidly-variable loads - possible methods are not yet fully exploited. The tests are considered to expand the applicability of modern construction materials, plastic and composites. Completed studies are not possible without the correct description of the properties of this type of materials. The use of well-known models for hyperelastic materials: reduced polynomial, Ogden's and non-linear models, allows us to have the correct description of the properties of the tested materials. Isotropic materials are analyzed in the theory of hyperelasticity, which presupposes the existence of the positive features of elasticity and specific energy of the natural state of the body. It will consider any form of deformation of the body for large deformations and processes that take into account the thermal effects during manufacturing. Models materials together with modifications may be used to evaluate the energy absorption, proposed to be used in the description of the simulation performed using the program Abaqus. For the materials considered the relationship between stresses and strains, which are dependent on the material properties can be determined. The use of the modified Ogden's model makes it possible to accurately determine the description of the material, which makes it possible to increase the accuracy and effectiveness of the simulation. The carried out research allow for an even better way to make a selection of the material and its properties.

Acknowledgment

I would like to thank the Organising Committee of the 12th Conference on Dynamical Systems – Theory and Applications for the possibility of presenting, and publishing of our article in the conference proceedings in *Dynamical Systems Theory* – summary of 34 best papers of university teachers and students, researchers and engineers.

References

- [1] Dudziak, M. and Mielniczuk, J. *Non-classical Models of the Materials in Machine Design*. Publisher Institute for Sustainable Technologies, Radom, 2001.
- [2] Boczkowska, A. and Babski, K. Modeling compression characteristics and properties of polyurethane materials used in the construction of machines. In: *Polimery 7/8*, vol. LIII, Warszawa, 2008.
- [3] Desphande, V. and Fleck, N. Isotropic Constitutive Model for Metallic Foams. *Journal of the Mechanics and Physics of Solids* **48**, Radom, 2000.
- [4] Iwanowski, A. and Osinski, J. *Evaluation of Energy-Consuming of Elastic-Plastic Stiff Foam in Case of Huge Volumetric Deformation*. Machine Dynamics Problems, Warszawa, 2003.
- [5] Ogden, R. *Nonlinear Elasticity with Application to Material Modeling*. Institute of Fundamental Technological Research, Polish Academy of Sciences, Lecture Notes 6, Warszawa, 2003.
- [6] Osinski, J. and Rumianek, P. Simulation of energy dissipation during impacts with hyper-elastic elements. *Machine Dynamics Research* **36** (2) (2003) 87–98.
- [7] Osinski, J. and Rumianek, P. Application of modified Ogdens model for describing features of composites with gas phase. *Machine Dynamics Research* **36** (2) (2003) 76–83.



Mathematical Modeling of the Hydro-Mechanical Fluid Flow System on the Basis of the Human Circulatory System

W. Parandyk*, D. Lewandowski and J. Awrejcewicz

*Department of Automation, Biomechanics and Mechatronics, Lodz University of Technology,
B. Stefanowskiego 1/15, 90-924 Lodz, Poland*

Received: March 31, 2014; Revised: January 19, 2015

Abstract: The primary objective of this study is to examine a human/mammal circulatory system. Considering structures and operating rules of a natural, biological circulatory system one can easily state that it is possible to create an analogous hydromechanical dynamic system. Noting the similarities and taking into account blood and vessels features there is a mathematical model given that includes differential equations of the fluid mechanics. Additionally a stand/analog consisted of hydraulic and electronics elements is presented. A prototype of the circulatory system is proposed with a construction of the heart as a bicapsular pumping unit powered by external pneumatic system. Solving the equations describing biological system, gives opportunities to examine some external and internal risk factors, model input signals and activity under different conditions.

Keywords: *mathematical modeling; fluid flow; circulatory system; biomechanics.*

Mathematics Subject Classification (2010): 93A10, 93A30.

1 Introduction

Considering anatomy and operating principles of biological human/mammal circulatory system (cardiovascular system) one can state that structurally it should be regarded as a hydro-mechanical closed-loop system. Because of the fact that anatomically, considered system is well-examined structure with application of a wide range of fields of science devoted to it (see [4-6]), we are able to exploit available knowledge combining with

* Corresponding author: <mailto:wiktor.parandyk@dokt.p.lodz.pl>

mechanics to create both simulation and mathematical system and laboratory structure, which yields possibility to make a comparison of numerical and experimental results.

Analyzing the state of knowledge regarding the mentioned problem and owing to the results presented in reference [7], the functional analysis of the biological circulatory system has been carried out to develop hydraulic system scheme. The proposed hydraulic system dynamics is governed by ordinary differential equations. An important feature of presented model is an oscillating forcing function that refers to the periodic signal of the heartbeat with the highlighted following phases of the heart muscle contractions. According to the biological data, selected parameters have been empirically estimated that characterize the mechanical properties (see [3]) of the system (the vascular elasticity, the flow resistance, the viscosity of a hydraulic fluid, the stroke volume) while checking the reliability of the results against the statistical data for the interesting physical quantities of the circulatory system. It seems to be obvious that the complexity of the biological structure of the vascular system carries implications in terms of structural simplification of the laboratory. An enormous number of small body capillary vessels or bronchioles capillary net and their branches, where gas exchange occurs, additionally the strict connection with opened lymphatic system is structurally an issue not to wade. To get the highly comparative to natural flow conditions there were implemented both the flow direction and resistance control hydraulic components. Moreover, because of the fact that one of the most significant natural blood vessels properties elasticity, has to be considered, the rigid hydraulic hoses were complemented by adjustable, vulnerable capsules so that the ripple of the blood vessels can be reflected during the operation of the system (including different venous and arteria compliance). The artificial heart construction (pump) was also proposed as a pneumatically controlled bicapsular, diaphragm pumping unit whereby the greatest structural and functional similarity to anatomical system was obtained. The hydraulic structure was expanded by a measurement system using absolute pressure sensors and measurement data acquisition module. Thanks to this construction, we are able to keep up with changes of the measured relevant values.

The creation of a complete simulation model and developing laboratory rig by another mechanical components gives possibility to examine the system behaviour under various conditions meaning input pattern signal disorders and changes (heart rythm). Moreover, it is also possible to generate artificial pathological conditions such as for example ventricular tachycardia or cardiac arrhythmias.

2 Simulation Model

2.1 The hydro-mechanical model basis

The following assumptions are used while carrying out the analysis of the working fluid flow in the considered closed system:

- the working fluid in the system is incompressible;
- differences in elevation as it flows in a horizontal arrangement do not exist;
- mass forces (inertial forces) do not affect the movement of the fluid;
- the flow is laminar.

It can be concluded that in the proposed model, the only physical factor causing the movement of the fluid is external, pressure forcing signal (eg, the pressure generated by

the movement of the piston pump). It is convenient, therefore, to describe the flow in the system, using the mass conservation principle (indestructibility of matter).

As shown in Figure 1, we can write the law of conservation of mass in the analytical form for the volume V , and the surrounding control surface S :

$$\frac{dm}{dt} = \int \int_S \rho v_N dA, \quad (1)$$

where m is the fluid mass contained in the volume V , ρ is the fluid density, v_N is the velocity vector, normal to the element of the control surface dS .

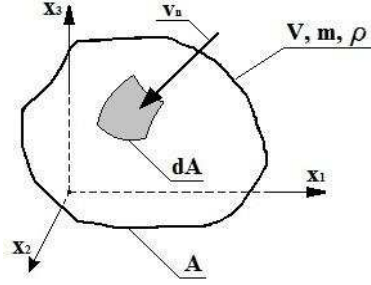


Figure 1: Model of fluid volume area.

Because in the real system, important for the analysis, flows through hydraulic elements (throttle valves, leakage, fluid supply elements, the hydraulic casing and fluid compliance, the volume changes of the cylinder-source of the fluid motion) are modeled as discrete object/elements, we are able to use the discrete instead of continuous model. As a result of the discretization of the model (see Figure 1), the equation (1) takes the following form:

$$\frac{dm}{dt} = \sum_{i=1}^n \rho v_{N_i} \Delta A_i, \quad (2)$$

This is the datum form of the equation, and after some trivial transformations (see [1]) the mass elementary flows balance equation is obtained:

$$\sum_{i=1}^n Q_i = \pm A \dot{x} + (C_0 + C_0 \frac{p}{E} + \frac{V_0}{E} \pm \frac{A}{E} x) \dot{p}, \quad (3)$$

where: dotted x and p in the notation given are respectively $\frac{dx}{dt}$ and $\frac{dp}{dt}$, A is the cylinder working surface, x is the movement coordinate of the piston, C_0 is coefficient of compliance of the deformable elements in the system, p is a pressure, V_0 is the initial volume of the fluid, E is the Young's modulus of the hydraulic fluid.

Of course, the applied notation of either '+' or '-' in a component of the equation is based on the direction of the forcing flow (in the present case the hydraulic cylinder piston movement direction). Other terms of the equation express the elementary flows associated with the deformation of both the elements and medium.

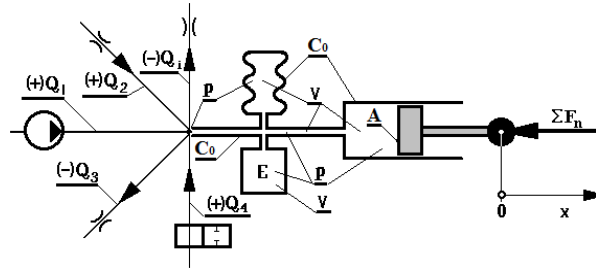


Figure 2: The physical model of the hydro-mechanical system [1].

2.2 The human cardiovascular system versus hydro-mechanical model

The diagram of the physical model of the hydro-mechanical system (shown in Figure 2) can be easily applied to a biological system of blood circulation in the human body. It should be emphasized that the circulatory system is a closed-loop system so the overall balance of mass elementary flows must be zero.

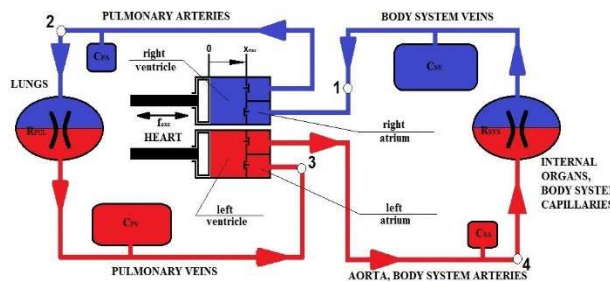


Figure 3: Hydro-mechanical model of the human circulatory system.

In order to simulate the respective mechanical properties of components of the human circulatory system, the model includes some important quantities that describe selected parameters (according to [3]). Referring to Figure 3, the chosen values follow:

- C_{SV} – reduced, average compliance of body system veins;
- C_{PV} – reduced, average compliance of pulmonary veins;
- C_{SA} – reduced, average compliance of body system arteries;
- C_{PA} – reduced, average compliance of pulmonary arteries;
- R_{SYS} – reduced flow resistance through internal organs and body system capillaries;
- R_{PUL} – reduced flow resistance through pulmonary vessels.

In the developed model (Figure 3), there is the clear separation of the two subcircuits (analogous to a biological system - the small and large circulatory system). Because both subcircuits are powered by a dual-chamber pumping unit (by assumption) that simulate

human heart, there are necessary elements which separate both circuits and perform biological function of the atria and vessels valves that are simply return one-way valves operating on the logical scheme based on the forcing cylinder movement direction. Since each of the four valves (two for each chamber) can have two states: 'open' or 'closed', they act as hydraulic return valves and from the mathematical point of view we can easily describe their operation by using the indicator function of the piston velocity

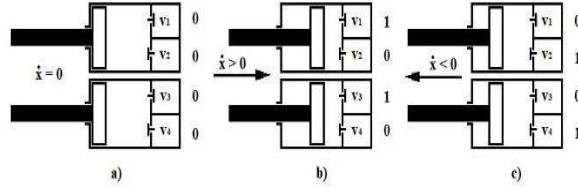


Figure 4: Valves states depending on the cylinder movement direction.

Of course, there are three cases that must be taken into account during the operation of the system (Figure 4). If the pressure cylinder is fixed, the system has no flow, and the valves v_1 , v_2 , v_3 and v_4 are closed (Figure 4a). In two other cases (Figure 4b,c), one of the pairs of valves in each chamber will remain open to allow flow in a closed system.

An important issue is the forcing (cadency/timing) function with the course corresponding to the various stages (phases) of contraction of the heart muscle. The cylinder motion, and thus the cyclic velocity changes which determine the flow control, is enforced by a periodic function with three phases distinguished: pause, diastole - atrial contraction, systole - ventricular contraction. Distribution of the following phases in the one time period of the function has a significant impact on the speed of the cylinder, and consequently on the waveform of the pressure pulsations in the system.

Obviously the nature of the excitation shown (Figure 5) can be disrupted by changing the period or duration of the different phases, thereby simulating changes in heart rate or some pathological cardiac states. Excitation function can be expressed as some conversion of a sinusoidal function, and it may have the form as given:

$$f(t) = -\sin(t)[\text{sgn}(\sin(t)) + 1] + 1. \quad (4)$$

Closely related to the function of the excitation is the velocity of the piston and thus the status of the valves in the chambers (Figure 4). The dynamics of a hydraulic closed structure (Figure 3) is governed by a system of four equations of elementary mass flow balance in the selected points shown in Figure 3. The number 1 indicates the point at which the flow in body system veins is being balanced. As the 2-nd we established the system of the pulmonary arteries, as 3-rd pulmonary venous system and 4-th the body system arteries. The equations follow:

$$(p_4 - p_1) \cdot R_{SYS} = A_{CYL} \cdot \dot{x} \cdot \begin{cases} -1 & \text{for } \dot{x} < 0 \\ 0 & \text{for } \dot{x} > 0 \\ 0 & \text{for } \dot{x} = 0 \end{cases} + C_{SV} \cdot \dot{p}_1, \quad (5)$$

$$-(p_2 - p_3) \cdot R_{PUL} = A_{CYL} \cdot \dot{x} \cdot \begin{cases} 1 & \text{for } \dot{x} > 0 \\ 0 & \text{for } \dot{x} < 0 \\ 0 & \text{for } \dot{x} = 0 \end{cases} + C_{PA} \cdot \dot{p}_2, \quad (6)$$

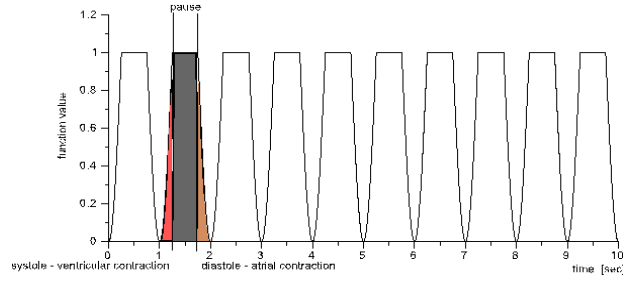


Figure 5: The forcing cadency function waveform.

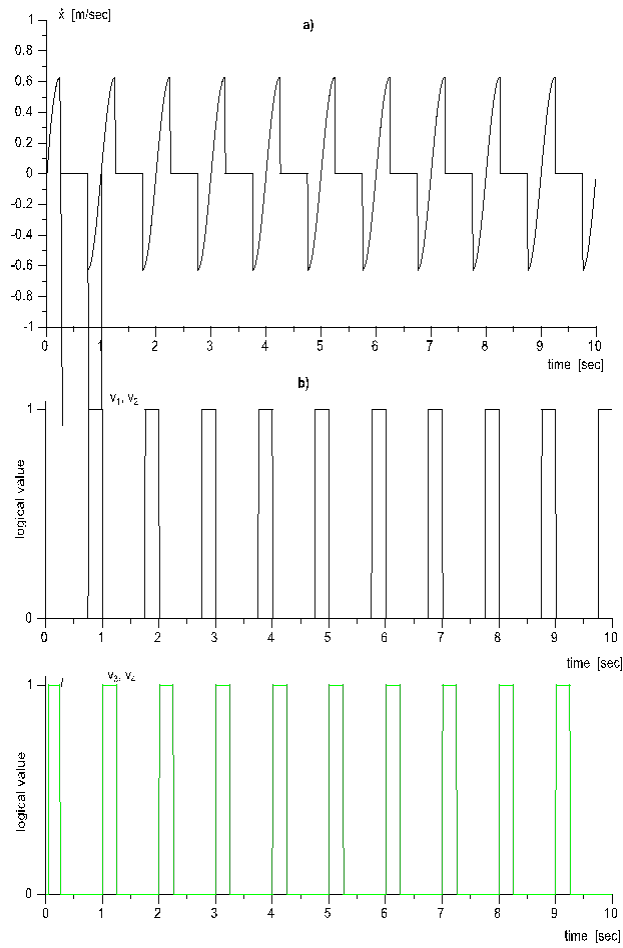


Figure 6: An example piston velocity waveform (a) and corresponding states of the valves (b).

$$(p_2 - p_3) \cdot R_{PUL} = A_{CYL} \cdot \dot{x} \cdot \begin{cases} -1 & \text{for } \dot{x} < 0 \\ 0 & \text{for } \dot{x} > 0 \\ 0 & \text{for } \dot{x} = 0 \end{cases} + C_{PV} \cdot \dot{p}_3, \quad (7)$$

$$-(p_4 - p_1) \cdot R_{SYS} = A_{CYL} \cdot \dot{x} \cdot \begin{cases} 1 & \text{for } \dot{x} > 0 \\ 0 & \text{for } \dot{x} < 0 + C_{SA} \cdot \dot{p}_4. \\ 0 & \text{for } \dot{x} = 0 \end{cases} \quad (8)$$

The left side of each equation contains the flow associated with the pressure difference on both sides of the point at which there is an increased flow resistance. The right side is reduced and simplified sum written for equation (3) of the elementary mass flow balance, wherein the first component of the total flow is associated with the movement of the piston with a working area and stroke defined. The second component is associated with compliance of hydraulic lines (blood vessels) system. Contained in brace bracket element is the mentioned pump piston velocity indicator, which describes the valves operations mathematically depending on the sign of the velocity. All equations (5) – (8) are coupled in pairs due to the construction of the entire system consisting of two sealed subsystems with a common pumping unit, with the work of which a common element is linked for all equations. It can be said that the simplified model of hydro-mechanical circulatory system has a common element in the form of heart unit that binds the entire differential equations system.

2.3 The numerical simulation results

The system dynamics equations (5) – (8) form the basis of the simulation model. They have been implemented as a block diagram in the SciLab Xcos system. Each of the described features, including timed transformed sine function and the pump piston velocity indicator is mapped to the system as a model block components associated with each other by signal connections.

Because of the fact that the essential element for the assessment of cardiovascular efficiency is the pressure in the blood vessels, the analyzed output signals of the system are arterial and venous pressures calculated for the given points of the system (Figure 3). Moreover, it is convenient to calculate fluid flows for each point mentioned that constitute a particular addend in equations given. By selecting appropriate coefficients of the equations of dynamics, based on biological data for compliance and flow resistance, it was possible to obtain pressure waveforms similar to real data (Table 1). It is obvious that selected human physiological conditions are considered, moreover the obtained results of the simulation are closely linked with the body system physiological state assumed in advance (heart rate, symmetry or asymmetry of pumping chambers operation, the length of the following phase in the cycle).

Table 1: The biological data of significant circulatory system parameters.

Resting heart rate		1.1 [Hz] (66 beats per minute)
Resting pressures	Body system veins pressure SYSTOLIC/DIASTOLIC p_1	2/0 [mmHg]
	Body system arteries pressure SYSTOLIC/DIASTOLIC p_4	120/70 [mmHg]
	Pulmonary veins pressure SYSTOLIC/DIASTOLIC p_3	5/0 [mmHg]
	Pulmonary arteries pressure SYSTOLIC/DIASTOLIC p_2	15-25/8 [mmHg]
Blood vessels compliance (veins to arteries)		$\frac{C_V}{C_A} \approx 20$
Blood flow resistance (system to pulmonary)		$\frac{R_{SYS}}{R_{PUL}} \approx 10$
Stroke volume (average)		$V_{STR} \approx 80[ml] = 80[cm^3]$

The numerical simulation results are presented, as the most significant pressure (Figure 7-10) and flow (Figures 11–15) waveforms and at selected points of the hydro – mechanical structure (Figure 3). For comparison purposes, the absolute pressure values are given in units of [mmHg], which are typical for the medical description. Because of the fact that flows in particular points are relatively small, they are presented in units of [cm³/sec].

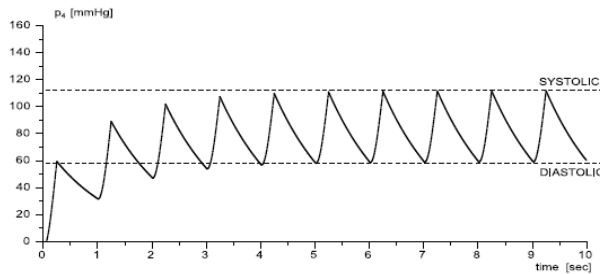


Figure 7: An example resting pressure waveform for a body system arterial structure.

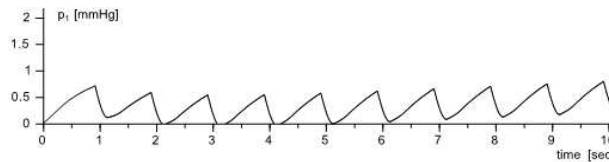


Figure 8: An example resting pressure waveform for a body system venous structure.

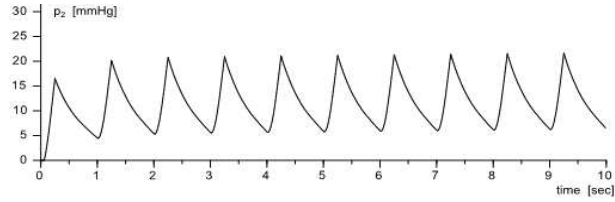


Figure 9: An example resting pressure waveform for a pulmonary arterial structure.

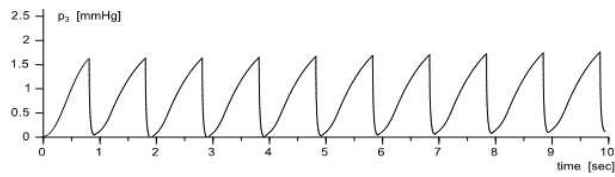


Figure 10: An example resting pressure waveform for a pulmonary venous structure.

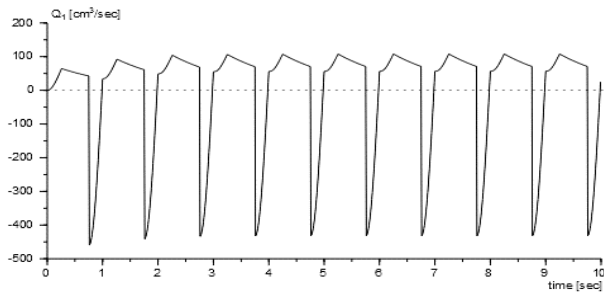


Figure 11: An example fluid volume flow waveform for a body system venous structure.

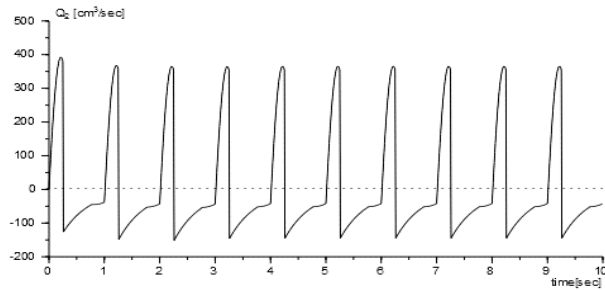


Figure 12: An example fluid volume flow waveform for a pulmonary arterial structure.

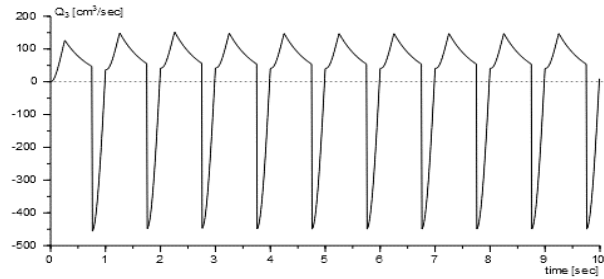


Figure 13: An example fluid volume flow waveform for a pulmonary venous structure.

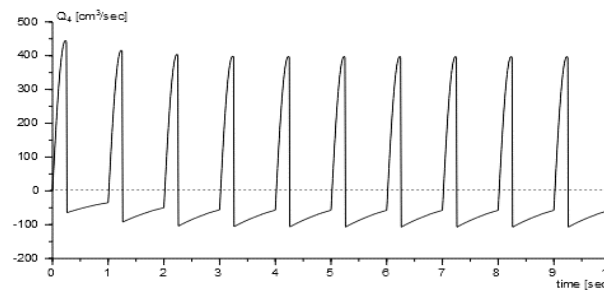


Figure 14: An example fluid volume flow waveform for a body system arterial structure.

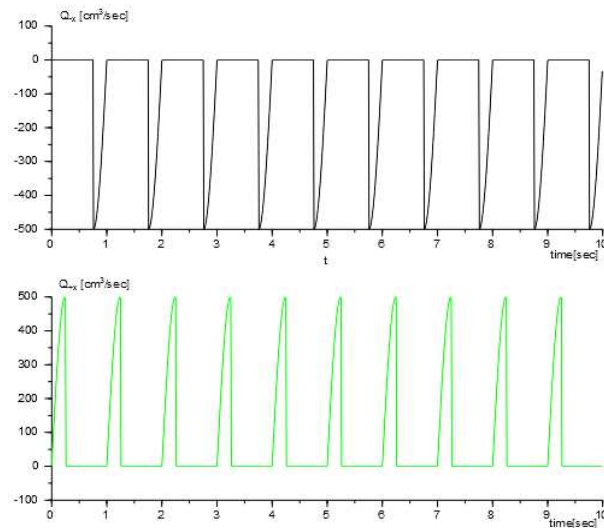


Figure 15: An example fluid volume flow waveforms for the flow occurrence caused by the piston movement: a) return movement direction '-'; b) right movement direction '+'.

Analysis of the exemplary pressure waveforms, shown in Figures 7-10, allows to detect similarities for the extreme pressure values in each waveform in comparison with biological data. Additionally, a common noticeable thing for both pressure and volume flow charts is a pulsation of each variables that is strictly connected with a pumping element operating phases. It has to be emphasize that fluid volume flow "-" sign (below zero point line) means that the fluid outflows from the particular point (on the other hand "+" sign represents fluid inflow). It should not be considered as a fluid movement direction changes, because it is stable by assumption. Observe that the described model is approximately idealized, which means that mechanical parameters used in the model were averaged and reduced to the selected points. The correctness of the simulation results consists in appropriate assumption of the hydro-mechanical structure operation, at this stage the numerical value is of the secondary importance.

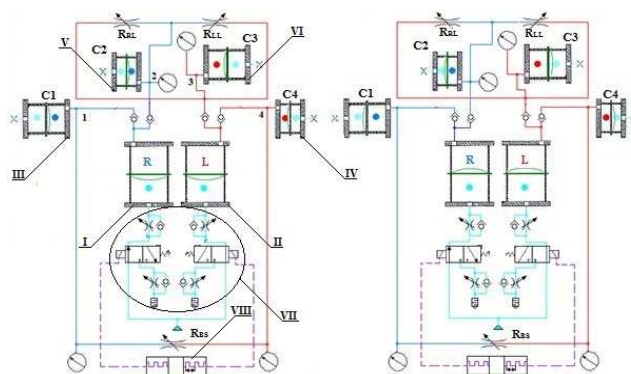


Figure 16: The scheme diagram of the pneumo-hydraulic structure: I – the right ventricle of the pumping unit, II – the left ventricle of the pumping unit, III – the compliance tank of the body venous system, IV – the compliance tank of the body arterial system, V – the compliance tank of the pulmonary arterial system, VI – the compliance tank of the pulmonary venous system, VII – pneumatic control system of the pumping unit operation, VIII – the electronic timing system (pattern generator).

3 The Experimental System Description

On the basis of the hydro-mechanical model shown in Figure 3, the laboratory rig was designed to achieve the flow effect for the proposed system. In contrast to the model system, the experimental rig is based on pneumatic and hydraulic structures combination, which optimally reflects the kind of work of the cardiac muscle and blood vessels. Figure 16 presents the schematic construction of the so far described measurement system.

Compared to the simulation model, structurally the dual mechanical pumping cylinder was replaced by diaphragm pneumo-hydraulic chambers. Deformable membrane separates the hydraulic and pneumatic parts. The increase in air pressure of the pneumatic system – setting the pneumatic valves to the open state by the electronic timing unit causes the deformation of the latex membrane, and thus the fluid flow in the system. The fluent and frictionless membranes movement reflects cardiac muscle operation in a better way. Furthermore, marked as III, IV, V and VI (see Figure 16) regulated compli-

ance tanks imitate respective blood vessels parameters. The system was also expanded by throttle valves corresponding to the flow resistance for the following: R_{RL} – blood flow resistance of the right lung, R_{LL} – blood flow resistance of the left lung, R_{BS} – blood flow resistance of the body vascular system. Moreover, in order to follow the pressure changes in the interesting points (indicated in Figure 16 as 1, 2, 3, 4) corresponding to the simulation model points four pressure sensors connected to the data acquisition unit were provided. Figure 17 shows the prototype laboratory appearance which is the first trial version being developed successively.

In order to check the quality and trend of measured pressure signals, there were some example, trial data registered in LabView environment which are shown below in Figure 18. Because of the fact that none of appropriate system parameters was selected/calculated at this stage, the resulting pressure waveforms should be regarded as trial and their accuracy should be evaluated only in terms of trend/course quality. It should be noted that the pressure waveforms in the recorded time period correspond to the subsequent pumping cycles (heart rate). Highly clear pressure signal pulsation may correspond to a systolic and diastolic pressure state. The experimental rig does not give an opportunity for tracking a volume flow values, so the comparison of this variable signal with simulation results was neglected at this stage. By calculating appropriate parameters for each hydraulic and pneumo-hydraulic laboratory components, we are able to obtain the correct pressure waveforms including also numerical values.

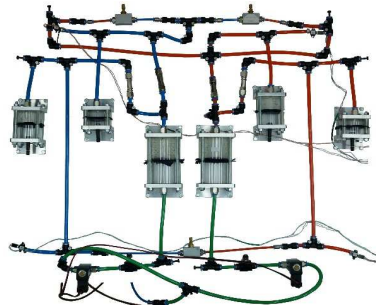


Figure 17: The operating part of the laboratory unit.

4 Summary

Starting from the basic laws of mechanics and taking into account certain simplifications and assumptions connected with the properties and phenomena occurring in the system, we are able to provide a mathematical description of almost any system. The really big challenge is trying to move a perfect biological system to the level of its corresponding mechanical analogue. Although a huge degree of complexity of the human cardiovascular system requires numerous simplifications, however, as it was shown it is possible to create a closed-loop hydraulic circuit and the simulation model that correspond to anatomical indeed. Interactive simulation model developed in any computing environment is only a general description of the purpose object. The main focus of the analysis on the further level is the appropriate parameters selection in order to obtain specific simulation and measurement results [2]. Further exploration of the simulation model and improving the

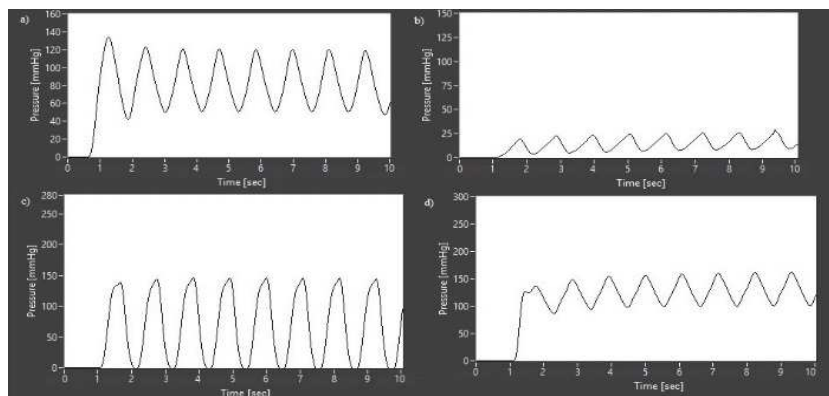


Figure 18: Trial, pressure waveforms recorded for selected points (Figure 11): a) in the point 4, b) in the point 1, c) in the point 3, d) in the point 2.

experimental laboratory will better define the operation of the system, and thus will give the possibility of a more reliable comparison of operating a closed hydraulic system in terms of biological circulatory system.

Acknowledgment

The paper has been presented during the 12th Conference on Dynamical Systems – Theory and Applications, Jydu, Poland, 2013.

References

- [1] Lewandowski, D. The creation and exploration of the pneumatic and hydraulic simulation models. In: *Scientific books of Kielce University of Technology, XII National Conference PNEUMA2000*. (2000) 199–210. [Polish]
- [2] Lewandowski, D. and Awrejcewicz, J. Modelling of the hydro-mechanical linear system controlled by a proportional valve. In: *Hydraulics and pneumatics 2012, International Scientific-Technical Conference book*. (2012) 121–127. [Polish]
- [3] Schneck, D.J. and Bronzino, J.D. *Biomechanics – Principles and Application*. Boca Raton, CRC Press LLC, 2003.
- [4] Dittrich, K. and Riesenberger, A. A model of the human circulatory system with an extended pulse simulator as a basis for artificial heart monitoring. In: *Biomedical Engineering* **30** (6) (1996) 359–361.
- [5] Siewnicka, A., Fajdek, B. and Janiszowski K. Simulation of Human Circulatory System with Coronary Circulation and Ventricular Assist Device. In: *Mechatronics-Recent Technological and Scientific Advances*. (2012) 679–683.
- [6] Conlon, M.J., Russel, D.L. and Mussivand, T. Development of a Mathematical Model of the Human Circulatory System. In: *Annals of Biomedical Engineering* **34** (9) (2006) 1400–1413.
- [7] Huang, F., Qian, W., Ruan, X. and Fu, X. Simulation of a Hydraulic System Duplicating the Human Circulatory System. In: *Intelligent Robotics and Applications Lecture Notes in Computer Science*. **8102** (2013) 427–433.



Six-Legged Robot Gait Analysis

B. Stańczyk* and J. Awrejcewicz

*Department of Automation, Biomechanics and Mechatronics,
Lodz University of Technology, Stefanowskiego 1/15, 90-924, Lodz*

Received: March 31, 2014; Revised: December 23, 2014

Abstract: This paper includes results of investigations of real six-legged robot. By the name of hexapod we call a robot that walks on six legs. Due to specific construction of legs, each leg has 3 degrees of freedom, prototype constructed by us allows to model gait of reptiles and insects. Presented system of rotation angle of each of the cells (servos) allows to analyze every single type of the movement. Applied measurement system allows also to measure current, and use it for calculation of power generated by motor. It allows to calculate power necessary for each type of the robot movement. Applied mathematical model allows for identification and check of the angular velocity, acceleration and moments generated by each of the robot cells separately. As a result it is possible to determine quality coefficients of different gait patterns of the robot, i.e. maximal speed or maximal load depending on the number of working legs. Obtained results were confronted with theoretical model of differential equations regulating gait of our hexapod.

Keywords: *hexapod, control, servo, gait, micro control.*

Mathematics Subject Classification (2010): 70E60.

1 Introduction

Nowadays mobile robotics is based mainly on the wheeled devices [1]. Due to the difficulties in the construction and control walking robots are much less common. Also, the equations used to describe the movements of the robot are less complicated for wheeled robots than in the case of the devices with legs [1]. However, due to the rapid development of technology, miniaturization and continuous growth of microcontroller productivity, robots with legs appear more and more frequently. Due to the desire to expand knowledge of the human gait most of robots subjected to the analysis are anthropomorphic, therefore in literature test results and structures of the two-legged robots are most

* Corresponding author: <mailto:bartchez@gmail.com>

common (i.e. see [2]). However, as far as we know there is no research on robots multi revenues in the six-legged.

In this paper, we present the results of real prototype of the six-legged (Hexapod) robot. Hexapod is a mobile robot, that is a vehicle equipped with electric motors by means of which it is capable of walking on its feet. In our case it is a design resembling insects (see Figure 1) and it moves using 18 engines. To maintain the balance only three legs are required, however for walking four are necessary. Additional two legs allow some leeway in walking and increase the reliability of the robot movements. Robot control is via a mobile phone equipped with a specially designed program that uses the serial data and Bluetooth networks. Originally developed software allows one to send movement data and then receive the information gathered by the sensors. Our robot is equipped with a wireless color camera with microphone, which is placed on the tail and is also controlled using a mobile phone. A special electronic system based on the ATmega128 microcontroller with 6 channels with pulse module which is programmable resolution from 2 to 16 bits, but now uses only two 16-bit channels to control 24 servos, enables separation of servo control signals.



Figure 1: View of the built walking six-feet mobile robot (hexapod).

Robot is equipped with a system for measurement of the rotation angle for each of the servos, what enables analysis of the individual movements. It also provides possibility of measurement of current through the motors, what can be used for approximation of the energy necessary for each type of the movements.

Pulse-width modulation (PWM), which is supplied to the controller of the servo has a constant frequency 50Hz and duration varying in a range of 0-13% (0-2,5MS), what allows to control all eight servos using single signal PWM, as shown in Figure 3.

According to equation (1), constructed robot can realize up to 11! different types of movements, what was initial point of the investigations of different gait possibilities.

$$N = (2k - 1)!, \quad (1)$$

where k denotes number of the legs, and N represents number of the movement types.

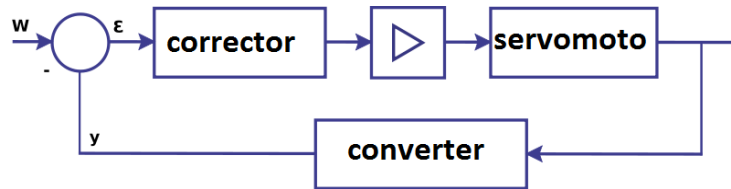


Figure 2: Block diagram of the servo.

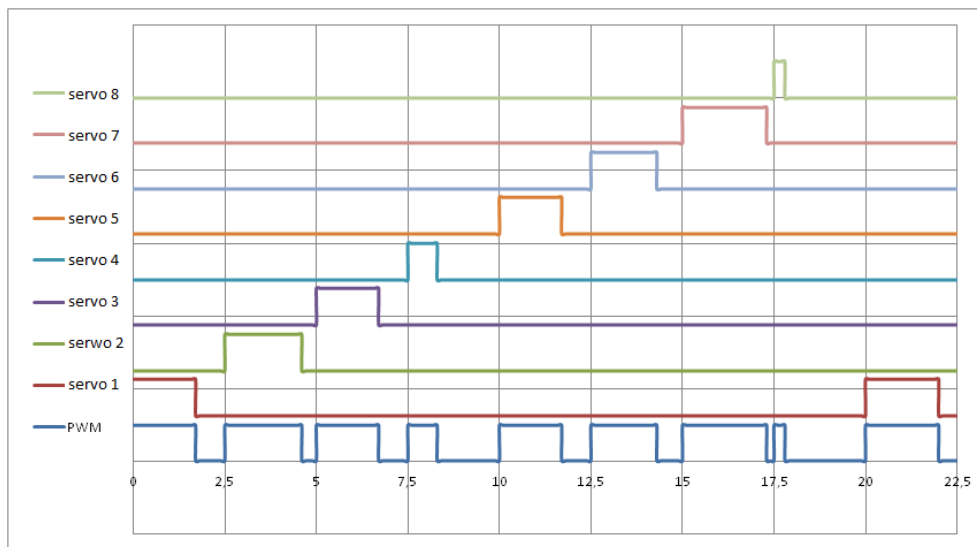


Figure 3: Division of the PWM control signal in dependence of designated servo.

2 Limbs Construction

Construction of the robot’s leg is based on the classical kinematic scheme of the insect. This pattern was chosen for its versatility and possibility to apply for investigations of the gait of both arthropods and reptiles. Moreover, chosen construction enables also to overcome wider range of the obstacles than in case of application of reptile or mammal kinematics. Figure 4 presents the scheme of the kinematic systems of mammals, reptiles and insects.

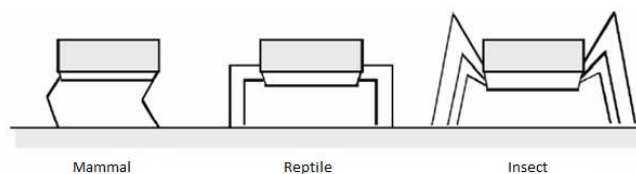


Figure 4: Possible configurations of robot legs.

Presented in Figure 5 scheme of the robot's leg is composed of three rotary cells (A, B, C) and three arms (of lengths l_1 , l_2 , l_3). The first cell (A) is attached to the robot's body and is perpendicular to its surface, what allows for forward-backward movements. Next cell is attached to the arm of length l_1 . This cell is responsible for up-down movement. Cell C is attached to the end of the arm of length l_2 in such a way, that its rotation axis is parallel to the axis of rotation of the cell B. To cell C attached is also additional arm, that serves as foot.

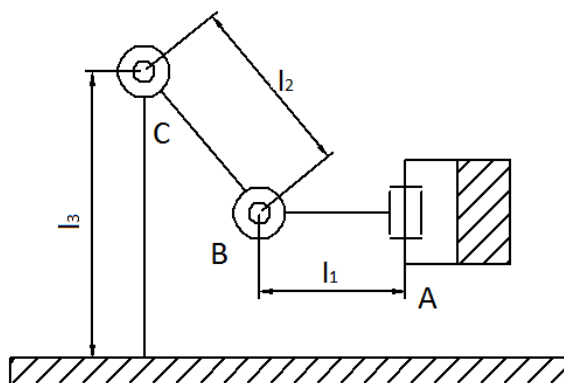


Figure 5: Scheme of the robot arm.

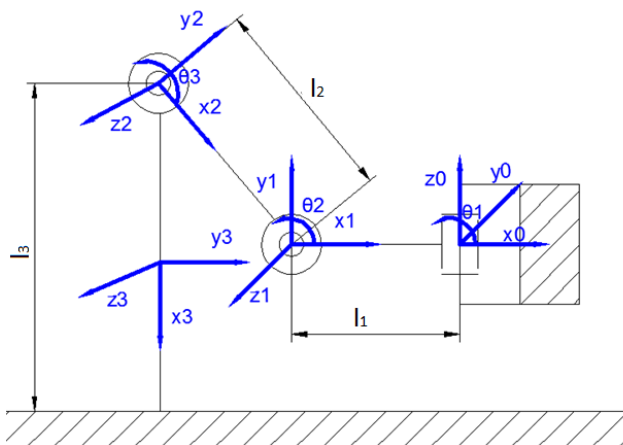


Figure 6: The kinematic scheme and arrangement of the coordinates.

Introduction of the articulated variables yields kinematic scheme of the robot's arm presented in Fig. 6. It is easy to notice, that it is similar to articulated scheme of the anthropomorphic manipulators (OOO). Application of the Denavit-Hartenberg theory allows for easy determination of the location of the end of the arm with respect to its attachment point and, what follows, for description of the gait sequences.

	Θ_{i-1}	λ_{i-1}	l_{i-1}	α_{i-1}
0 – 1	Θ_1	0	$-l_1$	90°
1 – 2	Θ_2	0	$-l_2$	0°
2 – 3	Θ_3	0	$-l_3$	0°

Table 1: Denavit-Hartenberg data (l_i - distance from the axis of Z_i to Z_{i+1} measured along the axis X_i ; α_i - angle between the axes Z_i and Z_{i+1} measured about X_i ; λ_i - distance from the axis X_{i-1} to X_i measured along Z_i ; Θ_i - angle between the axes X_{i-1} and X_i measured about Z_i).

Table 1 presents dependence between variables necessary for transition between coordinate systems. It was applied to derive the following matrices governing transition of variables between cells:

$$A_{0-1} = \begin{bmatrix} \cos \Theta_1 & 0 & \sin \Theta_1 & -l_1 \cos \Theta_1 \\ \sin \Theta_1 & 0 & -\cos \Theta_1 & -l_1 \sin \Theta_1 \\ 0 & 1 & 0 & 0 \\ 0 & 0 & 0 & 1 \end{bmatrix}, \quad (2)$$

$$A_{1-2} = \begin{bmatrix} \cos \Theta_2 & -\sin \Theta_2 & 0 & -l_2 \cos \Theta_2 \\ \sin \Theta_2 & \cos \Theta_2 & 0 & -l_2 \sin \Theta_2 \\ 0 & 0 & 1 & 0 \\ 0 & 0 & 0 & 1 \end{bmatrix}, \quad (3)$$

$$A_{2-3} = \begin{bmatrix} \cos \Theta_3 & -\sin \Theta_3 & 0 & l_3 \cos \Theta_3 \\ \sin \Theta_3 & \cos \Theta_3 & 0 & l_3 \sin \Theta_3 \\ 0 & 0 & 1 & 0 \\ 0 & 0 & 0 & 1 \end{bmatrix}. \quad (4)$$

The following transfer matrix (5) allows for mathematical description of the location of the end of the limb with respect to the coordinate system of attachment limb plane (it was calculated using Denavit-Hartenberg theory as a product of equations (2)–(4)):

$$T_{0-3} = A_{0-1} * A_{1-2} * A_{2-3} = \begin{bmatrix} c\theta_1(c\theta_2c\theta_3 - s\theta_2s\theta_3) & c\theta_1(c\theta_2c\theta_3 + s\theta_2c\theta_3) & s\theta_1 & c\theta_1(l_3(c\theta_2c\theta_3 - s\theta_2s\theta_3) - l_1 - l_2c\theta_2) \\ s\theta_1(c\theta_2c\theta_3 - s\theta_2s\theta_3) & -s\theta_1(c\theta_2c\theta_3 + s\theta_2c\theta_3) & -c\theta_1 & s\theta_1(l_3(c\theta_2c\theta_3 + s\theta_2s\theta_3) - l_1 - l_2s\theta_2) \\ c\theta_2c\theta_3 + s\theta_2s\theta_3 & c\theta_2c\theta_3 + s\theta_2s\theta_3 & 0 & l_3(c\theta_2s\theta_3 + s\theta_2c\theta_3) - l_2s\theta_2 \\ 0 & 0 & 0 & 1 \end{bmatrix}. \quad (5)$$

3 Research and Analysis of Operation Servo

In order to carry out preliminary research on the robot gait and qualitative factors to determine the energy consumption, walking speed and capacity, it is necessary to analyze work of the applied servos. Servos characteristic, being an integral nature of the actuator exhibits dynamics that does not interfere with the regulation, but introduces non-linearity. It implies the use of proportional equalizers (P controller) with high gain.

Observe that integrating characteristics of the actuator ensures theoretically zero static error. High gain in the main control line improves monitoring of the system after changes in pattern but it reduces the stability margin. It can be partially corrected by

a proportionally-derivational controller (PD), that plays a role of the corrector. Control module of the servo works with frequency 50 Hz, current provided to motor can be treated as a signal with constant frequency and varying duration, as shown in Figure 7. It can be noted, that in dependence on the load applied to the motor in servo, there is change in the duration of the current signal. Maximal current consumption by single servo is about 1,5 A with provided voltage 6 V.

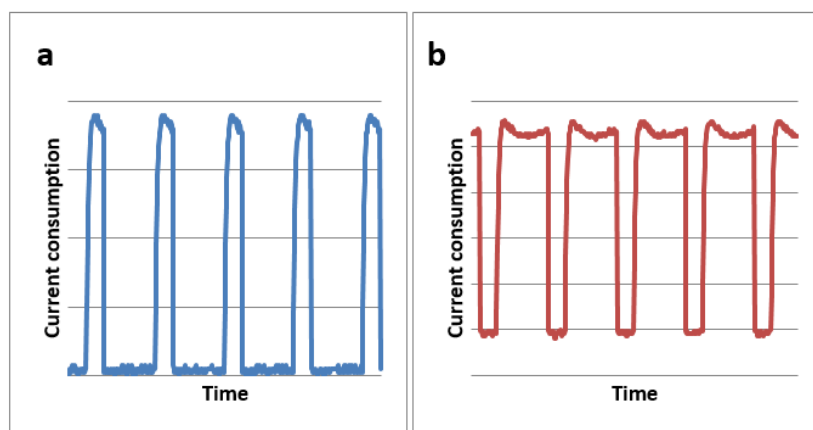


Figure 7: Change in the filling of a servos power signal for, low load on the servo(a), and high load on the servo(b).

In order to conduct research on robot gait, it is necessary to convert the signal with variable duration to analog continuous signal. For this purpose, a low-pass filter was constructed on the basis of a resistor and capacitor (RC). Unfiltered signal is shown in Figure 8a while the effect of the filter application is presented in Figure 8b.

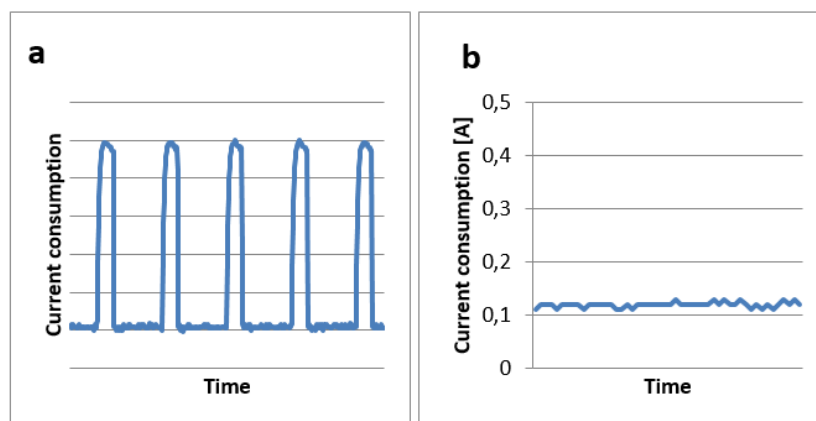


Figure 8: Conversion of the variable signal (a) to analog signal filling (b).

Introduction of signal filtration enabled to develop characteristics of dependence of the

current drawn by a servo from the moment generated on the output of the transmission. The results of the servos tests for variable load are presented in Figure 9. The graph shows that with the load increase the current consumption by the motor also increases. It can be seen that the increase in torque increases the motor current consumption up to a value of 1.5 A. As can be seen in Figure 9, when generating the maximum torque by the servo there occurs an increase of the current drawn by the motor from the value 1A up to 1.5 A.

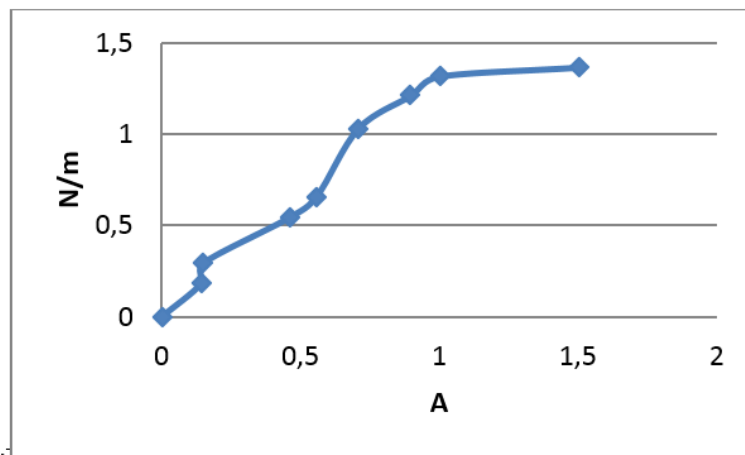


Figure 9: Measurement of intensity of the load servo.

With robot gait sequence as mentioned before, the robot having six legs is able to perform $11!$ different sequences of gait. First preliminary analysis has been subjected to a sequence of gait based on the movements of earth-boring dung beetle (*Geotrupes stercorarius*), because it has the same number of limbs as the constructed prototype robot. Constructed gait models are based on living organisms, what allows the analysis of movements created by millions of years of evolution. The quality of gait can be characterized by the use of qualitative indicators, such as minimum energy consumption, high speed and high performance. However, it is not always possible to get gait sequence that meets all the quality parameters. Therefore, analysis of relationships between different characteristics allows to choose the best solution for given situation.

The easiest way to present robots gait is to record the entire sequence (see Table 2). For simplicity, we assume that the first link takes only three positions and the second and third cells adopt the same angular position. Assumed positions are described below:

(i) the positions of movement for the first cell: 1 – Maximum withdrawal; 2 – middle position, 3 – maximum move forward;

(ii) the positions of movement of the second and third cell: 1 – maximum height, 2 – feet on the ground.

The legs move in pairs – the first motion is performed by legs 1 and 4, then 2 and 6, and finally 3 and 5. Data presented in table show that the movement of the robot is sequential, and always takes place in the same order. There are a number of limitations associated with the construction of the robot. The main limitation is the length of the movement depending on the dimension of the first robot arm and it is associated mainly

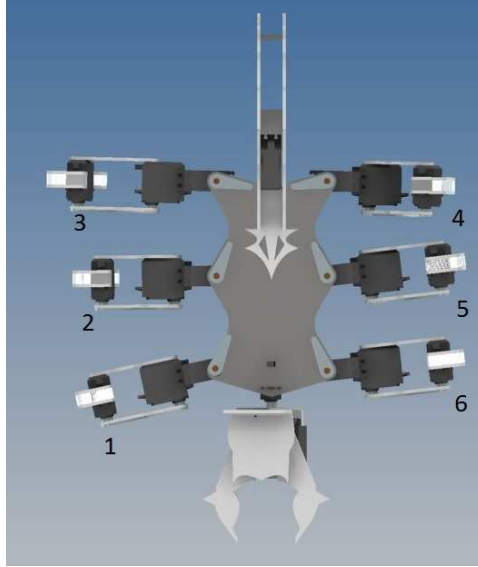


Figure 10: Order of robot limbs.

with the potential legs collisions.

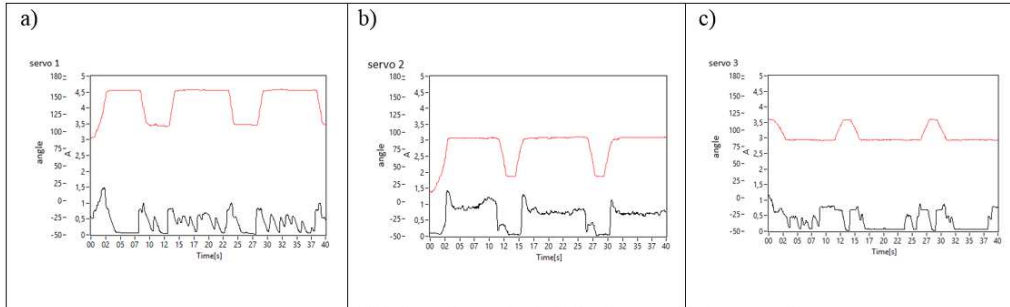


Figure 11: Measurement of the intensity of the load for a) servo 1, b) servo 2, c) servo 3.

Measurement of the intensity of the load for a) servo 1, b) servo 2, c) servo 3. In order to calculate the linear velocity of the end point of the robot leg, there should be introduced manipulator Jacobian. It is matrix J_0^N dimensions of $6 \times N$, where N is the number of segments of the kinematic system [8]. Such Jacobian may be introduced by the equation:

$$\begin{bmatrix} \dot{\vartheta}_0^N \\ \dot{\omega}_0^N \end{bmatrix} = J_0^N \dot{q}, \quad (6)$$

where: $\dot{\vartheta}_0^N$ is a vector of linear velocity of the endpoint of the kinematic system in basic coordinate system (point of the foot attachment to the body), $\dot{\omega}_0^N$ is the angular velocity vector for the end of a kinematic system in the basic coordinate system and \dot{q} is velocity

Leg 1									
Cell 1	1	1	2	2	3	3	3	1	1
Cell 2, 3	1	1	1	1	1	1	2	2	1
Leg 2									
Cell 1	1	1	2	2	3	3	3	1	1
Cell 2, 3	1	1	1	2	2	1	1	1	1
Leg 3									
Cell 1	1	1	2	2	3	3	3	1	1
Cell 2, 3	2	2	1	1	1	1	1	1	1
Leg 4									
Cell 1	1	1	2	2	3	3	3	1	1
Cell 2, 3	1	1	1	1	1	1	2	2	1
Leg 5									
Cell 1	1	1	2	2	3	3	3	1	1
Cell 2,3	2	2	1	1	1	1	1	1	1
Leg 6									
Cell 1	1	1	2	2	3	3	3	1	1
Cell 2, 3	1	1	1	2	2	1	1	1	1

Table 2: Record of robot gait sequence.

vector in each of the joint in a natural coordinate system. For each component, \dot{q} consists of the angular velocities (ω_i) in the case of joint rotation or linear velocities (ϑ_i) in the case of prismatic joints.

According to equation (6) the Jacobian is composed of the elements for the calculation of both linear and angular velocities. Therefore, introduced are the following two Jacobian parts: J_ω (the angular velocity) and J_ϑ (for flow velocity):

$$J_0^N = \begin{bmatrix} J_\vartheta \\ J_\omega \end{bmatrix}. \tag{7}$$

To apply this definition to our data, it is necessary to define Z_i as a unit vector in the Z axis for the i -th component of the system in relation to the basic coordinate system, and O_i as a vector derived from the basic coordinate system (O_0) to the i -th element of the coordinate system (O_i).

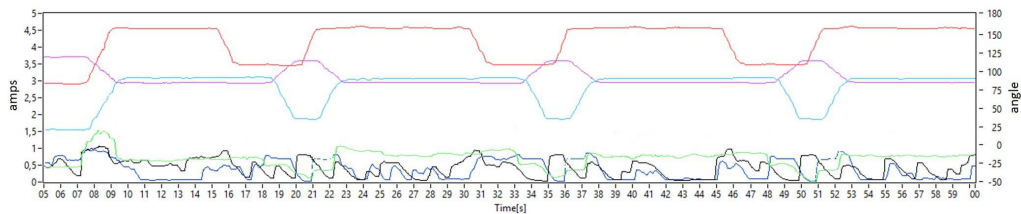


Figure 12: Measurement of the intensity of the load for comparison of the load for all three servos in one leg.

Figure 12 presents the analysis of walking robot in time with respect to the rotation

angle of the servo and power consumption for all three cells in the one leg. Basing on equation (6) it is possible to numerically calculate that the theoretical speed of walking robot is approximately 0,006 m/s and a theoretical average power consumption is of the order of 0.6 A/h (0.0002 A/s). The obtained theoretical results were compared with the measured values, and the differences between real and calculated values were in a range of 6-10%.

4 Conclusions

Conducted simulations show similar theoretical and measurement results, leading to the conclusion that they are correctly performed. Preliminary results enable to determine the power consumption of working actuator. On the other hand, servo analysis is applied for determination of the speed of basic biologically inspired gait. As shown in Figure 11, the most loaded is servo 2. Further research on the robots potential movement possibilities will increase knowledge in this field and will allow for a better understanding of insects gait. This may lead to a better understanding of the advantages and disadvantages of each of the gait sequences and help to create an optimal solution for the most six-legged robots in dependence on their application.

Acknowledgment

This paper was presented during the 12th Conference on Dynamical Systems - Theory and Applications held in Lodz, Poland on 2-5 December 2013.

References

- [1] Giergiel, M., Hendzel, Z. and Żyński, W. *Modeling and Control of the Mobile Wheel Robots*. PWN, Warsaw, 2002. [Polish].
- [2] Zielińska, T. *Walking Machines*. PWN, Warsaw, 2003. [Polish]
- [3] Morecki, A. and Knapczyk, J. *Basics of robots*. Warsaw, WNT, 1999. [Polish]
- [4] Tchoń, K., Mazur, A., Dulęba, I., Hossa, R. and Muszyński, R. *Manipulators and Mobile Robots – Models, Movement Planning, Control*. Akademicka Oficyna Wydawnicza PLJ, Warsaw, 2000. [Polish]
- [5] Jezierski, E. *Basic Course in Robotics*. TUL Press, Lodz, 2002. [Polish]
- [6] Kozłowski, K. and Dutkiewicz, P. *Modeling and Identification in Robotics*. Poznan Technical Univeristy Press, Poznan, 1996. [Polish]
- [7] Kozłowski, K., Dutkiewicz, P. and Wróblewski, W. *Robots Modelling and Control*. PWN, Warsaw, 2003, [Polish]
- [8] Spong, M. W., Vidyasagar, M. *Robot Dynamics and Control*. WNT, Warsaw, 1997.



Constrained Motion of Mechanical Systems and Tracking Control of Nonlinear Systems: Connections and Closed-form Results

Firdaus E. Udwardia^{1*} and Harshavardhan Mylapilli²

¹ *Departments of Aerospace and Mechanical Engineering, Civil and Environmental Engineering, Mathematics, Systems Architecture Engineering, and Information and Operations Management, University of Southern California, Los Angeles, California, USA.*

² *Department of Aerospace and Mechanical Engineering, University of Southern California, Los Angeles, California, USA.*

Received: March 31, 2014; Revised: December 15, 2014

Abstract: This paper aims to expose the connections between the determination of the equations of motion of constrained systems and the problem of tracking control of nonlinear mechanical systems. The duality between the imposition of constraints on a mechanical system and the trajectory requirements for tracking control is exposed through the use of a simple example. It is shown that given a set of constraints, d'Alembert's principle corresponds to the problem of finding the optimal tracking control of a mechanical system for a specific control cost function that Nature seems to choose. Furthermore, the general equations for constrained motion of mechanical systems that do not obey d'Alembert's principle yield, through this duality, the entire set of continuous controllers that permit exact tracking of the trajectory requirements. The way Nature seems to handle the tracking control problem of highly nonlinear systems suggests ways in which we can develop new control methods that do not make any approximations and/or linearizations related to the nonlinear system dynamics, or its controllers. More general control costs are used and Nature's approach is thereby extended to general control problems.

Keywords: *nonlinear mechanical systems; constraints; tracking control; closed form controllers; d'Alembert's principle; nonideal constraints.*

Mathematics Subject Classification (2010): 93A10, 93A30.

* Corresponding author: <mailto:fudwadia@usc.edu>

1 Introduction

Sir Isaac Newton described the field of mechanics in his preface to the Principia in the following words [1]:

“In this sense rational mechanics will be the science of motions resulting from any forces whatsoever, and the forces required to produce any motions, accurately proposed and demonstrated.”

Today, while the first part of Newton’s definition of mechanics has become our usual understanding of this field, the second part is usually relegated primarily to the field of control theory. Indeed, the problem that Newton famously solved was a control problem: the determination of the forces required to be acting on the planets so that their motions obey the observed motions described by Kepler’s first two laws.

To illustrate the view point of Newton, let us consider an elementary example, the problem of finding the equations of motion of a spherical pendulum like the one shown in Figure 1. The problem of finding the equation of motion of this simple system, which consists of a particle of mass m constrained to move so that it is always at a fixed distance, L , from its fixed point of support, O , in a nonuniform gravitational field, can alternatively be looked at from the dual stand-point of tracking control.

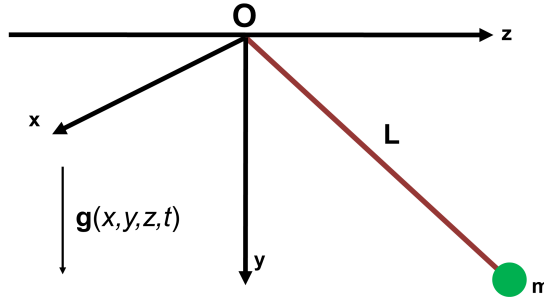


Figure 1: A spherical pendulum.

Consider a particle of mass m moving in a nonuniform gravitational field; it is now required to determine the control force that needs to be applied to this particle so that it is constrained to lie, at each instant of time t , on the sphere S^2 defined by the relation

$$\varphi(x, y, z, t) := x^2(t) + y^2(t) + z^2(t) - L^2 = 0. \quad (1)$$

We will show that this control problem can be handily approached using the theory of constrained motion of mechanical systems. Let us denote the 3 by 1 vector (the 3-vector) $q := [x \ y \ z]^T$. Clearly, the equation of motion of the particle as it freely moves in the nonuniform gravitational field in which the acceleration due to gravity at any point is $g(x, y, z, t)$ (see Figure 1), is simply given by the equation

$$M \ddot{q}(t) := m I_3 \ddot{q}^T = [0 \ mg(x, y, z, t) \ 0]^T := Q, \quad (2)$$

where I_3 is the 3 by 3 identity matrix. The acceleration of the particle at any time t , can be written as the 3-vector $a(q, t) = [0 \ g \ 0]^T$. [From here on, we shall drop the arguments of the various quantities, unless needed for clarity.] We shall refer to equation (2) as the *unconstrained* (or uncontrolled) *equation of motion* for the mechanical system. A control theorist may prefer to call the equation a description of the ‘plant’ whose trajectories need to be controlled so that they satisfy the control requirement stated in (1). In order to achieve this, an additional force will need to be applied to the particle so that its acceleration is altered from $a(q, t)$, and its equation of motion now becomes

$$M \ddot{q} = Q + Q^C. \tag{3}$$

This additional force, Q^C , which is a 3-vector, that needs to be applied to the constrained system can be viewed as the force of constraint that ensures that equation (1) is satisfied. It can also, from a dual perspective, be seen as the control force that must be applied to the system described by (2), so that it satisfies the trajectory requirement (1) that is imposed on it.

The initial conditions $q(0)$, and $\dot{q}(0)$ whose components could be chosen arbitrarily in the case of system (2) can no longer be chosen arbitrarily. Instead, the components of $q(t)$ must satisfy relation (1) at each instant of time (and hence also at the initial time); also, the components of $\dot{q}(t)$ must satisfy the relation

$$x(t) \dot{x}(t) + y(t) \dot{y}(t) + z(t) \dot{z}(t) = 0, \tag{4}$$

at each instant of time (and hence also at the initial time). Equation (4) is obtained by differentiating equation (1) with respect to time. One may want to further differentiate equation (4) to obtain the relation

$$x(t) \ddot{x}(t) + y(t) \ddot{y}(t) + z(t) \ddot{z}(t) = -\dot{x}^2(t) - \dot{y}^2(t) - \dot{z}^2(t), \tag{5}$$

which can be written in matrix-vector form as

$$A \ddot{q} = b, \tag{6}$$

where $A := [x \ y \ z]^T$, and $b = -\dot{x}^2(t) - \dot{y}^2(t) - \dot{z}^2(t)$. We note that for a given set of initial conditions that satisfy equations (1) and (4) at $t = 0$, equation (6) is equivalent to equation (1). This simple example thus illustrates the connections between the problem of constrained motion and the problem of tracking control. Specifically, we find the following analogous concepts given in Table 1. As we go along, we will extend and refine

Analytical Dynamics	Control Theory
Unconstrained System	Uncontrolled System, or Plant
Constrained System	Controlled System
Constraints	Trajectory Requirements
Constraint Force	Control Force, or Control

Table 1: Analogous Concepts in Analytical Dynamics and Control Theory.

this preliminary table. In what follows, we will move back and forth between these dual concepts, allowing ourselves to be aided in our understanding of constrained motion to expose new insights into trajectory control, and vice versa.

2 General Constrained Mechanical Systems and the Trajectory Control Problem

Our spherical pendulum problem is an illustrative ‘toy problem’ created simply to provide some insights into the connections that we are trying to establish. The problem could, of course, have been made considerably more challenging by requiring that the point of support, O , move over a surface say $\phi(q, \dot{q}, t) = 0$, and/or requiring that the pendulum’s length varies in a prescribed manner so that $L(t) = f(q, \dot{q}, t)$. We can now frame the general problem of constrained motion in analytical dynamics as follows:

1. Consider an unconstrained (uncontrolled) nonlinear nonautonomous mechanical system described by the equation

$$\begin{aligned} M(q, t) \ddot{q} &= Q(q, \dot{q}, t), \\ q(0) &= q_0 \text{ and } \dot{q}(0) = \dot{q}_0, \end{aligned} \quad (7)$$

where M is a positive definite n by n matrix, and q is an n -vector,

2. We require this system to satisfy the m consistent constraints (trajectory requirements) given by the relations

$$\phi_i(q, t) = 0, \quad i = 1, 2, \dots, h, \quad (8)$$

and

$$\psi_i(q, \dot{q}, t) = 0, \quad i = h + 1, h + 2, \dots, m. \quad (9)$$

3. We need to find a constraint (control) force, Q^C , so that the constrained (controlled) system described by

$$\begin{aligned} M(q, t) \ddot{q} &= Q(q, \dot{q}, t) + Q^C(q, \dot{q}, t), \\ q(0) &= q_0 \text{ and } \dot{q}(0) = \dot{q}_0, \end{aligned} \quad (10)$$

exactly satisfies trajectory requirements (8) and (9).

We shall assume that q_0 and \dot{q}_0 satisfy the trajectory requirements (8) and (9) at time $t = 0$. Later on, we will relax this condition. We define the acceleration of the uncontrolled (unconstrained) system by

$$a(q, \dot{q}, t) = M^{-1}(q, t)Q(q, \dot{q}, t). \quad (11)$$

Also, assuming sufficient smoothness, we can differentiate the h equations in the set (8) twice with respect to time (as we just did in our toy problem, see (5)), and the $(m - h)$ equations in the set (9) once with respect to time, to obtain the relation

$$A(q, \dot{q}, t) \ddot{q} = b(q, \dot{q}, t), \quad (12)$$

where A is an m by n matrix of rank k . Each row of the matrix A corresponds to one of the trajectory requirements in the sets (8) or (9).

3 The Control Force Q^C

Having now laid out some of the underlying concepts relevant to the duality between the problem of constrained motion and the problem of tracking control, let us concentrate in this section on how one might determine the control force Q^C . Before we embark on this, it might be worthwhile going back to our toy problem and investigating if such a force Q^C indeed exists, so that the trajectory requirement (1) is always satisfied, and if so, whether it can be uniquely found. That such a force Q^C exists, is obvious, because we know the equation of motion of a pendulum and so we know that a right hand side for equation (3) exists so that the constraint (1) is *exactly* satisfied for all time, given that the initial conditions satisfy the constraints. So there most-likely exists a control that is Lipschitz continuous, as we require in mechanics so that the solution of (3) is unique and it concurs with practical observations of the motions of a pendulum. Our next question is then, can Q^C be uniquely found ?

Unfortunately, not ! For the spherical pendulum, at each instant of time, we have the following six unknowns: the three components of the 3-vector \ddot{q} , and the three components of the 3-vector Q^C . At each instant of time, starting with a given state (q, \dot{q}) of the system, we have the three equations given by the set in (3) and an additional equation of constraint (1) (or alternately (6)) – a total of 4 equations. The number of unknowns exceeds the number of equations by two, and hence, at each instant of time, the problem of finding the 6 unknowns (accelerations and control forces) of the system is underdetermined ! To get them uniquely we would need to have two more independent equations. Moving to our dual vision of the problem as one of trajectory control, there must then be an infinity of control forces (controllers) Q^C that can *exactly* track the trajectory expressed by equation (1) !

However, the equation of motion of a spherical pendulum, which satisfies the constraint (trajectory requirement), *is* unique – hence Q^C is unique – and its motion pretty well agrees with what is in fact physically observed. So clearly, Nature must then be picking the constraint force (control force) Q^C in such a manner so as to satisfy some additional criterion – one which somehow yields the (additional) two missing equations, and yields a unique answer for the control force !

3.1 D’Alembert’s and Guass’s principle, and the cost function

Flipping back to our understanding of constrained motion, we may then ask, how does Nature pick the constraint force Q^C so that the motion of our spherical pendulum matches our physical observations ? This is a problem that was first attacked by d’Alembert, and later on, more generally, by Lagrange [2]. Lagrange came up with the precise statement of what is today called d’Alembert’s principle or prescription. D’Alembert’s prescription is as follows:

The constraint force Q^C is such that for all vectors $v(t) \neq 0$ that satisfy the relation $Av = 0$, Nature seems to require that $v^T Q^C = 0$.

The nonzero vectors v that satisfy the relation $Av = 0$ are called virtual displacements, and the quantity $W^C = v^T Q^C$ is referred to as the total work done by the forces of constraint under virtual displacements. And this prescription, somewhat miraculously – for any general mechanical system – generates the correct number of additional equa-

tions so that the constraint force Q^C in equation (10) can be uniquely found at each instant of time!

To see how this works for our spherical pendulum, observe that the rank of our matrix A in (6) is 1, and so the null space of this 1 by 3 matrix is 2. Thus at each time t , there are two linearly independent 3-vectors v_1 and v_2 that satisfy the relation $Av = 0$ which we can find. D'Alembert's prescription then requires that $v_1^T Q^C = 0$, and $v_2^T Q^C = 0$. These two additional equations used with the four equations (the three equations in set (3) and equation (6)) that we had previously, yield the six equations needed for finding the six unknowns – \ddot{q} and Q^C – at each instant of time. What is more astonishing is that d'Alembert's prescription yields the constraint force Q^C which when used in equation (10) yields the motion, $q(t)$, of the mechanical system that is fairly close, in numerous situations, to what is actually observed in the physical world; hence, its enormous value in modeling physical systems.

To summarize, we cannot, in general, determine the constraint force Q^C uniquely. D'Alembert's principle generates additional equations (exactly the right number) to give us a unique Q^C at each instant of time, which causes the constrained system to move in a manner that is in concert with physical observations. It turns out that this prescription of d'Alembert regarding the constraint force Q^C is exactly the same as the following condition on the constraint (control) force Q^C from the dual viewpoint [3]. This condition, called Gauss's Principle, is the following: From all those control (constraint) forces Q^C that can exactly satisfy the trajectory requirements (8) and (9), Nature chooses that control force Q^C that minimizes the control cost given by

$$J(t) = [Q^C(q, \dot{q}, t)]^T M^{-1}(q, t) Q^C(q, \dot{q}, t) = \|Q^C\|_{M^{-1}}^2 \quad (13)$$

at *each instant of time*. As seen from (13), $J(t)$ is simply the square of the weighted L_2 norm of the control force, Q^C .

So we see that d'Alembert's prescription in mechanics – a prescription that causes mathematical models of constrained mechanical system to suitably predict the physically observed motions of these systems – has a dual that says that Nature appears to be constantly solving an optimal control problem, minimizing the cost function $J(t)$ given in (13). But unlike most control engineers today, who would prefer to minimize $\int_0^T J(t)dt$, where T is some final time over which the control is executed, Nature seems to do this minimization *at each instant of time*. Also, the so-called weighting matrix that she uses in the cost function is M^{-1} . This is indeed clever! For example, imagine a multi-body system, with several masses, that is described by equation (7). Say we want to control this system so that it satisfies some given trajectory requirements given by relations (8) and (9). Realizing that the larger masses require larger forces to be exerted on them to cause them to move, Nature attempts to satisfy these requirements (constraints) on this multi-body system, by being in favor of applying forces to the smaller masses – hence, the weighting by the matrix M^{-1} .

We have so far only considered the properties of the constraint force Q^C , without answering the question: what *is* it? Can one find it explicitly, in closed form? We do that next.

3.2 Closed form solution to the optimal tracking control problem for nonlinear, nonautonomous mechanical systems using the theory of constrained motion

The problem of finding the constraint force Q^C that Nature uses has a long and varied history. The problem was first formulated by Lagrange [2], and has been worked on by numerous scientists and engineers [3–9]. A simple expression for the explicit form of the control force was obtained in 1992, and it is given by [10]

$$Q^C = -M^{1/2}(AM^{-1/2})^+(Aa - b), \tag{14}$$

where X^+ denotes the Moore-Penrose inverse of the matrix X [11, 12]. The equation of motion of the constrained system, which may be thought of as the fundamental equation of mechanics, can thus be explicitly written *in extensio*, using relation (10), as

$$M(q, t)\ddot{q} = Q(q, \dot{q}, t) + Q^C(q, \dot{q}, t), \tag{15}$$

where

$$Q^C(q, \dot{q}, t) = -M^{1/2}(q, t)[A(q, \dot{q}, t)M^{-1/2}(q, t)]^+[A(q, \dot{q}, t)a(q, \dot{q}, t) - b(q, \dot{q}, t)].$$

What now might be gleaned from a controls point of view from relation (15)? First, we observe that $a(q, \dot{q}, t)$ (see equation (11)) is the acceleration of the uncontrolled (unconstrained) system. However, to track the given trajectory described by the set of equations (8) and (9), the acceleration of the system needs to satisfy the trajectory requirement (12). Hence, the extent to which the acceleration, a , of the uncontrolled system does not satisfy this trajectory requirement is simply

$$e(q, \dot{q}, t) := [A(q, \dot{q}, t)a(q, \dot{q}, t) - b(q, \dot{q}, t)]. \tag{16}$$

This is in fact the error in the satisfaction of the trajectory constraint at time t by the acceleration (at that time) of the uncontrolled system. The expression for Q^C above says that this error signal is fed back to the system (7), just the way a modern-day control engineer might want to do negative feedback control! We also observe that Nature seems to choose a control gain matrix whose elements are, in general, highly nonlinear functions of q , \dot{q} , and t . It is given explicitly by

$$K(q, \dot{q}, t) := M^{1/2}(q, t)[A(q, \dot{q}, t)M^{-1/2}(q, t)]^+. \tag{17}$$

Thus the control methodology used by Nature, so that the uncontrolled system (7) exactly tracks the trajectory requirements stated in sets (8) and (9), can be encapsulated by the relation

$$M(q, t)\ddot{q} = Q(q, \dot{q}, t) - K(q, \dot{q}, t)e(q, \dot{q}, t), \tag{18}$$

where K is the gain matrix and e is the error signal. Lastly, we point out that Nature appears to use an error signal for its feedback control law that is related to accelerations, and not to displacements, nor to velocities, or to integrals of the displacement, as is commonly done in control theory. She appears to be basing her feedback on ensuring that the *accelerations* of the controlled system satisfy the trajectory requirement given in (12); and yet, cleverly enough, as seen from the expression for the feedback error e in (16), she involves only the state (q, \dot{q}) of the mechanical system. The tracking controller

given by equation (18) is not only optimal in that it minimizes the cost $J(t)$ given in (13), but it yields *exact* tracking; for, the set of equations (8) and (9) are the integrals of motion of the nonlinear system described by (15) (or, (18)). The minimal control cost at each instant of time is explicitly given by

$$J(t) = [Q^C]^T M^{-1} Q^C = \left\| (AM^{-1/2})^+ (Aa - b) \right\|^2. \quad (19)$$

As mentioned before, the closed form expression in equation (14) for the control force Q^C that nature uses satisfies the trajectory requirements. She gets this unique control force by minimizing the control cost $J(t)$ given in (13), which is simply the square of the weighted L_2 norm of control force, Q^C . Nature picks the weighting matrix to be the positive definite matrix $M^{-1}(q, t)$ and thereby produces control forces that are in conformity with the physically observed motions of constrained systems. However, what if the control engineer wants to use a different weighting matrix in his cost function? Namely, suppose (s)he wants to minimize at each instant of time the cost

$$J(t) = [Q^C(q, \dot{q}, t)]^T N(q, t) Q^C(q, \dot{q}, t) = \| Q^C \|_N^2, \quad (20)$$

where $N(q, t)$ is a positive definite matrix. Using our dual perspective, this may also be thought of as a generalization of Gauss's Principle (in mechanics), wherein we use a weighting matrix in our control cost minimization that may be different from M^{-1} . It turns out that the unique control that minimizes this control cost is given (instead of equation (14)) by [14]

$$Q^C = -N(q, t)^{-1/2} A_N^+ (Aa - b) = -N^{-1} M^{-1} A^T [A(MNM)^{-1} A^T]^+ (Aa - b), \quad (21)$$

where $A_N = A(q, \dot{q}, t) M(q, t)^{-1} N(q, t)^{-1/2}$. There is one last point that is worth mentioning. We had assumed that the initial conditions of the controlled system satisfy the trajectory requirements (8) and (9). What if the initial conditions do not lie on the so-called manifold described by the trajectory requirements? If one is close to the trajectory manifold, then instead of thinking of the trajectory requirements (8) and (9) as $\phi_i(q, t) = 0$ and $\psi_i(q, \dot{q}, t) = 0$, one could consider the trajectory requirement as [13]

$$\ddot{\phi} + \Sigma \dot{\phi} + K\phi = 0, \quad \text{and} \quad \dot{\psi} = -\Lambda\psi, \quad (22)$$

where ϕ and ψ are h - and $(m - h)$ -vectors that contain the ϕ_i 's and ψ_j 's respectively. The matrices Σ , K , and Λ can be chosen so that the solutions ϕ and ψ to the equations (22) tend to zero asymptotically as $t \rightarrow \infty$, so that the constraints $\phi_i = 0$ and $\psi_i = 0$ are ultimately satisfied. These equations lead to trajectory requirements which can again be stated in the form of Equation (12), and the control force is again given explicitly by equation (21)! The parameters that are used in the matrices Σ , K , and Λ control the rate and nature of convergence of the trajectories of the dynamical system towards the manifolds, $\phi_i(q, t) = 0$ and $\psi_i(q, \dot{q}, t) = 0$.

To illustrate the nature of this control force, let us go back to our toy problem of controlling a mass m in a time varying gravity field so that it lies on the surface $\varphi(x, y, z, t) := x^2(t) + y^2(t) + z^2(t) - L^2 = 0$. The uncontrolled equation of motion is given by (2) in which M and Q are defined, and $a = M^{-1}Q = [0 \ g(x, y, z, t) \ 0]^T$. We use the constraint equation

$$\ddot{\varphi} + c\dot{\varphi} + k\varphi = 0, \quad c > 0, \quad k > 0, \quad (23)$$

whose solution as $t \rightarrow \infty$ is $\varphi = 0$. Denoting, as before, $q := [x \ y \ z]^T$, this constraint can be rewritten as

$$A\ddot{q} = [x \ y \ z] \ddot{q}^T = -\dot{q}^T \dot{q} - c\dot{q}^T q - (k/2)(q^T q - L^2) := b. \quad (24)$$

Knowing M, Q, A, b , equation (21) then gives

$$Q^C = -\frac{mN^{-1}}{(AN^{-1}A^T)} q^T \{gy + \dot{q}^T \dot{q} + c\dot{q}^T q + \frac{k}{2}(q^T q - L^2)\}, \quad (25)$$

where N is a user-specified positive definite matrix. We note that the control is nonlinear and no approximations related to the nonlinear nature of the ‘plant’ are made. No *a priori* assumptions (such as a linear PD controller) are made about the controller either, and the control minimizes the control cost given in (20) at each instant of time.

Flipping back to analytical dynamics, our closed form equation given by (15) for the constrained motion of the system (10) presupposes that d’Alembert’s prescription is valid for every mechanical system. What if it isn’t? Constraint forces that do not obey d’Alembert’s prescription are called nonideal, and often such systems are referred to as systems with nonideal constraints.

3.3 Mechanical systems with nonideal constraints and the set of controllers for exact trajectory control

The difficulty of incorporating systems with nonideal constraints into the framework of Lagrangian mechanics – though such systems are fairly commonplace in the physical world – arises because of the following two main reasons:

1. We need to have the specification of constraints to be general enough so as to encompass problems of practical utility.
2. The specification must, in order to comply with physical observations, yield the accelerations of the constrained systems uniquely when using the math-ware of analytical dynamics that has been developed over the last 250 years.

It is for this reason that most texts and treatises on mechanics summarily dispatch these systems beyond their boundaries, early on in their treatments of analytical dynamics (see [15] and [16]).

The main problem is how to modify and extend d’Alembert’s principle. One way of doing this would be to extend d’Alembert’s prescription to say that *at each instant of time, the work done by the force of constraint is prescribed for the specific system at hand*. Such a principle would then state that [17]:

$$\begin{aligned} & \text{For any virtual displacement } v(t) \text{ at time } t, \text{ the work done by the} \\ & \text{force of constraint } W^C := v^T Q^C \text{ is prescribed to be equal to } v^T C(q, \dot{q}, t), \end{aligned} \quad (26)$$

where the n -vector $C(q, \dot{q}, t)$ is prescribed by the mechanician for the given, specific system being modeled. The prescription of C can be done through experimentation, and/or by analogy with other systems, or otherwise. At any given instant of time t , W^C can be positive, negative, or zero; this allows the possibility that energy can be fed into the system at the constraint, or it can be removed at the constraint. When $C \equiv 0$ for all time t , this extension of d’Alembert’s principle reverts to d’Alembert’s prescription.

For any sufficiently smooth C , one can find the explicit equation of motion for such a constrained system that satisfies exactly the constraint requirements (8) and (9) (or alternately (12)). Dropping the arguments of the various quantities, the equation is [17]

$$M \ddot{q} = Q - M^{1/2} B^+ (Aa - b) + M^{1/2} (I - B^+ B) M^{-1/2} C := Q + Q^C, \quad (27)$$

where $B(q, \dot{q}, t) = A(q, \dot{q}, t) M(q, t)^{-1/2}$. We notice that the first two terms on the right hand side of the first equality in equation (27) are identical to those on the right hand side of equation (15), the nonideal nature of the constraint force having simply added an additional term on the right hand side, for any given prescribed smooth function $C(q, \dot{q}, t)$. By choosing the Lipschitz continuous function $C(q, \dot{q}, t)$ arbitrarily, equation (27) provides all the possible Lipschitz continuous controllers [17] that can make the uncontrolled system (7) exactly track the trajectory requirements specified by equations (8) and (9). Clearly, the second and third members on the right hand side in the first equality of (27) are M -orthogonal, and so

$$J(t) = \|B^+(Aa - b)\|^2 + \|(I - B^+ B) M^{-1/2} C\|^2.$$

The addition of the second term on the right hand side increases the cost from its optimal value of $\|B^+(Aa - b)\|^2$ to that now provided. As before, more generally, when the weighting matrix in the control cost is N instead of M^{-1} the explicit control that causes system (10) to exactly satisfy the trajectory requirements (8) and (9) is given in closed form by [14],

$$Q^C = -N(q, t)^{-1/2} A_N^+ (Aa - b) + N^{-1/2} (I - A_N^+ A_N) M^{-1/2} C \quad (28)$$

for arbitrary continuous functions $C(q, \dot{q}, t)$ and the equation of motion becomes

$$M \ddot{q} = Q - N^{-1/2} A_N^+ (Aa - b) + N^{-1/2} (I - A_N^+ A_N) M^{-1/2} C := Q + Q^C. \quad (29)$$

The second and third members in the first equality above are now N -orthogonal and the control cost now becomes

$$J(t) = \|Q^C\|_N^2 = \|A_N^+ (Aa - b)\|^2 + \|(I - A_N^+ A_N) M^{-1/2} C\|^2. \quad (30)$$

We can now expand Table 1 to expose the various analogous concepts that we have developed (see Table 2).

4 Example

In this section, we provide an example that utilizes the connections we have developed between analytical dynamics and control of nonlinear systems.

Energy control of nonlinear mechanical systems has become important nowadays and various energy harvesting schemes are being developed. We consider here the problem of energy control of a highly nonlinear mechanical system and approach it by using the connections that have been developed in the previous sections between analytical dynamics and control. The fundamental equation of mechanics (equations (14) and (15)) is used to obtain the explicit nonlinear control force required to achieve the desired energy control.

Analytical Dynamics	Control Theory
Unconstrained System $M(q, t) \ddot{q} = Q(q, \dot{q}, t)$	Uncontrolled System, or Plant $M(q, t) \ddot{q} = Q(q, \dot{q}, t)$
Constrained System $M(q, t) \ddot{q} = Q(q, \dot{q}, t) + Q^C(q, \dot{q}, t)$	Controlled System $M(q, t) \ddot{q} = Q(q, \dot{q}, t) + Q^C(q, \dot{q}, t)$
Constraints $\ddot{\phi} + \Sigma \dot{\phi} + K\phi = 0,$ $\dot{\psi} = -\Lambda\psi$	Trajectory Requirements $\phi_i(q, t) = 0, i = 1, 2, \dots, h$ $\psi_i(q, \dot{q}, t) = 0, i = h + 1, h + 2, \dots, m.$
Gauss's Principle (GP) $J(t) = [Q^C(q, \dot{q}, t)]^T M^{-1}(q, t) Q^C(q, \dot{q}, t)$	Control Cost $\int_0^T [Q^C(q, \dot{q}, t)]^T M^{-1}(q, t) Q^C(q, \dot{q}, t) dt$
Constraint Force with GP $Q^C = -M^{1/2}(AM^{-1/2})^+(Aa - b)$	Control Force, or Control
Optimal at EACH Instant of time	Optimal over the interval of time $[0, T]$
Generalized Gauss's Principle $J(t) = [Q^C(q, \dot{q}, t)]^T N(q, t) Q^C(q, \dot{q}, t),$ where $N > 0$	$\int_0^T [Q^C(q, \dot{q}, t)]^T N(q, t) Q^C(q, \dot{q}, t) dt,$ where $N > 0$
Equations of motion for Nonideal Constraints $M\ddot{q} = \{Q - N(q, t)^{-1/2} A_N^+(Aa - b) + N^{-1/2}(I - A_N^+ A_N)M^{-1/2} C(q, \dot{q}, t)\}$	Full set of continuous controllers that satisfy trajectory requirements for arbitrary continuous $C(q, \dot{q}, t)$.

Table 2: Analogous Concepts in Analytical Dynamics and Control Theory (detailed).

We consider a 3-DOF fixed-fixed Toda chain [18] as shown in Figure 2. Let m_i denote the mass of the i -th particle ($i = 1, 2, 3$) in the chain. The displacement of the mass m_i as measured from its equilibrium position is denoted by q_i , and its velocity is denoted by \dot{q}_i . Given any nonzero initial energy state, H_0 of the chain, our aim is to stabilize the chain at a different nonzero desired energy level, H^* . And to achieve this, control can be applied to one or more of these three masses.

In the present example, we control the energy of the chain by actuating the first mass, m_1 , alone. We shall impose the requirement, that the energy of the system be increased to the desired value H^* as a constraint on the mechanical system, and the constraint force that will cause this constraint to be satisfied will then be the requisite control force that would need to be applied to the mass m_1 . We begin with a description of the Toda

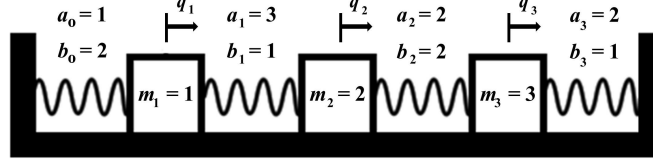


Figure 2: A 3-DOF fixed-fixed Toda chain.

potential.

(i) Toda Potential and Spring Force: The expression for the nonlinear potential of the Toda spring [18] is given by

$$u(q) = \frac{a}{b} e^{b q} - a q - \frac{a}{b}, \quad a > 0, b > 0, \quad (31)$$

whereas its exponential spring force $F_s(q)$ can be derived from its potential as

$$F_s(q) = -F_{restoring}(q) = \frac{\partial u(q)}{\partial q} = a (e^{b q} - 1). \quad (32)$$

A plot of the Toda spring potential and the Toda spring force is shown in Figures 3 and 4, respectively. For sufficiently small displacement, the spring force is approximately linear. However, the nonlinearity of the force gains prominence as the displacement increases. As can be inferred from Figure 4, a larger force is required to stretch the spring by a unit distance than is required to compress it. Hence, the Toda chain considered possesses spring elements that are stronger in tension than in compression. Such systems arise frequently in structural sub-systems such as the stringers in suspension bridges.

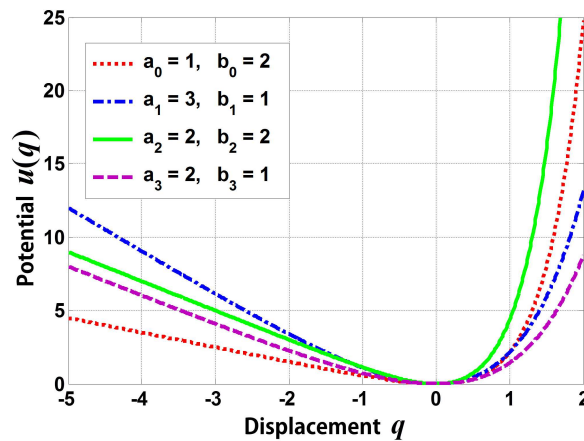


Figure 3: Toda Spring Potential.

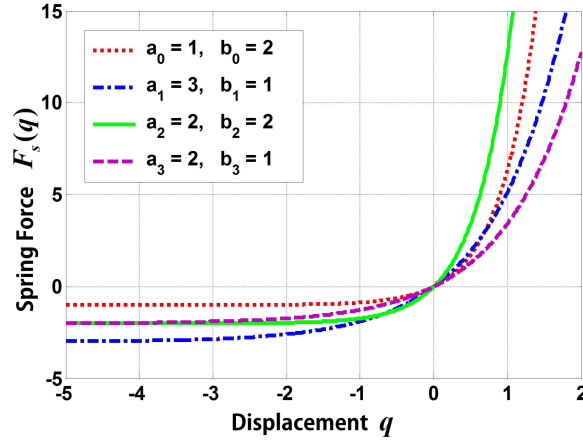


Figure 4: Toda Spring Force.

(ii) Unconstrained System: Consider the 3-DOF fixed-fixed Toda chain as shown in Figure 2. The total energy of the chain can be written down as

$$H(q, \dot{q}) = \sum_{i=1}^3 \left[\frac{1}{2} m_i \dot{q}_i^2 \right] + \sum_{i=0}^3 \left[\frac{a_i}{b_i} e^{b_i(q_{i+1} - q_i)} - a_i (q_{i+1} - q_i) - \frac{a_i}{b_i} \right], \quad (33)$$

where $q_0 \equiv q_4 \equiv 0$ describe the boundary conditions of the fixed-fixed chain. The equations of motion of the unconstrained (uncontrolled) system can be written down in matrix form as $M\ddot{q} = Q$, or more explicitly as

$$\begin{bmatrix} m_1 & 0 & 0 \\ 0 & m_2 & 0 \\ 0 & 0 & m_3 \end{bmatrix} \begin{bmatrix} \ddot{q}_1 \\ \ddot{q}_2 \\ \ddot{q}_3 \end{bmatrix} = \begin{bmatrix} a_1(e^{b_1(q_2 - q_1)} - 1) - a_0(e^{b_0(q_1)} - 1) \\ a_2(e^{b_2(q_3 - q_2)} - 1) - a_1(e^{b_1(q_2 - q_1)} - 1) \\ a_3(e^{b_3(-q_3)} - 1) - a_2(e^{b_2(q_3 - q_2)} - 1) \end{bmatrix}. \quad (34)$$

We take, for example, the initial conditions of this Toda chain to be

$$\begin{aligned} q_1(0) &= 1, \quad q_2(0) = 2, \quad q_3(0) = 1, \\ \dot{q}_1(0) &= 2, \quad \dot{q}_2(0) = 0, \quad \dot{q}_3(0) = 2. \end{aligned} \quad (35)$$

Figure 2 shows the parameter values of the masses (m_i , $i = 1, 2, 3$) used as well as the parameter values a_i , b_i , $i = 0, 1, 2, 3$ that characterize the four different Toda springs. Using these parameter values and the initial conditions given in (35), the unconstrained equations of motion given in (34) can be numerically integrated. We note that for all the simulations presented in this section, the equations of motion have been integrated using the ‘ode45’ scheme in the Matlab environment with a relative integration error tolerance of 10^{-10} and an absolute error tolerance of 10^{-13} . Figure 5 (top) shows a plot of the displacements of the three masses from $t = 0$ to $t = 10$ time units for the unconstrained (uncontrolled) system.

The unconstrained Toda chain is a conservative system and the energy, being an integral of motion, remains constant throughout the duration of the simulation (see

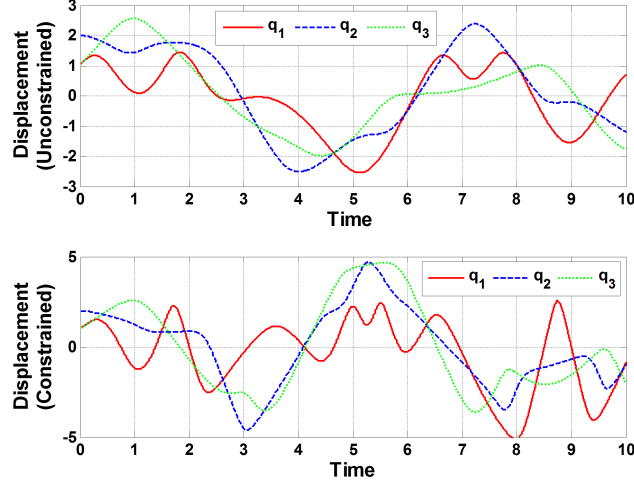


Figure 5: Time history of displacements for the unconstrained system (top) and constrained system (bottom).

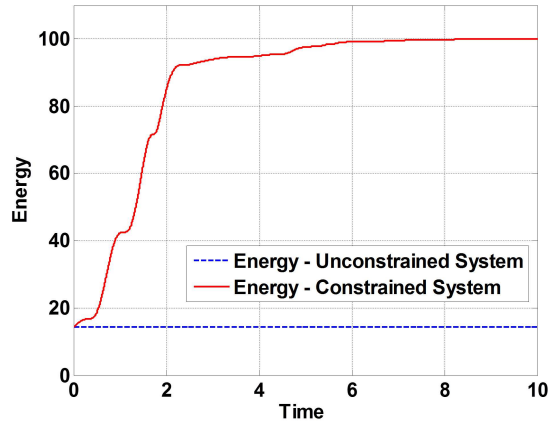


Figure 6: Time history of energy of the 3-DOF Toda chain.

dotted line in Figure 6). For the parameter values chosen, the energy level of the chain is $H_0 = 14.22$ units. Our aim is to increase the energy of the chain to a new and different value.

(iii) Constraints: We shall assume that we want the nonlinear Toda chain described by equation (34) (with the parameter values as shown in Figure 2) to have an energy level $H^* = 100$ units by controlling only mass m_1 . In order to achieve this control objective, we impose the following two types of constraints on the unconstrained system. The first deals with our objective to change the energy of the system to its desired value, H^* ; the second deals with the fact that we want to achieve this by actuating just a single mass from amongst the three masses in the chain, namely, only mass m_1 (see Figure 2).

1. *Energy Control Constraint*: The energy control constraint is given by

$$\frac{d}{dt}(H(q, \dot{q}) - H^*) + \beta(H(q, \dot{q}) - H^*) = 0, \quad (36)$$

where $\beta > 0$. The solution to this differential equation shows that as $t \rightarrow \infty$, $H(q, \dot{q}) \rightarrow H^*$. Notice that this constraint allows the 3-DOF Toda chain to be started from any arbitrary initial energy state H_0 (see equation (22)) so that it reaches its desired energy state, H^* , as $t \rightarrow \infty$.

2. *No-Control Constraints*: Since no control force is to be applied to masses m_2 and m_3 of the Toda chain, the second and third equations in the equation set (34) must remain unchanged in the controlled system. Therefore, the unconstrained equations of motion of masses m_2 and m_3 are themselves the constraints and guarantee that no control is applied to either of these two masses! Thus, in addition to the energy constraint given by (36), the unconstrained system (equation (34)) is also subjected to the following two constraints.

$$\begin{bmatrix} m_2 & 0 \\ 0 & m_3 \end{bmatrix} \begin{bmatrix} \ddot{q}_2 \\ \ddot{q}_3 \end{bmatrix} = \begin{bmatrix} a_2(e^{b_2(q_3 - q_2)} - 1) - a_1(e^{b_1(q_2 - q_1)} - 1) \\ a_3(e^{b_3(-q_3)} - 1) - a_2(e^{b_2(q_3 - q_2)} - 1) \end{bmatrix}. \quad (37)$$

When this set of constraints (equations (36) and (37)) are expressed in the general constraint matrix form of equation (12), we obtain $A\ddot{q} = b$, or more explicitly

$$\begin{bmatrix} m_1\dot{q}_1 & m_2\dot{q}_2 & m_3\dot{q}_3 \\ 0 & m_2 & 0 \\ 0 & 0 & m_3 \end{bmatrix} \begin{bmatrix} \ddot{q}_1 \\ \ddot{q}_2 \\ \ddot{q}_3 \end{bmatrix} = \begin{bmatrix} \dot{q}^T Q - \beta(H - H^*) \\ a_2(e^{b_2(q_3 - q_2)} - 1) - a_1(e^{b_1(q_2 - q_1)} - 1) \\ a_3(e^{b_3(-q_3)} - 1) - a_2(e^{b_2(q_3 - q_2)} - 1) \end{bmatrix}. \quad (38)$$

- (iv) *Explicit Control Force*: With the matrices M, Q, A, b at our disposal, the control force Q^C can be calculated using (14) and is given by

$$Q^C(q, \dot{q}) = \begin{bmatrix} -\xi_o (H - H^*) m_1 \dot{q}_1 \\ 0 \\ 0 \end{bmatrix}, \quad (39)$$

where the value of $\beta = \xi_o m_1 \dot{q}_1^2$ has been chosen to avoid any singularities in the control force, which might arise when the actuated mass m_1 has zero velocity. In the present example, for illustration, the positive constant ξ_o has been chosen to be 0.03. The control force (equation (39)) obtained is optimal and it minimizes the control cost given by (20) at each instant of time, with $N = M^{-1}$. Notice from equation (39) that the control force acting on the first mass appears to make it move like a self-excited oscillator!

- (v) *Dynamics of Constrained System*: The equations of motion of the constrained (controlled) Toda chain can now be written down using equations (14) and (15), where M and Q are given by (34), and Q^C is given in (39). A plot of the displacements of the three masses of the controlled system (using the parameters shown in Figure 2), is shown in Figure 5 (bottom) from $t = 0$ to $t = 10$ time units. A plot of the time history of the

energy is depicted in Figure 6 for the constrained system. The solid line in the figure shows that the application of the control force has resulted in an increase of the energy of the 3-DOF Toda chain from an initial energy level of $H_0 = 14.22$ units to the desired energy level of $H^* = 100$ units. Figure 7 shows a plot of the time history of the nonlinear control force acting on the first mass to achieve the desired transition. Once the desired energy level is attained, the control force automatically becomes zero and we make use of the conservative nature of the chain to remain at the desired energy level for all future time.

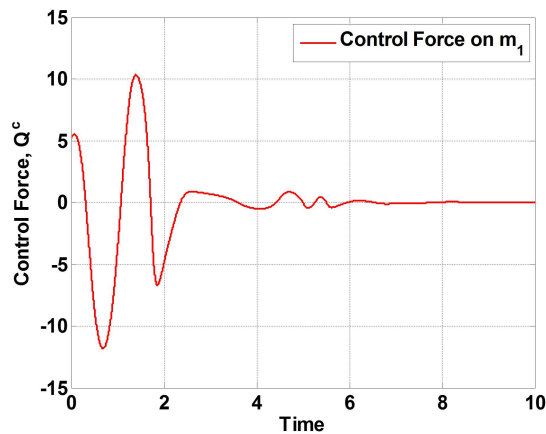


Figure 7: Time history of control forces acting on the 3-DOF Toda chain

It can be shown with some effort that the nonhomogeneous Toda chain that we have considered is controllable using control on just mass m_1 in the sense that the system can be “moved” from any arbitrary energy state $H_0 \neq 0$ to any other energy state $H^* \neq 0$ using the control described in (39). We don’t prove that here, since it will take us too far afield from the central theme of this paper.

5 Conclusions and Open Problems

In this paper, we have established a connection between the problem of constrained motion and the problem of control of nonlinear mechanical systems. An example illustrating the development of exact, closed-form energy control of a highly nonlinear multi-degree of freedom system that utilizes this connection has been demonstrated. The developments outlined herein form just the beginnings of a new path to our understanding of the synthesis of analytical dynamics and control. Numerous open questions remain unanswered, such as, robustness of control, extensions to multi-body dynamics and the dynamics of continua, and applications to robotics, space systems, and fluid mechanical systems.

Acknowledgment

This paper was presented at the Opening Plenary Session of the 12th Conference on Dynamical Systems Theory and Applications, Lodz, Poland, December 2-5, 2013.

References

- [1] Newton, I. *Mathematical Principles of Natural Philosophy. Vol. 1*. Berkeley: University of California Press, 1962.
- [2] Lagrange, J.L. *Mechanique Analytique*. Paris: Mme Ve Courcier, 1811.
- [3] Udwadia, F.E. and Kalaba, R.E. *Analytical Dynamics: A New Approach*. Cambridge: Cambridge University Press, 1996.
- [4] Gauss, C.F. Über ein Neues Allgemeines Grundgesetz der Mechanik. *J. Reine Angewandte Math.* **4** (1829) 232–235.
- [5] Jacobi, C.G.J. *Vorlesung über Dynamik*. Berlin: G. Reimer, 1884.
- [6] Gibbs, J.W. On the fundamental formulae of dynamics. *Amer. Journ. Math.* **2** (1879) 49–64.
- [7] Appell, P. Sur une Forme Generale des Equations de la Dynamique. *C. R. Acad. Sci., Paris* **129** (1899) 459–460.
- [8] Dirac, P.A.M. *Lecture on Quantum Mechanics*. New York: Yeshiva University Press, 1964.
- [9] Poincaré, H. Sur une Forme Nouvelle des Equations de la Mechnique. *C. R. Acad. Sci., Paris* **132** (1901) 369–371.
- [10] Udwadia, F.E. and Kalaba, R.E. A new perspective on constrained motion. *Proc. Roy. Soc. Lon., Series A* **439** (1992) 407–410.
- [11] Moore, E.H. On the reciprocal of the general algebraic matrix. *Bull. Amer. Math. Soc.* **26** (1920) 394–395.
- [12] Penrose, R. A generalized inverse of matrices. *Proc. Cambridge Phil. Soc.* **51** (1955) 406–413.
- [13] Udwadia, F.E. A new perspective on the tracking control of nonlinear structural and mechanical systems. *Proc. Roy. Soc. Lon. A* **459** (2003) 1783–1800.
- [14] Udwadia, F.E. Optimal tracking control of nonlinear dynamical systems. *Proc. of the Royal Society of London, Series A* **464** (2008) 2341–2363.
- [15] Goldstein, H. *Classical Mechanics*. New York: Addison-Wesley, 1976.
- [16] Pars, L.A. *A Treatise on Analytical Dynamics*. Woodbridge, Connecticut: Oxbow Press, 1972.
- [17] Udwadia, F.E. and Kalaba, R.E. What is the general form of the explicit equations of motion for constrained mechanical systems? *J. App. Mech.* **69** (2002) 335–339.
- [18] Toda, M. *Theory of Nonlinear Lattices*. New York: Springer-Verlag, 1989.



Transcritical-like Bifurcation in a Model of a Bioreactor

J. Villa, G. Olivar* and F. Angulo

*Universidad Nacional de Colombia - Sede Manizales, Facultad de Ingeniería y Arquitectura,
Departamento de Ingeniería Eléctrica, Electrónica y Computación,
Percepción y Control Inteligente - ABC Dynamics,
Bloque Q, Campus La Nubia, Manizales, 170003 - Colombia*

Received: March 31, 2014; Revised: December 23, 2014

Abstract: A non-standard bifurcation, similar to a transcritical one, in a model of a bioreactor has been detected. This happens in a periodically-forced system with restrictions on the state space. The bioreactor is periodically fed with substrate. In the mathematical model, a periodic orbit approaches (without hitting) the restriction surface as a bifurcation parameter is varied. The way the orbit approaches the switching surface in the three-dimensional state space is such that it becomes parallel to the restriction surface. This phenomenon is somehow analogous to a transcritical bifurcation since another periodic orbit exists inside the restriction surface, but they do not collide. Full model and bifurcation description are shown.

Keywords: *bifurcation; bioreactor; periodically-forced; nonlinearity.*

Mathematics Subject Classification (2010): 34C23, 34C25, 34D20, 37C27.

1 Introduction

The biological wastewater treatment uses different techniques to create optimum environmental conditions that promote the removal of organic matter by using microorganisms. One of the most common is the activated sludge system, which uses aeration for bacteria [1, 2].

A least-used system, although it is a current research topic, is the Anaerobic Digestion, which operates in the absence of oxygen. The UASB (Upflow Anaerobic Sludge Blanket, or Upflow Anaerobic Reactor) is a type of tubular bioreactor operating in continuous mode and in upflow. These systems have an additional advantage because they can treat effluents with high organic load wastewater from agriculture and food industry tasks. The

* Corresponding author: <mailto:golivart@unal.edu.co>

efficiency of this system is estimated to be a reduction of the COD (Chemical Oxygen Demand) of approximately 80%. COD is the parameter used to characterize the organic water pollution. This organic matter, in natural conditions, may be slowly biodegradable to CO₂ and H₂O. It can take from several days to a few million years, depending on the type of organic matter and biodegradation conditions. Another advantage is the energy production (methane). This also implies a low sludge production compared to aerobic digestion [5, 8].

1.1 Operation

In high-load reactors, UASB is one of the most used in the world. Its main advantage is due to the fact that it retains the biomass without the need for support. It does so through the formation of grains, which makes the reactor more economical and gives technical advantages over other advanced reactors. In general, the success of this reactor relies in that the grains forming the bioparticles are very active and thick. This gives the characteristics of a compact reactor without plugging problems, and without the high costs of traditional packaging.

Anaerobic degradation process is carried out in four stages: hydrolysis, acidogenesis, acetogenesis and methanogenesis.

- Hydrolysis : In this stage the extracellular enzymes of fermentative bacteria are responsible for converting the insoluble organic matter into soluble molecules. This complex molecules breaking is carried out in order for the bacteria to digest organic matter. This stage is very important for effluents treatment with a high content of organic matter.
- Acidogenesis : The compounds formed in the hydrolytic stage are absorbed through the cell wall of acidogenic bacteria. This performs an internal degradation process through microorganisms metabolism which produces carbon dioxide, hydrogen and volatile fatty acids (AGV).
- Acetogenesis : AGVs are converted into acetic acid through the effect of acetogenic bacteria, which also produce hydrogen and carbon dioxide.
- Methanogenesis : At this stage, methane is produced by the activity of a group of bacteria, which have two routes for gas generation. On the one hand, the acetoclastic path, where acetic acid molecules are converted into methane and carbon dioxide. On the other hand, we have the hydrogenophilic path, where methane is produced by a reduction reaction of carbon dioxide with hydrogen.

A complete and comprehensive model for anaerobic digestion called "The IWA (International Water Association) Anaerobic Digestion Model No 1 (AMD1)" features 26 state variables and 19 biological reaction schemes [6]. This model allows for standardization of existing systems and is a starting point for the development of specific models. Without losing sight of its limitations, a mathematical model can be an important tool to understand the kinetics of the processes involved, and to develop and implement good systems for the design and control of wastewater treatment plants.

Our model in this paper takes into account the material balance equations of three state variables: biomass (expressed as volatile suspended solids concentration), substrate (expressed as chemical oxygen demand COD) and volatile fatty acids (VFA). It is based on a kinetic model unstructured and non-segregated. It considers a total reaction which

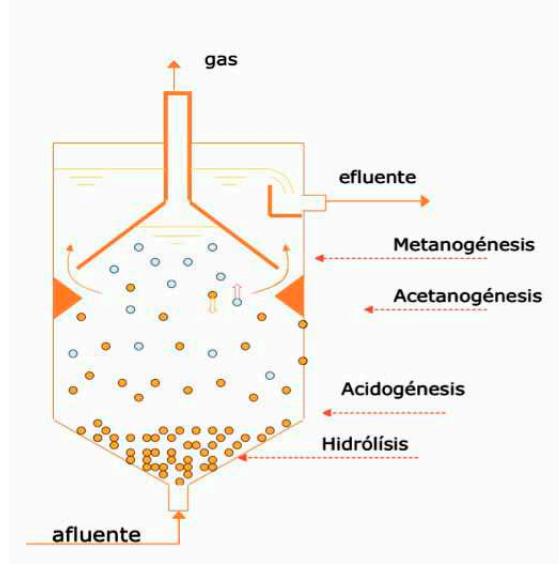


Figure 1: Scheme of an UASB.

groups various microbial colonies within the volatile soluble solids (VSS), and substrates involved in chemical oxygen demand (COD) [4].

2 Modeling

Round 1950, Monod suggested that the bacteria growth rate depends not only on the microorganisms concentration, but also on the substrate concentration [3]. It is currently accepted that conversion of soluble substrates during anaerobic stage is governed by Monod equation, which describes this relationship in a way similar to the one proposed for the Michaelis-Menten enzyme-substrate interaction.

$$\mu = \mu_{max} \frac{S}{K + S} \quad (1)$$

and we have

$$\dot{S} = D(S^{in} - S) - Y(\mu_{max} \frac{S}{K + S})X, \quad (2)$$

$$\dot{X} = D(X^{in} - \alpha X) + (\mu_{max} \frac{S}{K + S})X. \quad (3)$$

In this paper we consider the concentrations of substrate and biomass in the input current as periodic functions like

$$S^{in}(t) = S^{in}(1 + \beta \cos(\omega t)), \quad (4)$$

$$X^{in}(t) = X^{in}(1 + \delta \cos(\omega t)). \quad (5)$$

Thus our final model is

$$\dot{S} = D(S^{in}(1 + \beta \cos(\omega t)) - S) - Y\left(\mu_{max} \frac{S}{K + S}\right)X, \quad (6)$$

$$\dot{X} = D(X^{in}(1 + \delta \cos(\omega t)) - \alpha X) + \left(\mu_{max} \frac{S}{K + S}\right)X, \quad (7)$$

where S is the substrate concentration in the reactor (mg / l COD), D is the dilution factor (d^{-1}), S^{in} is the substrate concentration in the inlet stream (mg / l COD), $\alpha = 1 - \eta$ where η is the efficiency of the separator (0.93), X is the biomass concentration in the reactor (mg / l VSS), X^{in} is the biomass concentration in the inlet stream, μ_{max} is the maximum growth rate of microorganisms (d^{-1}), K is the Monod constant, also called half-saturation constant (kg COD/m³), β is the amplitude of the forcing function for the substrate, δ is the amplitude of the forcing function for the biomass and finally, ω is the frequency of the forcing functions.

Since both S and X must fulfill $S \geq 0$ and $X \geq 0$ for meaningful operation, we consider $X = 0$ and $S = 0$ as restriction surfaces.

3 Analysis

We study four cases:

3.1 First case

We first consider that we have no forcing. This is, the amplitude for the forcing is zero. Also we consider that the inflow wastewater contains biomass.

Thus we take

$$\beta = 0, \quad \delta = 0, \quad X^{in} = 240,$$

(certain values for parameters are taken from experiments in [7]).

Then, for the equilibrium points we have

$$D(S^{in} - S) - Y\left(\mu_{max} \frac{S}{K + S}\right)X = 0, \quad (8)$$

$$D(X^{in} - \alpha X) + \left(\mu_{max} \frac{S}{K + S}\right)X = 0. \quad (9)$$

After some algebraic operations we get

$$X = (S^{in} + YX^{in} - S)/(\alpha Y)$$

and thus

$$(\mu_{max} - D\alpha)S^2 + (DS^{in}\alpha - DK\alpha - \mu_{max}S^{in} - Y\mu_{max}X^{in})S + DK\alpha S^{in} = 0.$$

The values for the parameters were taken from the experimental work in Munoz [7]. $D = 3$, $S^{in} = 3000$, $X^{in} = 240$, $\mu_{max} = 1.32$, $\alpha = 0.07$, $Y = 3.35$ and $K = 5522$.

Two equilibriums are obtained, but one of them is not physically possible.

3.2 Second case

In general, the input current does not contain biomass composition. Thus we consider now that we have no forcing and no biomass in the inflow

$$\beta = 0, \quad \delta = 0, \quad X^{in} = 0.$$

We have then

$$D(S^{in} - S) - Y\left(\mu_{max}\frac{S}{K+S}\right)X = 0, \quad (10)$$

$$D(-\alpha X) + \left(\mu_{max}\frac{S}{K+S}\right)X = 0. \quad (11)$$

By inspection, we can deduce that both equations are fulfilled when $X = 0$, which corresponds to bioreactor washout condition. This is bad operation for the reactor.

Also, an equilibrium point is found for

$$S = DK\alpha/(\mu_{max} - D\alpha)$$

and

$$X = (S^{in}\mu_{max} - DS^{in}\alpha - DK\alpha)/(Y\alpha),$$

which is physically possible.

3.3 Third case

Now we consider that $\omega = 0$, thus we do not have periodic forcing. But we still have the effect of parameters β and δ . We also consider that wastewater has biomass. Thus,

$$\omega = 0, \quad X^{in} = 240,$$

and the equations for the equilibrium points are

$$D(S^{in}(1 + \beta) - S) - Y\left(\mu_{max}\frac{S}{K+S}\right)X = 0, \quad (12)$$

$$D(X^{in}(1 + \delta) - \alpha X) + \left(\mu_{max}\frac{S}{K+S}\right)X = 0. \quad (13)$$

After some algebra we get

$$X = (S^{in}(1 + \beta) + YX^{in}(1 + \delta) - S)/(\alpha Y)$$

and then

$$(\mu_{max} - D\alpha)S^2 + (DS^{in}(1 + \beta)\alpha - DK\alpha - \mu_{max}S^{in}(1 + \beta)\mu_{max}X^{in}(1 + \delta))S + DK\alpha S^{in} = 0.$$

For positive β and δ we obtain two equilibriums, but one of them is always unfeasible.

3.4 Forth case

We consider again that we have no periodic forcing but we have influence through β and δ . Moreover, we assume now that we have no biomass in the input flow. Thus,

$$\omega = 0 \quad X^{in} = 0.$$

Then, the equations for the equilibrium points are

$$D(S^{in}(1 + \beta) - S) - Y\left(\mu_{max} \frac{S}{K + S}\right)X = 0, \quad (14)$$

$$D(-\alpha X) + \left(\mu_{max} \frac{S}{K + S}\right)X = 0. \quad (15)$$

Similarly to the second case, we have an equilibrium point which corresponds to washout condition ($X = 0$), and a second equilibrium at

$$S = DK\alpha / (\mu_{max} - D\alpha)$$

and

$$X = (S^{in}(1 + \beta)\mu_{max} - DS^{in}(1 + \beta)\alpha - DK\alpha) / (Y\alpha),$$

which is physically feasible.

In summary, balance characteristics depend on the value of X^{in} . When the input current is present, biomass generates two equilibrium points, but only one is physically meaningful. On the other hand, when we have no input biomass, one of the equilibrium points corresponds to washout.

4 Numerical Results

We consider now real periodic forcing where $\omega \neq 0$. No closed-form solutions are available now and thus we rely on numerical simulations.

The following figures (Figs. 2–4) show waveforms, orbits in the phase space and bifurcation diagrams when we vary the most significant parameter, namely the dilution factor D . The almost non-smooth point in the bifurcation diagrams is due to washout condition. At this point, both periodic orbits (one corresponding to washout, inside the restriction surface; and another one without touching the restriction surface) get infinitely closer. We called this phenomenon a transcritical-like bifurcation since although there is not really a qualitative change in the state space (and thus it is not a bifurcation), it resembles very much a transcritical bifurcation. Moreover, from a practical view, both orbits are indistinguishable and can be considered as if the washout orbit is the only one which exists.

4.1 Transcritical-like bifurcation

In this subsection we describe an exotic bifurcation which is found in the system.

Namely, since in this case we have a periodic forced system, the natural phase space is $\mathbb{S} \times \mathbb{R}^2$, where \mathbb{S} corresponds to the unit circle.

Then, as parameter D is increased, two periodic orbits, one lying in the washout condition, with $X = 0$ and another one with $X \neq 0$ approach. The non-washout periodic orbits aligns with the washout one as parameter D increases, and gets infinitely closer to it. This behaviour is not generic and thus we consider it as a non-standard bifurcation (see Figs. 5–7).

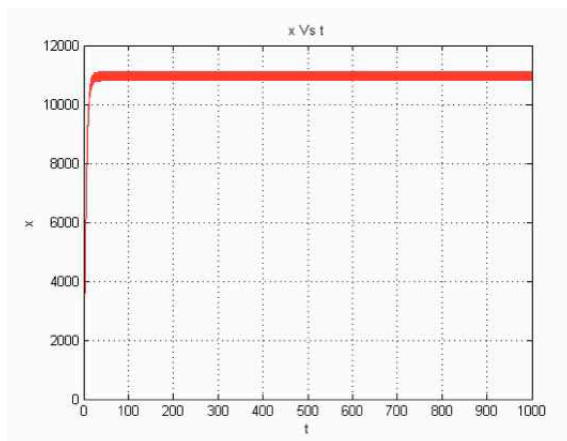


Figure 2: Waveform for the biomass evolution when $D = 5$.

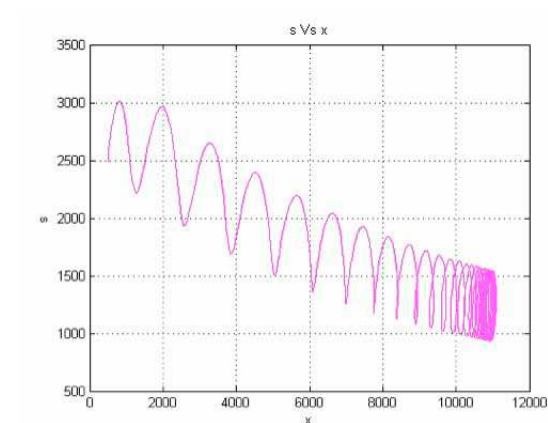


Figure 3: Orbit in the phase space when $D = 5$.

5 Conclusion

Based on dynamic analysis of the model, it was found that in general, the study of an UASB reactor has good stability to different operating conditions, especially when the effluent to be treated is from a leachate. This is because in this case the washout phenomenon can occur.

The system stops working properly under washout conditions. According to the results of different simulations, the parameters that most influence this condition are the dilution factor D (which is related to the speed with which the effluent passes through the reactor) and the solid – liquid – gas separator efficiency parameter α .

Numerical simulations showed that, depending on the biomass which is present in the inflow, washout or good operations are possible. Also, when periodic forcing is considered, periodic orbits can be found, as expected. A non-standard transcritical-like bifurcation of periodic orbits was also found.

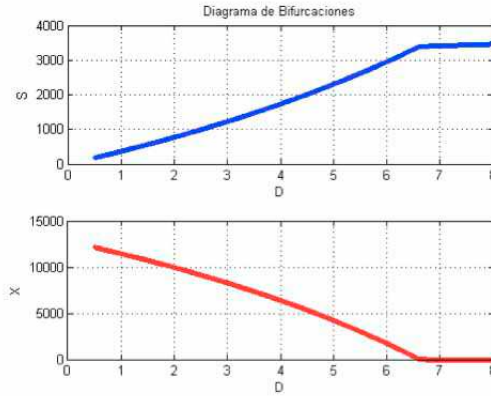


Figure 4: Bifurcation diagrams for the substrate and the biomass as parameter D (dilution time) is varied.

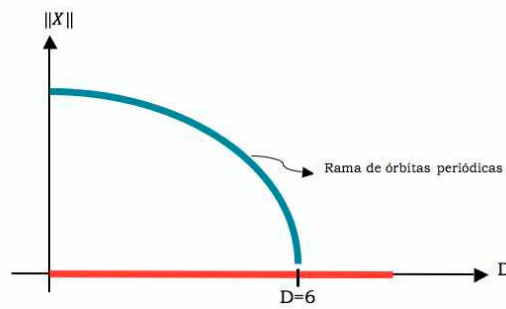


Figure 5: Bifurcation diagram as parameter D is varied. Two periodic orbits get infinitely closer at a transcritical-like bifurcation point.

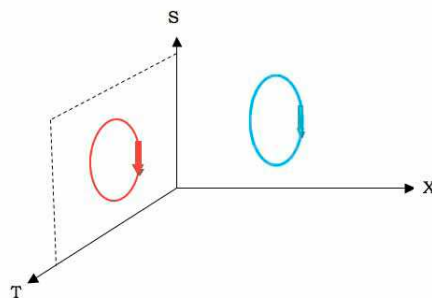


Figure 6: Two periodic orbits which coexist in the phase space. One of them corresponds to washout condition since $X^{in} = 0$.

Acknowledgment

This paper was presented at the 12th Conference on Dynamical Systems - Theory and Applications, December 2-5, 2013, Lodz, POLAND. The authors acknowledge support

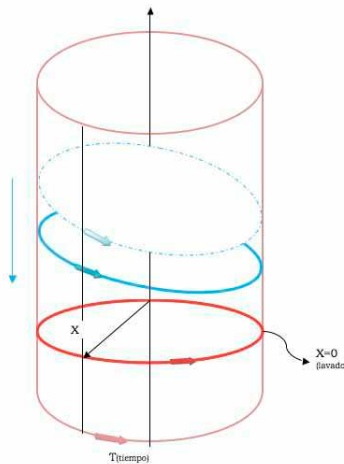


Figure 7: Coexistence of two periodic orbits in the natural space, close to collision.

from Universidad Nacional de Colombia, DIMA projects.

References

- [1] Zanabria, O. and Modelagem, A. *Identificao e Controle de Sistemas de Tratamento de lodo Ativado con Remocao de Nitrogenio*. Sao Paulo, Universidade de Sao Paulo, 2002.
- [2] Henze, M., Van Loosdrecht, M., Ekama, G. and Brdjanovic, D. *Biological Wastewater Treatment. Principles, Modeling and Design*. London, IWA Publishing, 2008.
- [3] Konak, A.R. Derivation of generalised Monod equation and its application. *Journal of Applied Chemistry and Biotechnology* **24** (8) (2007) 453–455.
- [4] May, M.Wu. and Hickey, R. Dynamic Model for UASB Reactor Including Reactor hydraulics, Reaction and Diffusion. *Journal of Enviromental Engineering* **23** (1997) 244–252.
- [5] Ahn, J.H. and Forster, C.F. *A comparison of Mesophilic and Thermophilic Anaerobic Up-flow Filters*. Bioresource Technology, 1999.
- [6] Batstone, D.J., Keller, Angelidakis, R.I., Kalyuzhny, S.V., Pavlostathis, S.G., Rozzi, A. and Sanders W.T. The IWA Anaerobic Digestion Model No 1 (ADM1). In: *Proc. of the 9th World Congress on Anaerobic Digestion*. Amberes, Belgium, 2001
- [7] Munoz, R. and Angulo, F. Aproximación de estimación de estados en un reactor UASB. *Revista Colombiana de Tecnologías Avanzadas* **1** (2006) 27–33. [Spanish]
- [8] Sotomayor, O.A.Z., Park, S.W. and García C. A simulation benchmark to evaluate the performance of advanced control techniques in biological wastewater treatment plants. *Brazilian Journal and Chemical Engineering* **18** (2001) 81–101.



Cooperation of One and Multi-Joint Muscles

B. Zagrodny* and J. Awrejcewicz

*Lodz University of Technology, Department of Automation, Biomechanics and Mechatronics,
Stefanowskiego Str. 1/15 Lodz, Poland*

Received: March 31, 2014; Revised: January 7, 2015

Abstract: In this paper an analysis of equations describing single and multi-joint muscles cooperation during movement of limb segments is presented. Additionally, the Pareto-optimum problem is considered for the human upper limb in case of movement in sagittal plane. Uncertainty of this problem and some additional physiological restrictions such as angular range of motion or tissue tension are described. Moreover, effects of practical verification based on the video analysis of the volunteers arm movement and its lack of reproducibility are addressed. Examination of the artificial arm prototype shows similar behaviour to the human biological musculo-skeletal system. Furthermore, results of comparison with those obtained by other authors are shown.

Keywords: *biomechanics; muscle cooperation; motion analysis.*

Mathematics Subject Classification (2010): 93A30.

1 Introduction

The structure of biological systems is complex, which causes serious challenging problems in their control. The occurred imperfections, external actions on the objects under investigations or fatigue of musculo-skeletal systems affect trajectories of motion, their speed and precision of repetitions. It is conjectured that a movement of biological system is not determined along one fixed trajectory. Namely, there are infinite number of admissible paths of moving from one point to another one. In order to verify the hypothesis a mathematical model of cooperation of one and multi-joint muscles of the human upper limb during motions is proposed and analysed. This model is used to illustrate the way of cooperation of any number of single and multi-joint flexors and extensors of an arm

* Corresponding author: <mailto:bartlomiej.zagrodny@p.lodz.pl>

and forearm. Moreover, inability to determine exactly one trajectory, which is Pareto-optimal solution for the existing biological limitations, is also shown. On the other hand, it is proved that the set of admissible trajectories is narrow. Obtained theoretical results are verified in an experiment based on the repeatability of the human arm movement. In order to record the trajectories of movement a video analysis is used. The presented model is also applied to analysing the human walking on the treadmill and the obtained results are compared with earlier results concerning the issue. More sophisticated models, in this line, can be applied to analysing any system of the repeatable movement of the human body.

2 Mathematical Description of Problem

2.1 Notation and physiological description

Let us introduce a problem of a forearm flexion undergoing following muscle actions. The following notation is applied:

- (i) m, r – one joint flexors muscles of forearm and arm, respectively;
- (ii) n – two joint flexors;
- (iii) o, s – one joint extensors of forearm and arm, respectively;
- (iv) p – two joint extensors muscles.

Figure 1 presents an example of such system for a few of these muscles. Furthermore, the following nomenclature is used:

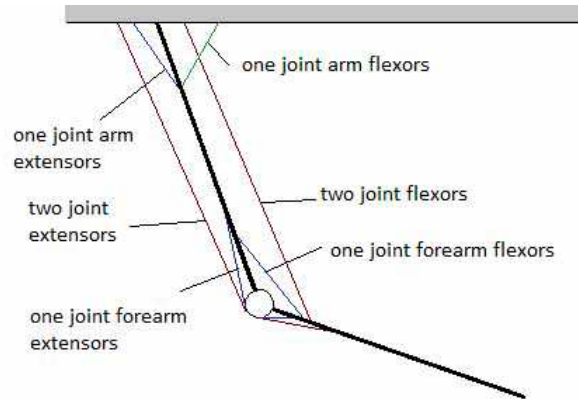


Figure 1: Example of the one and two joint muscles extensors and flexors system.

- (i) $z_{(rj)a}$ – one joint arm flexors, $a \in (1, \dots, r)$;
- (ii) $z_{(pj)b}$ – one joint forearm flexors, $b \in (1, \dots, m)$;
- (iii) $z_{(2)c}$ – two joint flexors, $c \in (1, \dots, n)$;
- (iv) $p_{(rj)d}$ – one joint arm extensors, $d \in (1, \dots, s)$;

- (v) $p_{(pj)e}$ – one joint forearm extensors, $e \in (1, \dots, o)$;
- (vi) $p_{(2)f}$ – two joint extensors, $f \in (1, \dots, p)$.

It is well known that contraction of the flexors causes flexion of the limb and contraction of the extensors causes extension assuming that they act stronger than its antagonists. For a precise movement they have to cooperate in an appropriate way (see [2-9]).

2.2 Formulation of the mathematical problem

Let us consider a forearm flexion. In this particular case the muscles z_{pj} and z_2 have to contract, whereas the muscles p_{pj} and p_2 have to reduce their tension. If the contraction is strong enough and not compensated by p_2 , then we will observe also an arm flexion, what is undesirable in this case. To prevent this movement a contraction of p_{rj} muscles has to occur. This will compensate a momentum of two joint muscles yielding a movement of a forearm only. Similarly, such cooperation will happen in the case of other limbs movements. In what follows we analyse this problem in the case of arm and forearm movement in the sagittal plane. In the considered model it is assumed that each muscle contributes to the creation of the momentum acting on the joint.

We define it as follows:

$$M_i = r_i \cdot F_i, \tag{1}$$

where r means forces arm acting with respect to the joint with axis of rotation (see Figure 2). This arm is defined as a function of muscle length and limb flexion angle. Observe that it is different for each muscle.

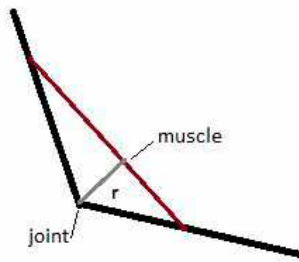


Figure 2: Example of defining forces arm acting on a joint.

The following forces momentum are acting on the elbow joint:

- (i) flexing forearm: $M_{zp} = \sum_{i=1}^r M_{(zpj)i} + \sum_{i=1}^n M_{(z2)i}$;
- (ii) straightening forearm: $M_{pp} = \sum_{i=1}^o M_{(ppj)i} + \sum_{i=1}^p M_{(p2)i}$.

On the shoulder joint the following forces momentum are acting:

- (i) flexing arm: $M_{zr} = \sum_{i=1}^r M_{(zrj)i} + \sum_{i=1}^n M_{(z2)i}$;
- (ii) straightening arm: $M_{pr} = \sum_{i=1}^o M_{(prj)i} + \sum_{i=1}^p M_{(p2)i}$.

Moments of the straightening forces are defined as the product of force F_i and constant radius block d .

Hence it follows, that sum of momentum acting on the joint are:

(i) for elbow joint: $M_l = M_{zp} + M_{pp}$;

(ii) for arm joint: $M_r = M_{zr} + M_{pr}$.

A movement in one joint is caused by muscles lengths and tensions (forces) change involved in the movement, which belong to the physiological phenomenon ([2, 4, 6]). This means that we have to consider these equations as a system. Only in this way we can correctly and completely describe the problem.

Introducing the following notation:

$$\begin{aligned} \sum_{i=1}^r M_{(zpj)i} &= Z_p; \sum_{i=1}^n M_{(z2)i} = Z_2; \sum_{i=1}^r M_{(zrj)i} = Z_r; \\ \sum_{i=1}^o M_{(ppj)i} &= P_p; \sum_{i=1}^p M_{(p2)i} = P_2; \sum_{i=1}^s M_{(prj)i} = P_r. \end{aligned} \quad (2)$$

The system dynamics is governed by the following system of equations:

$$\begin{cases} Z_p + Z_2 + P_p + P_2 = 0, \\ Z_r + Z_2 + P_r + P_2 = 0. \end{cases} \quad (3)$$

This yields:

$$Z_p + P_p = Z_r + P_r. \quad (4)$$

It can be observed that two joint muscles do not compensate a movement in an adjacent joint. Transforming this equation into a quotient form and assuming according to physiological behaviour that $Z_r + P_r \neq 0$, we obtain:

$$\frac{Z_p + P_p}{Z_r + P_r} = 1. \quad (5)$$

From that we can observe that when the flexor forces increase, the force P_p have to decrease or $Z_r + P_r$ have to increase.

However, this equation, with these conditions is not marked – there is infinitely many solutions. This is reflected in the actual behaviour of the muscular system. During movement it do not realise the ideal of one operating model. It can be explained by the imperfection of the nervous system, muscle fatigue or other physiological or environmental reasons.

In order to obtain the best solution, optimisation methods are used, such as minimising the cost function of energy, assuming that individual muscles can not exceed the maximum physiological tension. It is also possible to consider optimisation problem based on minimising the tension σ of a muscle.

Let us consider the following Pareto minimisation problem:

$$\{\sigma_i\}, \sigma_i = \frac{F_i}{S_i \text{ anat}}, \quad (6)$$

where σ_i means i -th muscle tension and F_i denotes force generated by i -th muscle, S_i *anat* means anatomical cross-section area of i -th muscle.

We denote by J the following objective function:

$$J : \mathbb{R}_+^{r+m+s+o} \implies \mathbb{R}_+^4, \tag{7}$$

$$J(\sigma_1, \dots, \sigma_n) = \left(\sum_{i=1}^r \sigma_i, \sum_{i=r+1}^{r+m} \sigma_i, \sum_{i=r+m+1}^{r+m+s} \sigma_i, \sum_{i=r+m+s}^l \sigma_i \right), \quad l = r + m + s + o. \tag{8}$$

We minimise the function J with the following conditions:

$$\begin{aligned} 0 \leq \sigma_i, \quad \sigma_i \leq \sigma_{max}, \quad i = 1, \dots, l, \\ \sum_{i=r+1}^{r+m+s} S_i \sigma_i r_i(\alpha) = \sum_{i=1}^r S_i \sigma_i r_i(\alpha) + \sum_{i=r+m+s}^l S_i \sigma_i r_i(\alpha), \end{aligned} \tag{9}$$

where

$$\sum_{i=r+1}^{r+m+s} S_i \sigma_i r_i(\alpha) - \sum_{i=r+m+s}^l S_i \sigma_i r_i(\alpha) = M, \tag{10}$$

and M is the momentum generated by the flexors. Moreover:

$$\begin{aligned} \sigma_1 = \sigma_2 = \dots = \sigma_r; \\ \sigma_{r+1} = \sigma_{r+2} = \dots = \sigma_{r+m}; \\ \sigma_{r+m+1} = \sigma_{r+m+2} = \dots = \sigma_{r+m+s}; \\ \sigma_{r+m+s+1} = \sigma_{r+m+s+2} = \dots = \sigma_l. \\ M > 0. \end{aligned} \tag{11}$$

Even if we know σ_i *max*, $i = 1, \dots, l$, $\alpha \in (0, \pi)$, S_i , the problem still is indeterminate, that is there exist infinitely many solutions. For obvious reasons some of them are more important for us than others. To choose them an additional criterion have to be added, that is a scalar function have to be supplemented to the objective function (for example, such as the function of the cost of energy $E(\sigma)$, which limits the number of Pareto-optimal solutions). Moreover, it is also possible to enter additional, physiological restrictions (see Section 3), so the set of admissible solutions becomes narrower.

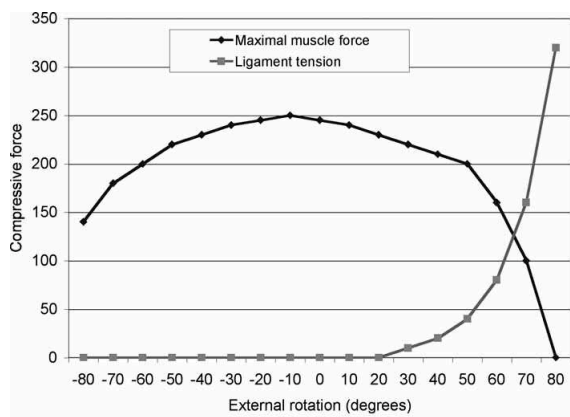
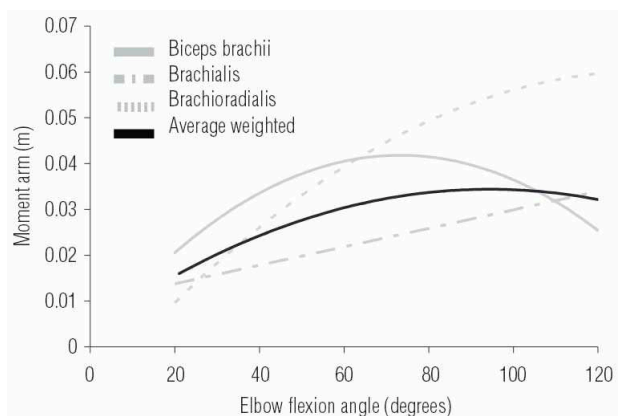
3 Physiological Movement Restrictions

First of these restrictions concerns the limbs range of motion, and is provided in Table 1.

This introduces restrictions on the angles of abduction/adduction, flexion/extension and reversion/inversion of the limb or its segments. It can be combined with a stress distribution in the individual muscle. Another physiological condition is the phenomenon of the optimal length of the muscles and increase of tissue resistance (see for example Figure 3) in the extreme positions of the limb or change in limb muscle an its moments (see Figure 4). It can be seen that muscles not always work in optimal range, which moreover does not always cover an optimal moment arm.

Table 1: International Standard Orthopaedic Measurements Norm for an upper limb.

Joint	Plane of motion	Norm International Standard Orthopedic Measurements [deg]
Shoulder	S	50-0-170
	F	170-0-0
	T	30-0-135
	R(F90)	90-0-80
	R(F0)	60-0-70
Elbow	S	0-0-150
Forearm	R	90-0-80
radio-carpal	S	50-0-60
	F	20-0-30

**Figure 3:** Corelation between muscular and capsular tension during arm movement [10].**Figure 4:** Moment arm for main forearm muscles and respective weighted mean moment arm [11].

Overlapping of the conditions leads to a reduction of possible solutions. However, as mentioned, the last of restrictions should make the solution possible. Not cost-effective (energy or due to excessive stretching of tissue) will be eliminated by the central nervous system. So there will be some narrow family of solutions. This is confirmed by the experience, the results of which are presented in Figure 5. It is also shown experimentally, using a prototype of artificial arm, that this argumentation is correct.

4 Practical Verification of the Problem

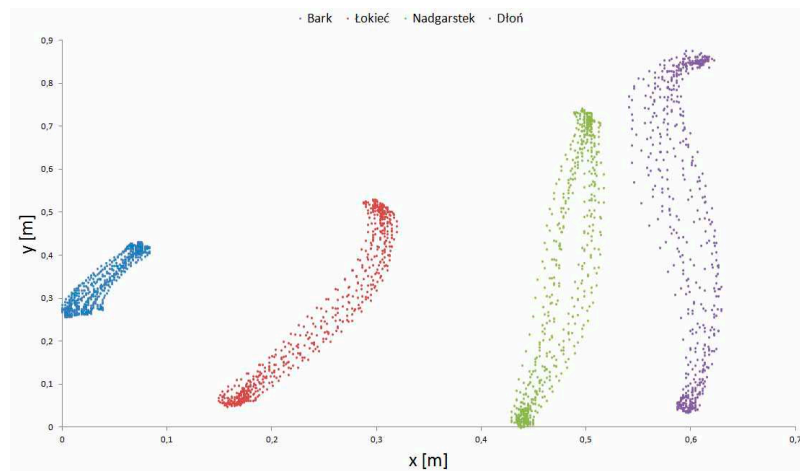


Figure 5: Repeatability of arm and forearm trajectories during subsequent cycles. Shoulder (blue), elbow (red), wrist (green) and palm (violet) trajectories (an example) [1] (with permission).

Coordinates of the upper limb joints that during the test were marked with reflective markers were determined by analysing software, specially developed for this purpose. Markers were illuminated coaxially to the optical axis of the lens to obtain maximum of reflectivity. The obtained results show that in studied biological systems there are no fixed trajectories. Five volunteers were examined. Their task was to raise their arm in the following manner:

- (i) start from point on the level of their knees;
- (ii) finish at a specific point above their heads;
- (iii) complete the motion while sitting, without standing up;
- (iv) complete the motion ten times.

Points were marked on the rack. No other restriction in arm movements were applied. Luminescent markers were placed on the shoulder joint, elbow, wrist and small finger. It is shown that the biological system, which is the upper limb human, does not have well-determined trajectory.

5 Conclusions

Due to many factors (imperfections of central nervous system phenomena, onset of muscle fatigue and other human and environmental factors), each trajectory was different. These observations confirmed the study published in the references [8] and [9]. In the first one,

trajectory has been studied as the dependence of the position of the wrist the and in the second one movement were analysed in the transverse plane. It was also found that for each of movement the strategy was different (different phases of motion at different speeds, different bending angles of the limb). This means another work of muscles each time, which can be an illustration of an uncertainty muscles cooperation problem (see also [1]). For each cycle, volunteer make the movement in a slightly different manner (different speeds, limb flexion angles, etc.). There are as many solutions as combinations that meet a specified target. In this particular case, there are also some biological and physiological constraints such as maximum bending angles of the joints, the maximum force that can generate muscle action. When analysing the results, it was hypothesised that the differences between the two depend on the state of the musculo-skeletal injuries or illnesses completed. Paper [2] confirms the observations of muscle cooperation during movement. The authors have presented a measurement of EMG signals, which shows that in the case of movement in one or two joints, an activation of muscles that spanning a stationary joint was observes.

Acknowledgements

Authors want to thank Ph.D. Michał Ludwicki for permission to use his motion analysis programm. This paper have been presented during the 12 th Conference on Dynamical Systems - Theory and Applications.

References

- [1] Andrysiak, T., Awrejcewicz, J., Ludwicki, M. and Zagrodny, B. On the human arm motion camera tracking system. *Vibrations in Physical Systems* **XXV**, Poznań (2012) 41–46.
- [2] Gribble, P. L. and Ostry, D. J. Compensation for Interaction Torques During Single- and Multijoint Limb Movement. *Journal of Neurophysiology* **82** (1999) 2310–2326.
- [3] Fick, R. *Handbuch der Anatomie des Menschen*. Jena, Gustav Fisher, vol. 2, 1910.
- [4] Reicher, M. *Human Anatomy. General Anatomy, Bones, Joints and Ligaments, Muscles*. Warsaw, Medical Publisher PZWL, 1976. [Polish]
- [5] Siemieski, A. *Inverse Optimisation Problem of Interacting Skeletal Muscles*. Wrocaw, Studies and Monographs of the Academy of Physical Education in Wrocaw, nr. 87, 2007. [Polish]
- [6] Sokoowska-Pituchowa, J. ed. *Human Anatomy*. Warsaw, Medical Publisher PZWL, 1989. [Polish]
- [7] Wojnicz, W. *Modelling and Simulation of the Skeletal Arm-forearm System Behaviour*. Ph.D. thesis. Gdask-d, 2008.
- [8] Wang, X. Three-dimensional kinematic analysis of influence of hand orientation and joint limits on the control of arm postures and movements. *Biological Cybernetics* **80** (1999) 449–463.
- [9] Okadome, T. and Honda, M. Kinematic construction of the trajectory of sequential arm movements. *Biological Cybernetics* **80** (1999) 157–169.
- [10] Frederick, A., Matsen, M.D. and Chebli, C. Principles for the Evaluation and Management of Shoulder Instability. *Lippitt, MDThe Journal of Bone and Joint Surgery* **88** (3) (2006) 647–659.
- [11] Loss, J. and Candotti, C. Comparative study between two elbow flexion exercises using the estimated resultant muscle force. *Brazilian Journal for Physical Therapy*, Sao Carlos **12** (6) (2008) 502–510.